CLAUDE OPUS 4.5

EDITED BY ADAM S. JERMYN

LECTURES ON MAGNETOHYDRODYNAMIC

Contents

Preface

These lectures aim to build physical intuition for magnetohydrodynamics—the physics of conducting fluids threaded by magnetic fields. The subject spans an enormous range: from laboratory plasma experiments to accretion disks around black holes, from Earth's liquid iron core to the eleven-year solar cycle. What unites these phenomena is a single coupling: moving conductors generate currents, currents create magnetic fields, and those fields exert forces that change the motion. This feedback loop creates the rich dynamics of MHD.

We assume familiarity with classical electromagnetism—Maxwell's equations, the Lorentz force, electromagnetic energy. We do not assume extensive fluid mechanics background; we will build what we need as we go. The emphasis throughout is on physical pictures and order-of-magnitude estimates before mathematical machinery. We want you to *feel* why magnetic fields and flows couple as they do, and to develop intuition for when MHD applies, when it breaks down, and what phenomena it explains.

The book has three parts. In Part I (Chapters 1–5), we establish the foundations: the coupling between fields and flows, the MHD equations and their approximations, the remarkable "frozen-in flux" property, magnetic pressure and tension, and MHD waves. In Part II (Chapters 6–11), we explore equilibria, instabilities, and dynamics: the confinement problem that motivates fusion research, the tokamak, current-driven and pressure-driven instabilities, the magnetorotational instability that drives accretion, and magnetic reconnection. In Part III (Chapters 12–15), we go deeper into applications: MHD turbulence, dynamo theory, stellar magnetism, and the spectacular engines of accretion disks and jets.

Part I

Foundations

1
Why Magnetism and Flow Intertwine

1.1 The Dance of Current and Field

Watch a lightning bolt. In a fraction of a second, a channel of air transforms from insulator to conductor, and current surges through it. But the channel doesn't hold still—it writhes, branches, flickers across the sky. Why? The current creates a magnetic field; that field exerts forces on the current; those forces reshape the channel; the new shape changes the current distribution; and so on, in a feedback loop faster than the eye can follow. The lightning bolt is dancing with its own magnetic field.

Now consider something grander: the Sun's corona, that ghostly halo visible during eclipses. The corona is a million degrees hot—far hotter than the six-thousand-degree surface below it. This is deeply puzzling. Heat flows from hot to cold, so how can the outer atmosphere be hotter than the surface beneath? The answer involves magnetic fields threading through conducting plasma, twisted and braided by convective motions, storing energy and releasing it in flares and coronal loops. The same physics that makes lightning dance makes the Sun's atmosphere seethe.

And in the laboratory: liquid sodium pumped through pipes at high speed, spontaneously generating magnetic fields. Experiments in Riga and Karlsruhe that recreate, in a room-sized apparatus, the physics that gives Earth its magnetic field.

What unites these phenomena? Whenever a conductor moves through a magnetic field, or a magnetic field changes near a conductor, something happens. Currents are induced. Those currents feel forces. The forces change the motion. You cannot understand the field without understanding the flow, or the flow without understanding the field. They are coupled, and that coupling is the subject of magnetohydrodynamics—MHD.

1.2 *A Wire Loop Falls Through a Magnet*

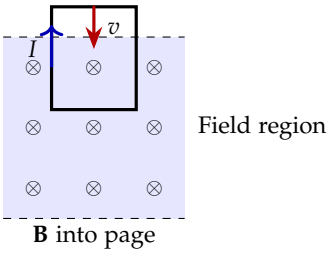

Figure 1.1: A wire loop falling into a region of magnetic field. As it enters, the changing flux induces a current that opposes the motion.

Let us begin with the simplest possible example: a rectangular loop of wire falling through a region of magnetic field. This is freshman physics, but it contains the seed of everything that follows.

Imagine a loop of copper wire, 10 cm on a side, with total resistance $R = 0.01\ \Omega$. Above the loop is empty space; below is a region where a uniform magnetic field $B = 0.1$ T points into the page. The loop is released and begins to fall.

As the loop enters the field region, the magnetic flux through it increases. Faraday's law is unforgiving: a changing flux induces an electromotive force. The EMF drives a current, and that current flows in a direction that opposes the change—this is Lenz's law, nature's way of resisting disturbance.

Let us calculate. If the loop falls at speed $v = 1$ m/s and has width $L = 0.1$ m, then the rate of flux change is

$$\frac{d\Phi}{dt} = BLv = (0.1\ \text{T})(0.1\ \text{m})(1\ \text{m/s}) = 0.01\ \text{V}.$$

This EMF drives a current $I = \mathcal{E}/R = 0.01\ \text{V}/0.01\ \Omega = 1$ A through the loop.

Now comes the crucial part. The current-carrying wire, in the portion that has entered the magnetic field, feels a force. The bottom segment of the loop carries current horizontally (say, to the right), and the magnetic field points into the page. The Lorentz force $\mathbf{F} = I\mathbf{L} \times \mathbf{B}$ points *upward*—opposing the fall.

The magnitude of this braking force is

$$F = BIL = (0.1\ \text{T})(1\ \text{A})(0.1\ \text{m}) = 0.01\ \text{N}.$$

Compare this to the gravitational force on a 10-gram loop: $mg \approx 0.1$ N. The magnetic braking force is about 10% of gravity. The loop falls, but more slowly than it would in empty space.

You might ask: where does the energy go? The kinetic energy the loop would have gained from falling is instead dissipated as heat in the wire's resistance. The current $I = 1$ A flowing through $R = 0.01\ \Omega$ produces Joule heating at a rate $I^2R = 0.01$ W. Energy is conserved; it simply goes into warming the wire rather than speeding up the fall.

This is the essence of MHD in miniature: motion creates currents, currents feel forces, forces affect motion. The loop and the field are coupled. You cannot analyze one without considering the other.

1.3 From Wire to Fluid

The wire loop is instructive, but MHD concerns itself with continuous conducting media—plasmas, liquid metals, saltwater. Let us see how the same physics extends.

Imagine replacing the wire loop with a blob of conducting fluid—say, liquid mercury. The mercury falls through the magnetic field just as the wire did. But now there is no discrete "loop"; instead, currents flow throughout the volume of the fluid, following paths determined by the field geometry and the fluid's motion.

The key equations remain the same. In a conductor moving with velocity $\mathbf{v}$ through a magnetic field $\mathbf{B}$, the effective electric field in the conductor's rest frame is

$$\mathbf{E}' = \mathbf{E} + \mathbf{v} \times \mathbf{B}.$$

This is just the motional EMF, now expressed as a field rather than an integrated voltage. If the conductor obeys Ohm's law, the current density is

$$\mathbf{J} = \sigma \mathbf{E}' = \sigma(\mathbf{E} + \mathbf{v} \times \mathbf{B}),$$

where σ is the electrical conductivity.

This equation is the heart of MHD. It says that motion through a magnetic field ($\mathbf{v} \times \mathbf{B}$) drives currents, just as an applied electric field would. The currents, once established, create their own magnetic fields (via Ampère's law) and feel forces (via the Lorentz force). The force per unit volume on the fluid is

$$\mathbf{f} = \mathbf{J} \times \mathbf{B}.$$

This force enters the fluid's equation of motion, changing how it flows. The changed flow alters $\mathbf{v} \times \mathbf{B}$, which changes the currents, which changes the forces... and we have a fully coupled system.

You might ask: why doesn't this feedback loop always run away? Sometimes it does—that's called an instability, and we'll spend several chapters on instabilities. But often the system settles into a balance, with the magnetic forces providing a kind of friction or tension that resists certain motions while permitting others.

1.4 The Coupling at Work: Two Examples

Let us make this concrete with two examples that span the range of MHD phenomena.

Magnetic Braking in Metallurgy

In steel production, molten metal must be cast into molds without excessive turbulence. Turbulence creates defects—bubbles, inclusions,

uneven cooling. One solution is electromagnetic braking: apply a strong magnetic field across the flow of liquid steel.

The physics is exactly our falling loop, writ large. Liquid steel has conductivity $\sigma \approx 7 \times 10^5$ S/m. If it flows at $v \sim 1$ m/s through a field $B \sim 0.3$ T, the induced current density is roughly

$$J \sim \sigma v B \sim (7 \times 10^5)(1)(0.3) \sim 2 \times 10^5 \text{ A/m}^2.$$

The braking force density is

$$f \sim JB \sim (2 \times 10^5)(0.3) \sim 6 \times 10^4 \text{ N/m}^3.$$

Over a region 0.1 m thick, this gives a pressure-like resistance of ~ 6000 Pa, comparable to the dynamic pressure of the flow itself. The field genuinely slows the steel.

This is MHD engineering: using the coupling between fields and flows to control industrial processes. No moving parts, no contact with the hot metal—just Maxwell's equations doing the work. One might call it "contactless plumbing," except that phrase lacks the gravitas demanded by engineering journals.

The Earth's Core

At the other extreme of scale, consider the Earth's liquid outer core. Here we have liquid iron at temperatures around 4000–5000 K, conductivity $\sigma \approx 10^6$ S/m, churning due to convection driven by the slow cooling of the planet.

The core is about 3500 km in radius. Convective velocities are tiny by everyday standards—perhaps 10^{-4} m/s, inferred from the slow drift of magnetic features at Earth's surface over decades. The magnetic field strength at the core-mantle boundary is about 5×10^{-4} T.

Let us estimate the motional EMF across the core:

$$\mathcal{E} \sim vBL \sim (10^{-4} \text{ m/s})(5 \times 10^{-4} \text{ T})(3.5 \times 10^6 \text{ m}) \sim 0.2 \text{ V}.$$

That's a fifth of a volt across 3500 kilometers! Not much by household standards, but with such enormous conductivity and volume, even this modest EMF drives substantial currents.

The current density can be estimated as

$$J \sim \sigma v B \sim (10^6)(10^{-4})(5 \times 10^{-4}) \sim 0.05 \text{ A/m}^2.$$

And the Lorentz force density:

$$f \sim JB \sim (0.05)(5 \times 10^{-4}) \sim 2.5 \times 10^{-5} \text{ N/m}^3.$$

This seems negligible—and compared to pressure forces in the core (which run to $\sim 10^{-2}$ N/m^3 from thermal buoyancy), it is small. The

magnetic forces are perhaps 1% of the buoyancy forces that drive convection.

You might ask: if magnetic forces are so weak, why do they matter? Because they have a special property: they can *organize* the flow in ways that pressure and gravity cannot. Magnetic fields impose structure, linking distant parts of the fluid. A magnetic field line is like a rubber band stretched through the core—pull on one end, and the other end feels it. This long-range coupling gives magnetic forces an influence far beyond their magnitude.

And there's something more: in the core, the currents that flow actually *create* the magnetic field in the first place. This is the geodynamo—a self-sustaining engine where convective motion generates magnetic field, and the magnetic field guides (and partially resists) the convection. Understanding how this works will occupy us in Chapter 13. For now, the point is simply that MHD in the core is inescapably coupled: you cannot compute the flow without knowing the field, and you cannot compute the field without knowing the flow.

1.5 Historical Interlude: Faraday's Saltwater

The coupling between conducting fluids and magnetic fields was recognized almost as soon as electromagnetic induction itself was discovered. Michael Faraday didn't just experiment with coils and magnets in his laboratory; he thought about the natural world.

In 1832, shortly after demonstrating induction, Faraday attempted to detect the EMF induced in the River Thames as it flowed through Earth's magnetic field. He dangled electrodes from Waterloo Bridge into the water and connected them to a galvanometer. The signal, he hoped, would reveal the river as a moving conductor in a planetary magnetic field.

The experiment failed—the signal was too small and too noisy to detect reliably. But Faraday's reasoning was impeccable. The Thames flows at perhaps 1 m/s; Earth's field has a vertical component of about 5×10^{-5} T in London; the river is perhaps 200 m wide. The expected EMF is

$$\mathcal{E} \sim vBL \sim (1)(5 \times 10^{-5})(200) \sim 0.01 \text{ V}.$$

Ten millivolts—detectable in principle, but swamped by electrochemical potentials between the electrodes and the dirty river water.

A century later, this same effect was successfully measured in ocean channels. The Gulf Stream, flowing through Earth's field, does indeed generate measurable voltages—a fact now used to monitor deep-ocean currents with seafloor cables. Faraday's physical intuition was correct; only his technology was inadequate.

The quantitative foundations of MHD came later. Hannes Alfvén, in the 1940s, developed the theory of hydromagnetic waves and the concept of "frozen-in" magnetic flux that we'll explore in Chapter 3. His work earned the 1970 Nobel Prize. Meanwhile, in 1937, Julius Hartmann and Freimut Lazarus performed careful experiments on mercury flowing through magnetic fields, establishing the basic physics of MHD channel flow. They were thinking about metallurgy and liquid-metal technology. They could not have imagined that the same equations would describe the solar corona.

1.6 The Essential Coupling

Let us now be precise about what makes MHD special. Many physical systems involve feedback—thermostats, predator-prey populations, electronic oscillators. What distinguishes the MHD coupling?

The answer lies in the structure of the equations. Start with Ohm's law in a moving conductor:

$$\mathbf{J} = \sigma(\mathbf{E} + \mathbf{v} \times \mathbf{B}).$$

Take the curl and use Faraday's law ($\nabla \times \mathbf{E} = -\partial \mathbf{B}/\partial t$) and Ampère's law ($\nabla \times \mathbf{B} = \mu_0 \mathbf{J}$ in the MHD limit where displacement current is negligible). After some vector calculus, you arrive at the *induction equation*:

$$\frac{\partial \mathbf{B}}{\partial t} = \nabla \times (\mathbf{v} \times \mathbf{B}) + \lambda \nabla^2 \mathbf{B},$$

where $\lambda = 1/(\mu_0 \sigma)$ is the magnetic diffusivity.

This equation tells you how the magnetic field evolves. The first term on the right describes how the flow drags and distorts the field—the "advection" or "frozen-in" effect we'll explore later. The second term describes how the field diffuses due to finite conductivity—the resistive decay that would cause any field to fade away if nothing regenerated it.

Meanwhile, the magnetic field affects the flow through the Lorentz force in the momentum equation:

$$\rho \frac{D\mathbf{v}}{Dt} = -\nabla p + \mathbf{J} \times \mathbf{B} + (\text{other forces}).$$

The $\mathbf{J} \times \mathbf{B}$ term feeds back into the velocity field $\mathbf{v}$, which appears in the induction equation, which determines $\mathbf{B}$, which determines $\mathbf{J}$...

This is a genuine two-way coupling. Not "the field affects the flow" or "the flow affects the field," but both simultaneously and inseparably. Solving MHD problems means solving these equations together, self-consistently.

You might ask: when does this coupling matter? When can we ignore it? The answer involves comparing the strength of the magnetic

force to other forces in the problem. We'll develop dimensionless parameters—the magnetic Reynolds number, the Alfvén Mach number, the plasma beta—to quantify this. But roughly: if the magnetic field is strong and the conductor is good, you cannot ignore the coupling.

1.7 Why "Magnetohydrodynamics"?

The name itself tells a story. "Magneto-" for magnetic fields. "Hydro-" for fluid flow (from the Greek for water, though MHD applies to any conducting fluid). "Dynamics" for the study of forces and motion.

The term was coined in the 1940s, during the explosive growth of plasma physics driven by both astrophysical curiosity and the quest for controlled fusion. One suspects the name was chosen by physicists who wanted to ensure their grant applications looked sufficiently impressive—"magnetohydrodynamics" has precisely the polysyllabic gravitas to make administrators nervous about cutting the budget. Before that, the coupling between fields and flows was studied piecemeal—by electrical engineers worried about eddy currents in motors, by geophysicists puzzling over Earth's field, by astrophysicists modeling sunspots. The unifying framework of MHD revealed that these were all facets of the same physics.

You might ask: is MHD just applied electromagnetism? In a sense, yes—Maxwell's equations plus Ohm's law plus fluid mechanics. But the combination is more than the sum of its parts. The coupling creates phenomena that exist in none of the parent subjects: Alfvén waves, magnetic reconnection, the dynamo effect, magnetorotational instability. These are emergent behaviors of the coupled system.

MHD is also an approximation. It assumes the fluid is dense enough to treat as a continuum, conducting enough that currents flow freely, and slow enough (compared to light) that we can ignore displacement currents and relativistic effects. When these assumptions fail—in dilute plasmas, at very high frequencies, near black holes—MHD gives way to more complete descriptions. But within its domain of validity, MHD is remarkably powerful.

1.8 What Lies Ahead

We have seen that conducting fluids and magnetic fields are coupled through Faraday's law and the Lorentz force. Motion induces currents; currents create fields; fields exert forces; forces change motion. This feedback loop is the engine of MHD.

But we have been waving our hands about "the equations." What

exactly are the equations of MHD? What approximations do we make? What phenomena do we neglect? The next chapter will derive the MHD equations carefully, starting from Maxwell and Newton and ending with a closed system we can solve.

We will then explore the remarkable consequences: magnetic flux frozen into moving fluid, the twin forces of magnetic pressure and tension, waves that propagate along field lines like vibrations on a string. And we will see how this simple physics—freshman electromagnetism plus fluid mechanics—explains phenomena from laboratory experiments to the most violent events in the universe.

The lightning bolt was just the beginning.

2
The Equations of a Conducting Fluid

2.1 The Art of Controlled Demolition

We want to write down the equations that govern a conducting fluid in a magnetic field. But here is the remarkable thing: we already know all the relevant physics. Maxwell's equations describe the electromagnetic fields. Newton's laws, in the form of fluid mechanics, describe the motion of matter. Ohm's law relates the current to the electric field. There is nothing fundamentally new to discover.

And yet, if we simply combined all those equations without approximation, we would have an unholy mess. Electromagnetic waves propagating at the speed of light. Charge separation on microscopic Debye scales. Plasma oscillations at frequencies we do not care about. Displacement currents modifying Ampère's law. The full equations describe physics from radio waves to gamma rays, from individual electrons to galaxy clusters—far more than we need for the conducting-fluid problems that interest us.

The art of MHD is knowing what to throw away. The "MHD approximation" is a controlled demolition of the full equations, keeping only the physics that matters for slow, large-scale, quasi-neutral conducting flows. We are building a simpler theory by deliberately ignoring phenomena that occur on scales too fast or too small to affect the dynamics we care about.

The payoff is a beautiful, closed set of equations—compact enough to write on a single page, rich enough to describe sunspots and planetary cores and fusion reactors. But we must earn this simplicity by understanding precisely what we are neglecting and when those approximations fail.

2.2 *Why We Can Ignore Displacement Current*

Let us begin with the most consequential simplification. Maxwell's equation relating the curl of the magnetic field to currents reads

$$\nabla \times \mathbf{B} = \mu_0 \mathbf{J} + \mu_0 \epsilon_0 \frac{\partial \mathbf{E}}{\partial t}.$$

The second term on the right—the displacement current—is what allows electromagnetic waves to propagate. It is essential for radio transmission, for light, for all of classical electrodynamics. Can we really throw it away?

Let us estimate when the displacement current matters. Consider a system of characteristic size L varying on a timescale τ. The electric field has magnitude E, and the current density is related to the field by Ohm's law: $J \sim \sigma E$, where σ is the electrical conductivity.

The displacement current density has magnitude

$$J_{\text{disp}} \sim \epsilon_0 \frac{\partial E}{\partial t} \sim \epsilon_0 \frac{E}{\tau}.$$

The ratio of displacement to conduction current is therefore

$$\frac{J_{\text{disp}}}{J_{\text{cond}}} \sim \frac{\epsilon_0 E/\tau}{\sigma E} = \frac{\epsilon_0}{\sigma \tau} = \frac{1}{\sigma \tau / \epsilon_0}.$$

For copper, $\sigma \approx 6 \times 10^7$ S/m. Even for a process as fast as $\tau =$ 1 millisecond:

$$\frac{J_{\text{disp}}}{J_{\text{cond}}} \sim \frac{8.85 \times 10^{-12}}{(6 \times 10^7)(10^{-3})} \sim 10^{-16}.$$

The displacement current is sixteen orders of magnitude smaller than the conduction current! We can neglect it without a second thought.

You might ask: when *would* the displacement current matter? When $\tau \sim \epsilon_0/\sigma \sim 10^{-19}$ s for copper. That is the timescale on which charge rearranges itself inside a conductor—effectively instantaneous for any macroscopic process.

There is another way to see this. Displacement current matters when electromagnetic waves are important, and EM waves travel at speed c. For waves to significantly affect dynamics on length scale L, we need the wave transit time L/c to be comparable to the timescale of interest τ. For $L = 1$ m, that means $\tau \sim 3$ nanoseconds. MHD phenomena—convection in stellar interiors, flow in liquid metal experiments, dynamics of fusion plasmas—are vastly slower.

The MHD ordering can be summarized as: $v \ll c$ and $L \gg c/\omega_p$, where ω_p is the plasma frequency. We are working in a regime where light-speed effects are negligible.

With displacement current gone, Ampère's law becomes simply

$$\nabla \times \mathbf{B} = \mu_0 \mathbf{J}. \tag{2.1}$$

This is a tremendous simplification. The current density is no longer an independent variable—it is determined entirely by the magnetic field configuration: $\mathbf{J} = (\nabla \times \mathbf{B})/\mu_0$.

2.3 *The Full Set of Starting Equations*

Before making further approximations, let us write down everything we have. The electromagnetic sector gives us Maxwell's equations:

$$\nabla \cdot \mathbf{E} = \rho_c/\epsilon_0 \tag{2.2}$$

$$\nabla \cdot \mathbf{B} = 0 \tag{2.3}$$

$$\nabla \times \mathbf{E} = -\frac{\partial \mathbf{B}}{\partial t} \tag{2.4}$$

$$\nabla \times \mathbf{B} = \mu_0 \mathbf{J} \tag{2.5}$$

where we have already dropped the displacement current in (2.5).

The fluid sector gives us the momentum equation:

$$\rho\left(\frac{\partial \mathbf{v}}{\partial t} + \mathbf{v}\cdot\nabla\mathbf{v}\right) = -\nabla p + \mathbf{J}\times\mathbf{B} + \rho\mathbf{g} + \nu\nabla^2\mathbf{v}, \tag{2.6}$$

where ρ is the mass density, p the pressure, $\mathbf{g}$ the gravitational acceleration, and ν the kinematic viscosity.

Mass conservation requires

$$\frac{\partial \rho}{\partial t} + \nabla\cdot(\rho\mathbf{v}) = 0. \tag{2.7}$$

We need an equation of state relating pressure to density and temperature. For an ideal gas:

$$p = \frac{\rho k_B T}{m}, \tag{2.8}$$

where m is the mean particle mass. From this we can define the sound speed

$$c_s = \sqrt{\frac{\partial p}{\partial \rho}} = \sqrt{\frac{\gamma k_B T}{m}} \tag{2.9}$$

for adiabatic processes. The sound speed sets how fast pressure disturbances propagate—a crucial velocity scale that we will compare to the magnetic velocity scales later.

For the solar photosphere at $T \sim 6000$ K with hydrogen ($m \approx m_p$), the sound speed is about 8 km/s. For a fusion plasma at $T \sim 10$ keV (about 10^8 K) with deuterium, it rises to several hundred km/s—the exact value depending on whether you use the electron or ion temperature and what ratio of specific heats you assume, but the order of magnitude is clear. These numbers will become important when we discuss MHD waves.

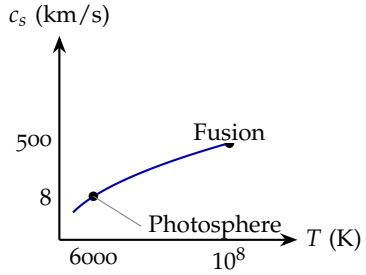

Figure 2.1: Sound speed increases with temperature. Solar photosphere: $c_s \sim 8$ km/s. Fusion plasma: $c_s \sim 500$ km/s.

Finally, we need Ohm's law relating current to electric field. The generalized form is

$$\mathbf{E} + \mathbf{v} \times \mathbf{B} = \eta \mathbf{J} + \frac{1}{ne}(\mathbf{J} \times \mathbf{B}) - \frac{1}{ne}\nabla p_e + \cdots \tag{2.10}$$

The left side is the electric field in the frame moving with the fluid. The right side includes resistive effects (the $\eta\mathbf{J}$ term), the Hall effect, electron pressure gradients, and potentially other terms we have omitted.

2.4 *The MHD Approximations*

Now let us make the approximations that define MHD.

Quasi-Neutrality

In a plasma or conducting fluid, any charge imbalance creates electric fields that immediately drive currents to neutralize it. The timescale for this neutralization is the inverse plasma frequency, ω_p^{-1}, which is typically 10^{-9} s or faster for laboratory plasmas.

The length scale over which charge separation can persist is the Debye length:

$$\lambda_D = \sqrt{\frac{\epsilon_0 k_B T}{ne^2}}.$$

For a fusion plasma with $n \sim 10^{20}$ m^{-3} and $T \sim 10$ keV, this is about 10^{-5} m—utterly negligible compared to the meter-scale structures we care about.

The MHD approximation treats the plasma as electrically neutral: the charge density ρ_c is essentially zero on the scales of interest. This does *not* mean there are no electric fields! Electric fields still arise from electromagnetic induction (Faraday's law) and from the motional $\mathbf{v} \times \mathbf{B}$ EMF. We simply do not use Gauss's law (2.2) to determine $\mathbf{E}$; instead, $\mathbf{E}$ comes from Ohm's law.

You might ask: if we set $\rho_c = 0$, how can there be currents? The currents arise from the *motion* of the (neutral) fluid through magnetic fields, not from net charge. The current $\mathbf{J}$ represents a slight difference in the velocities of electrons and ions, not an excess of one species over the other.

Simplified Ohm's Law

The generalized Ohm's law (2.10) contains several terms beyond simple resistivity. In standard MHD, we keep only the resistive term:

$$\mathbf{E} + \mathbf{v} \times \mathbf{B} = \eta \mathbf{J}. \tag{2.11}$$

When is this valid? The Hall term $(\mathbf{J} \times \mathbf{B})/ne$ becomes important when the ion gyroradius $r_i = m_i v_\perp / (eB)$ is comparable to the length scales of interest. The electron pressure term matters when there are sharp gradients in electron temperature or density.

For most MHD applications—stellar interiors, liquid metal experiments, large-scale plasma dynamics—these corrections are small. But they become crucial in certain situations. Magnetic reconnection, which we will study in Chapter 11, is profoundly affected by Hall physics. The simple Ohm's law (2.11) predicts reconnection rates that are far too slow; including the Hall term resolves the discrepancy.

You might ask: if the Hall term is so important for reconnection, why not include it from the start? Because it complicates the equations substantially, introducing new wave modes and new instabilities. The philosophy of MHD is to use the simplest model that captures the essential physics, then add corrections when they matter. We will see when they matter.

For now, we proceed with the simple form, remembering that it is an approximation with known limitations.

2.5 *The Induction Equation*

Here is where the magic happens. Let us combine our simplified equations to derive the evolution equation for the magnetic field.

Start with Faraday's law:

$$\frac{\partial \mathbf{B}}{\partial t} = -\nabla \times \mathbf{E}.$$

Substitute Ohm's law (2.11) solved for $\mathbf{E}$:

$$\mathbf{E} = -\mathbf{v} \times \mathbf{B} + \eta \mathbf{J}.$$

Use Ampère's law to write $\mathbf{J} = (\nabla \times \mathbf{B})/\mu_0$:

$$\mathbf{E} = -\mathbf{v} \times \mathbf{B} + \frac{\eta}{\mu_0} \nabla \times \mathbf{B}.$$

Take the curl:

$$\nabla \times \mathbf{E} = -\nabla \times (\mathbf{v} \times \mathbf{B}) + \frac{\eta}{\mu_0} \nabla \times (\nabla \times \mathbf{B}).$$

Using the vector identity $\nabla \times (\nabla \times \mathbf{B}) = \nabla(\nabla \cdot \mathbf{B}) - \nabla^2 \mathbf{B}$ and noting that $\nabla \cdot \mathbf{B} = 0$:

$$\nabla \times \mathbf{E} = -\nabla \times (\mathbf{v} \times \mathbf{B}) - \frac{\eta}{\mu_0} \nabla^2 \mathbf{B}.$$

Finally, substitute into Faraday's law:

$$\boxed{\frac{\partial \mathbf{B}}{\partial t} = \nabla \times (\mathbf{v} \times \mathbf{B}) + \lambda \nabla^2 \mathbf{B}} \tag{2.12}$$

where we have defined the **magnetic diffusivity**

$$\lambda \equiv \frac{\eta}{\mu_0} \tag{2.13}$$

with units of m^2/s.

This is the **induction equation**, and it is the heart of MHD. Let us understand its two terms.

The first term, $\nabla \times (\mathbf{v} \times \mathbf{B})$, describes **advection**—how the flow carries and distorts the magnetic field. If a fluid element moves, it drags the magnetic field with it. If the flow shears, the field is stretched. This term is responsible for the "frozen-in" behavior we will explore in the next chapter.

The second term, $\lambda \nabla^2 \mathbf{B}$, describes **diffusion**—how the magnetic field spreads out due to finite resistivity, like heat diffusing through a conductor or dye spreading in water. Without any flow to maintain it, any magnetic field configuration would eventually decay away through this diffusive process.

2.6 *The Magnetic Reynolds Number*

Which term dominates? Let us estimate their magnitudes for a system of size L with characteristic velocity V and magnetic field B.

The advection term scales as

$$|\nabla \times (\mathbf{v} \times \mathbf{B})| \sim \frac{VB}{L}.$$

The diffusion term scales as

$$|\lambda \nabla^2 \mathbf{B}| \sim \frac{\lambda B}{L^2}.$$

Their ratio defines the **magnetic Reynolds number**:

$$R_\mathrm{m} = \frac{\text{advection}}{\text{diffusion}} = \frac{VB/L}{\lambda B/L^2} = \frac{VL}{\lambda}. \tag{2.14}$$

This dimensionless number controls the character of MHD dynamics:

When $R_\mathrm{m} \ll 1$: Diffusion dominates. The magnetic field slips through the fluid, decaying on the diffusion timescale $\tau_\mathrm{diff} \sim L^2/\lambda$. This is the regime of small laboratory experiments and highly resistive plasmas.

When $R_\mathrm{m} \gg 1$: Advection dominates. The magnetic field is effectively "frozen" to the fluid, carried along with it like threads embedded in a moving gel. This is the regime of astrophysics and large-scale plasma physics.

When $R_\mathrm{m} \sim 1$: Both effects matter, and the full equation must be solved.

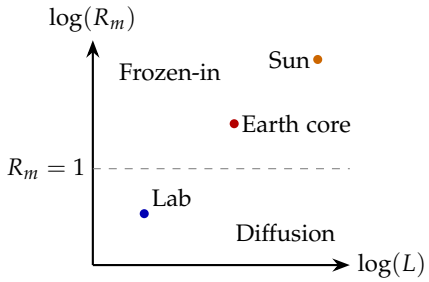

Figure 2.2: Magnetic Reynolds number increases with system size. Laboratory experiments struggle to reach $R_m > 1$; astrophysical systems easily exceed $R_m \sim 10^6$.

Let us put in numbers for some representative systems:

Laboratory liquid metal ($L \sim 0.1$ m, $V \sim 1$ m/s, $\lambda \sim 1$ m^2/s for liquid sodium):

$$R_{\mathrm{m}} \sim \frac{(1)(0.1)}{1} \sim 0.1.$$

Diffusion wins. This is why liquid metal dynamo experiments are so difficult—they operate right at the margin where $R_{\mathrm{m}} \sim 1$.

Earth's outer core ($L \sim 10^6$ m, $V \sim 10^{-4}$ m/s, $\lambda \sim 1$ m^2/s):

$$R_{\mathrm{m}} \sim \frac{(10^{-4})(10^6)}{1} \sim 100.$$

Advection wins handily. The geodynamo operates in the frozen-in regime.

Solar convection zone ($L \sim 10^8$ m, $V \sim 100$ m/s, $\lambda \sim 10^2$ m^2/s):

$$R_{\mathrm{m}} \sim \frac{(100)(10^8)}{10^2} \sim 10^8.$$

Overwhelmingly frozen-in. The Sun's magnetic field is dragged around by convection, sheared by differential rotation, wound up and amplified. Diffusion is almost irrelevant on dynamical timescales.

You might ask: why does size matter so much more than velocity? Because diffusion scales with L^2 while advection scales with L—the magnetic Reynolds number grows linearly with size. The same flow that barely stirs a laboratory beaker will utterly dominate diffusion in a planetary core. This is why astrophysicists work in the frozen-in limit almost always, while experimentalists in liquid-metal labs struggle to reach $R_{\mathrm{m}} \sim 1$.

2.7 *Diffusion Time Versus Dynamical Time*

You might ask: if diffusion is irrelevant for the Sun, why do sunspots disappear in a few weeks rather than lasting forever?

This question cuts to the heart of the distinction between diffusion and dynamics. Let us work through it carefully.

A sunspot is a region of strong magnetic field, roughly $B \sim 0.3$ T, with a radius of about $L \sim 10^7$ m (10,000 km). The magnetic diffusivity in the solar photosphere is $\lambda \sim 1$ m^2/s.[1]

[1] This comes from the Spitzer resistivity formula, which depends on temperature and is about $\eta \sim 10^{-6}$ Ωm for the photosphere.

The diffusion timescale is

$$\tau_{\mathrm{diff}} \sim \frac{L^2}{\lambda} \sim \frac{(10^7)^2}{1} \sim 10^{14} \text{ s} \sim 3 \text{ million years}.$$

If sunspots decayed by diffusion alone, they would persist for geological time!

But sunspots vanish in weeks. What gives?

The answer is that sunspots do not decay by diffusion—they are destroyed by *dynamics*. Convective motions in the photosphere, with velocities $v \sim 1$ km/s, operate on a timescale

$$\tau_{\rm dyn} \sim \frac{L}{v} \sim \frac{10^7}{10^3} \sim 10^4 \text{ s} \sim \text{hours}.$$

The ratio of these timescales is precisely the magnetic Reynolds number:

$$\frac{\tau_{\rm diff}}{\tau_{\rm dyn}} = \frac{L^2/\lambda}{L/v} = \frac{vL}{\lambda} = R_{\rm m} \sim 10^{10}.$$

The field is frozen to the plasma on dynamical timescales. When the sunspot disappears, the magnetic flux is not destroyed—it is *rearranged*, dispersed by convective motions into structures too small and fragmented to see as a coherent spot. The total unsigned flux may persist for much longer; it is only the organized structure that is lost.

This distinction is crucial throughout MHD. Diffusion times tell you how long a field would persist in a static medium. Dynamical times tell you how fast the field is rearranged. In high-$R_{\rm m}$ systems, the dynamics always wins.

2.8 *Historical Note: Alfvén and the Frozen Field*

The equations we have derived were known, in pieces, before the 1940s. Maxwell's equations dated from the 1860s. Fluid mechanics was well established. Ohm's law was understood. But nobody had synthesized them into a coherent framework for conducting fluids until Hannes Alfvén.

Alfvén was a Swedish physicist interested in cosmic electrodynamics—the physics of sunspots, cosmic rays, and magnetized plasmas in space. In a series of papers in the 1940s, he developed the theory of hydromagnetic waves (now called Alfvén waves) and articulated the concept of magnetic field lines "frozen" to the conducting fluid.

The frozen-in picture was controversial. Many physicists, trained to think of field lines as mathematical conveniences, were uncomfortable with the idea that these abstract curves could behave like physical strings embedded in a material. Sydney Chapman, the doyen of geomagnetism, was skeptical. The debate had the flavor of an argument between a mathematician who insists that π is merely a ratio and an engineer who wants to wrap it around a cylinder.

Alfvén won the 1970 Nobel Prize in Physics "for fundamental work and discoveries in magnetohydrodynamics with fruitful applications in different parts of plasma physics." His frozen-in picture became the conceptual foundation of space physics.

But Alfvén himself grew frustrated with how literally people took the picture. In his later years, he repeatedly warned against treating field lines as real objects.[2] They are useful for intuition, but the physics is in the equations, not in the visualization.

We will take the frozen-in theorem seriously in the next chapter—derive it properly, understand its limits, and see what it tells us about MHD dynamics. But we will also keep Alfvén's warning in mind.

[2] "The concept of frozen-in field lines is of great use when one starts to learn about cosmic plasmas. However, at a more advanced level it is misleading, especially in the case of reconnection." —Alfvén, 1976

2.9 The Complete MHD System

Let us collect the equations that define standard MHD. The induction equation:

$$\frac{\partial \mathbf{B}}{\partial t} = \nabla \times (\mathbf{v} \times \mathbf{B}) + \lambda \nabla^2 \mathbf{B}. \tag{2.15}$$

The momentum equation:

$$\rho \left(\frac{\partial \mathbf{v}}{\partial t} + \mathbf{v} \cdot \nabla \mathbf{v} \right) = -\nabla p + \frac{1}{\mu_0} (\nabla \times \mathbf{B}) \times \mathbf{B} + \rho \mathbf{g}. \tag{2.16}$$

Here we have used $\mathbf{J} = (\nabla \times \mathbf{B})/\mu_0$ to eliminate the current, and dropped viscosity for simplicity.

The continuity equation:

$$\frac{\partial \rho}{\partial t} + \nabla \cdot (\rho \mathbf{v}) = 0. \tag{2.17}$$

And an energy equation or equation of state to close the system. For an adiabatic ideal gas:

$$\frac{d}{dt} \left(\frac{p}{\rho^\gamma} \right) = 0, \tag{2.18}$$

or for incompressible flow simply $\nabla \cdot \mathbf{v} = 0$.

The constraint $\nabla \cdot \mathbf{B} = 0$ must be satisfied at all times. If it holds initially and the induction equation is used to evolve $\mathbf{B}$, it will continue to hold.[3]

These equations—four in all—are the foundation of MHD. Everything else we will study, from Alfvén waves to the geodynamo to accretion disk jets, emerges from this system.

[3] This follows from taking the divergence of the induction equation: $\partial(\nabla \cdot \mathbf{B})/\partial t = \nabla \cdot [\nabla \times (\mathbf{v} \times \mathbf{B})] + \lambda \nabla^2 (\nabla \cdot \mathbf{B}) = 0 + \lambda \nabla^2 (\nabla \cdot \mathbf{B})$. If $\nabla \cdot \mathbf{B} = 0$ initially, it stays zero.

2.10 What Lies Ahead

We now have the equations. But equations are just the beginning; what matters is understanding their behavior.

The induction equation contains a competition between advection and diffusion. In the limit where advection dominates ($R_\mathrm{m} \gg 1$), something remarkable happens: the magnetic field becomes "frozen" to the fluid, unable to diffuse through it. Field lines move with the

flow like elastic threads embedded in a deforming jelly. This is Alfvén's theorem, and we will derive it properly in the next chapter.

But first, consider what this means. If field lines are frozen in, they can be stretched, compressed, and twisted by fluid motions. Stretching a field line increases the magnetic energy density, like stretching a rubber band. That energy has to come from somewhere—it comes from the kinetic energy of the flow. The field exerts a back-reaction, a tension force, on the fluid. This is magnetic tension, and together with magnetic pressure, it gives magnetic fields a mechanical reality that we will explore in Chapter 4.

The MHD equations are deceptively simple. Within them lies a universe of phenomena—and we have only begun to explore it.

3
Frozen-In Flux and Alfvén's Theorem

3.1 Painting a Field Line

Imagine you could paint a magnetic field line with luminous dye and watch what happens. In a perfect conductor, that glowing line moves with the fluid. Stretch the fluid, and the field line stretches. Twist the fluid, and the field line twists. Compress the fluid perpendicular to the field, and the field grows stronger. The field line behaves as if it were a material thread embedded in the conducting medium.

This is Alfvén's theorem, and it sounds like a metaphor—the kind of loose talk physicists use at colloquia when they want to seem insightful without committing to a calculation. But here, for once, the loose talk is exactly right. The magnetic flux through any material surface—a surface that moves and deforms with the fluid—is exactly constant in time, provided the fluid is a perfect conductor.

The consequences are profound. Magnetic topology is preserved: knots in the field cannot untangle themselves; linked loops remain linked. Energy stored in twisted field configurations cannot easily escape. The frozen-in constraint shapes everything from solar flares to accretion disk dynamics.

But we must not forget that frozen-in is an approximation. Real conductors have finite resistivity. On small enough scales or long enough times, the field can slip through the fluid, diffusing and dissipating. Understanding when frozen-in holds, and when it fails catastrophically, is essential for understanding MHD phenomena.

3.2 Stretching a Flux Tube

Let us see the frozen-in constraint in action with the simplest possible example: stretching a tube of magnetized fluid.

Take a cylindrical tube of conducting fluid with magnetic field B_0 pointing along its axis. The tube has initial cross-sectional area A_0 and length L_0.

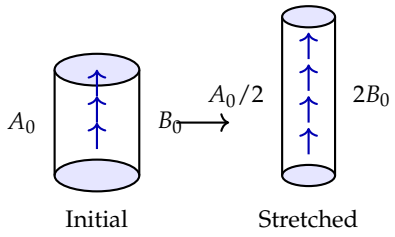

Figure 3.1: Stretching a flux tube: doubling the length halves the cross-section and doubles the field strength.

Now stretch the tube to twice its original length: $L_1 = 2L_0$. If the fluid is incompressible, the volume must remain constant, so the cross-sectional area shrinks: $A_1 = A_0/2$. (This is why pasta makers must work fast—their noodles are trying to conserve volume too.)

What happens to the magnetic field? The frozen-in constraint says that the magnetic flux through any material surface is conserved. Take a cross-section of the tube—a material surface that moves with the fluid. The flux through it is $\Phi = BA$. Since Φ is conserved:

$$B_0 A_0 = B_1 A_1 \quad \Rightarrow \quad B_1 = B_0 \frac{A_0}{A_1} = 2B_0.$$

The field has doubled! Stretching the fluid amplifies the magnetic field.

Let us check the energy budget. The magnetic energy density is $B^2/(2\mu_0)$. The initial energy is

$$U_0 = \frac{B_0^2}{2\mu_0} \times A_0 L_0.$$

The final energy is

$$U_1 = \frac{(2B_0)^2}{2\mu_0} \times \frac{A_0}{2} \times 2L_0 = \frac{4B_0^2}{2\mu_0} \times A_0 L_0 = 2U_0.$$

The magnetic energy has doubled. Where did this energy come from?

It came from the work done to stretch the tube against the magnetic tension. The field lines resist being stretched, like rubber bands. You have to do work to pull them longer, and that work goes into magnetic energy.

A Solar Example

This mechanism is not merely academic. It explains how sunspots get their intense magnetic fields.

Consider a flux tube in the Sun's convection zone with initial field $B_0 = 0.01$ T and cross-sectional area $A_0 = (1000\text{ km})^2 = 10^{12}\text{ m}^2$. Convective downdrafts grab the flux tube and drag it downward, stretching it. If the tube is stretched to three times its original length, the cross-section shrinks to $A_0/3$ and the field increases to $3B_0 = 0.03$ T.

Further stretching by buoyant rise through the convection zone can amplify the field to 0.1–0.3 T—precisely the field strengths observed in sunspots. We will return to this flux tube amplification mechanism in Chapter 14 when we discuss the solar dynamo. It is the key to understanding how the Sun builds and maintains its magnetic field.

3.3 *Deriving Alfvén's Theorem*

Let us now prove the frozen-in property rigorously. We start with the ideal MHD induction equation—the induction equation in the limit of zero resistivity:

$$\frac{\partial \mathbf{B}}{\partial t} = \nabla \times (\mathbf{v} \times \mathbf{B}). \tag{3.1}$$

We want to show that the magnetic flux through any material surface S is constant:

$$\frac{d\Phi}{dt} = \frac{d}{dt}\int_S \mathbf{B} \cdot d\mathbf{A} = 0.$$

The flux through a moving, deforming surface changes for two reasons. First, the magnetic field $\mathbf{B}$ changes in time at each point in space. Second, the surface S itself moves and deforms, sweeping through regions of different field.

The mathematical expression for this total derivative is[1]

$$\frac{d\Phi}{dt} = \int_S \frac{\partial \mathbf{B}}{\partial t} \cdot d\mathbf{A} + \oint_C \mathbf{B} \cdot (\mathbf{v} \times d\mathbf{l}), \tag{3.2}$$

where C is the boundary curve of S, and $\mathbf{v}$ is the velocity of the fluid (and hence of the material surface).

[1] This is Reynolds transport theorem applied to a vector field. The derivation can be found in any advanced fluid mechanics text.

The second term accounts for the flux swept out by the moving boundary. Using the vector identity $\mathbf{B} \cdot (\mathbf{v} \times d\mathbf{l}) = -(\mathbf{v} \times \mathbf{B}) \cdot d\mathbf{l}$ and Stokes' theorem:

$$\oint_C \mathbf{B} \cdot (\mathbf{v} \times d\mathbf{l}) = -\oint_C (\mathbf{v} \times \mathbf{B}) \cdot d\mathbf{l} = -\int_S \nabla \times (\mathbf{v} \times \mathbf{B}) \cdot d\mathbf{A}.$$

Substituting into (3.2):

$$\frac{d\Phi}{dt} = \int_S \left[\frac{\partial \mathbf{B}}{\partial t} - \nabla \times (\mathbf{v} \times \mathbf{B})\right] \cdot d\mathbf{A}.$$

But the ideal induction equation (3.1) tells us that the bracketed quantity is exactly zero! Therefore:

$$\boxed{\frac{d\Phi}{dt} = 0} \tag{3.3}$$

This is Alfvén's theorem: the magnetic flux through any material surface is conserved in ideal MHD.

3.4 *What Frozen-In Really Means*

The mathematical statement $d\Phi/dt = 0$ has several intuitive consequences:

Field lines move with the fluid. If we define a magnetic field line as the curve threading through a particular set of fluid elements, that

field line continues to thread through the same fluid elements forever. Field lines have a material identity—you can track them, name them, watch them evolve.

Flux is conserved through material loops. Take any closed loop of fluid elements. The magnetic flux threading that loop is constant in time. Shrink the loop, and the field inside it must intensify. Stretch the loop, and the field weakens.

Topology is preserved. This is the most profound consequence. If two field lines are linked—if one threads through the loop formed by the other—they remain linked for all time. If a field line is knotted, it stays knotted. No amount of smooth fluid motion can change the topology of the magnetic field.

You might ask: if field lines are frozen in, why do solar flares happen? Flares involve rapid reconfiguration of the magnetic field, breaking and reconnecting field lines. The answer is that frozen-in eventually fails. When the field develops steep gradients, the resistive term in the induction equation—negligible at large scales—becomes important locally. Field lines can slip through the fluid, reconnect, and release energy. We will study this process, called magnetic reconnection, in Chapter 11.

You might ask: is the frozen-in picture unique to MHD? No! Vortex lines in an inviscid fluid obey an identical theorem—they are frozen to the fluid. This is Kelvin's circulation theorem, and the mathematics is the same. Replace $\mathbf{B}$ with the vorticity $\boldsymbol{\omega} = \nabla \times \mathbf{v}$, and the induction equation becomes the vorticity equation for an ideal fluid.

3.5 *Magnetic Helicity: Topology Made Quantitative*

The topological content of a magnetic field—its knottedness, its linkage—can be quantified by a single number called magnetic helicity:

$$H = \int_V \mathbf{A} \cdot \mathbf{B}\, dV, \tag{3.4}$$

where $\mathbf{A}$ is the magnetic vector potential satisfying $\mathbf{B} = \nabla \times \mathbf{A}$.

In ideal MHD, helicity is exactly conserved. To see why, note that the time derivative of helicity is[2]

$$\frac{dH}{dt} = -2 \int_V \mathbf{E} \cdot \mathbf{B}\, dV.$$

In ideal MHD, $\mathbf{E} = -\mathbf{v} \times \mathbf{B}$, so

$$\mathbf{E} \cdot \mathbf{B} = (-\mathbf{v} \times \mathbf{B}) \cdot \mathbf{B} = 0,$$

since any vector is perpendicular to its own cross product. Therefore $dH/dt = 0$.

[2] The derivation involves some vector calculus and boundary terms that vanish for a closed system. See textbooks on MHD for details.

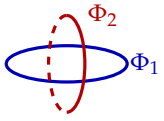

$H = \pm 2\Phi_1\Phi_2$

Figure 3.2: Two linked flux rings. Their helicity is $\pm 2\Phi_1\Phi_2$, with sign depending on the handedness of the linkage.

What does helicity measure physically? Consider two circular flux rings, each carrying magnetic flux Φ. If the rings are unlinked—far apart, not threading through each other—the helicity is zero. But if they are linked once (one ring passes through the hole of the other), the helicity is $H = \pm 2\Phi_1\Phi_2$, with the sign depending on the handedness of the linkage.

In ideal MHD, you cannot unlink the rings. That would require cutting a field line and rejoining it elsewhere, which is forbidden by the frozen-in constraint. Helicity conservation is the mathematical statement of this topological impossibility.

Even in resistive MHD, where frozen-in breaks down, helicity decays much more slowly than magnetic energy. Energy cascades to small scales and dissipates; helicity is more "rugged," surviving the turbulent cascade. This has profound consequences for the relaxation of magnetic fields in stars and in laboratory plasmas.

You might ask: why should we care about such an abstract quantity? Because helicity constrains how magnetic fields can evolve. A field with nonzero helicity cannot decay to zero—it must retain some structure. When a twisted coronal loop flares, releasing magnetic energy, the helicity is approximately conserved; this constrains what final states are accessible. We will see helicity again in Chapter 11 (reconnection) and Chapter 13 (dynamos), where it plays a central role.

3.6 *Compression and the B/ρ Invariant*

So far we have considered incompressible flows. What happens when the fluid compresses?

Consider a fluid element with density ρ and magnetic field $\mathbf{B}$ parallel to some direction. If the fluid compresses perpendicular to the field—squeezing the field lines closer together—the field strength increases. But so does the density.

The frozen-in constraint implies that for motions perpendicular to $\mathbf{B}$, the ratio B/ρ is conserved:[3]

$$\frac{d}{dt}\left(\frac{B}{\rho}\right) = 0.$$

[3] More precisely, (B/ρ) is constant following a fluid element for one-dimensional compression perpendicular to $\mathbf{B}$. The full statement involves the component of $\mathbf{B}/\rho$ along the direction of motion.

This makes physical sense. If you squeeze a bundle of field lines into a smaller volume, both the number of field lines per unit area (the field strength B) and the mass per unit volume (the density ρ) increase in the same proportion.

You might ask: what if the flow is compressible but the compression is along the field lines? Then the density changes but the field does not—the field lines are not being squeezed closer together, just

shortened. The frozen-in constraint still holds, but the relationship between B and ρ is different.

3.7 A Worked Example: The Z-Pinch

Let us see frozen-in flux in a laboratory context: the Z-pinch.

A Z-pinch is a cylinder of plasma with a large current flowing axially (in the z-direction). The current creates an azimuthal magnetic field B_ϕ that wraps around the plasma column. This field exerts an inward pressure on the plasma, pinching it radially.

Suppose the plasma also has an axial magnetic field $B_{z,0}$ initially. The initial radius is $R_0 = 1$ cm, and the pinch compresses the plasma to $R_1 = R_0/3 \approx 3$ mm.

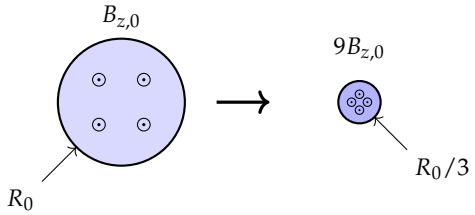

Figure 3.3: Z-pinch compression: reducing the radius by a factor of 3 increases the axial field by a factor of 9.

What happens to the axial field?

The axial flux must be conserved (frozen-in):

$$B_{z,0} \times \pi R_0^2 = B_{z,1} \times \pi R_1^2.$$

Therefore:

$$B_{z,1} = B_{z,0} \times \left(\frac{R_0}{R_1}\right)^2 = B_{z,0} \times 9 = 9B_{z,0}.$$

If $B_{z,0} = 0.1$ T initially, the compressed field is $B_{z,1} = 0.9$ T. The field increased by a factor of nine—the square of the compression ratio.

Let us check the energy. The magnetic energy in the axial field goes as $B_z^2 \times$ volume. The volume decreases as R^2, so:

$$\frac{U_1}{U_0} = \frac{B_{z,1}^2 \times R_1^2}{B_{z,0}^2 \times R_0^2} = \frac{81B_{z,0}^2 \times R_0^2/9}{B_{z,0}^2 \times R_0^2} = 9.$$

The magnetic energy increased ninefold. That energy came from the work done by the azimuthal field compressing the plasma—mechanical work converted to magnetic energy. This is one way Z-pinches can achieve intense magnetic fields and high temperatures.

3.8 Historical Note: The Frozen-In Controversy

When Hannes Alfvén proposed the frozen-in concept in the 1940s, it was not immediately embraced. Many physicists, trained to think of magnetic field lines as mathematical conveniences—contours of a potential, perhaps, or solutions to differential equations—were uncomfortable with the idea that these abstract curves could behave like material objects.

Sydney Chapman, the leading figure in geomagnetism, was particularly skeptical. For him, the global structure of Earth's magnetic

field was captured by spherical harmonic expansions, not by tracking individual field lines through a moving medium. The frozen-in picture seemed too mechanical, too literal.

Alfvén's genius was to recognize that in a perfect conductor, field lines *do* have a kind of material identity. You can track them, watch them evolve, see cause and effect as fluid motions stretch and twist the field. The picture is not merely a visualization aid; it captures the dynamics.

In later writings, Alfvén both celebrated and cautioned about frozen-in flux. The concept had proven enormously fruitful for space physics and astrophysics. But Alfvén worried that people took it too literally, forgetting that it is an approximation. In a 1976 paper, he wrote: "The concept of frozen-in field lines may be useful for pedagogical purposes... [but] in many cases its physical relevance is doubtful, and sometimes it is definitely misleading." The warning was characteristically blunt: frozen-in is a tool, not a truth.

We will heed his warning. Frozen-in is a powerful intuition, but it has limits. Knowing those limits is as important as knowing the theorem itself.

3.9 *When Frozen-In Fails*

The frozen-in theorem requires perfect conductivity: $\eta = 0$. Real materials have finite resistivity, so frozen-in is always an approximation. When does the approximation fail?

Recall the magnetic Reynolds number:

$$R_{\mathrm{m}} = \frac{vL}{\lambda},$$

where $\lambda = \eta/\mu_0$ is the magnetic diffusivity. When $R_{\mathrm{m}} \gg 1$, advection dominates and the field is effectively frozen in. When $R_{\mathrm{m}} \lesssim 1$, diffusion competes with advection, and the field can slip through the fluid.

But there is a subtlety. Even when the global R_{m} is enormous, the *local* R_{m} can be small if gradients are steep. If the field develops structure on scale $\ell \ll L$, then the relevant Reynolds number is $R_{\mathrm{m}\ell} = v\ell/\lambda$, which may be order unity even when $vL/\lambda \gg 1$.

This is exactly what happens in magnetic reconnection. The global field configuration has $R_{\mathrm{m}} \sim 10^{10}$ or more, but the field is forced into thin current sheets where ℓ becomes small enough that diffusion matters. In these sheets, field lines can slip through the plasma, break, and reconnect. The result is a topological change—linked field lines become unlinked—forbidden by ideal MHD but permitted when resistivity locally dominates.

You might ask: doesn't this mean frozen-in is useless, since it always fails somewhere? Not at all. Frozen-in controls the global evolution of the field. Reconnection events are localized in space and time. The overall topology changes slowly, punctuated by rapid reconnection episodes. Understanding MHD means understanding both the frozen-in evolution and the reconnection events that interrupt it.

3.10 Looking Ahead

We have established that magnetic field lines in ideal MHD behave like elastic threads frozen into the conducting fluid. Stretch the fluid, and the field amplifies. Compress it perpendicular to the field, and the field intensifies. Twist it, and the field twists. Topology is preserved—knots remain knotted, links remain linked.

But we have been vague about the forces involved. We said the field "resists" stretching, like a rubber band. But what is the actual force? How does it enter the momentum equation?

Magnetic fields exert two kinds of forces on conducting fluids: pressure and tension. Understanding these forces—their magnitude, their direction, their effect on fluid motion—is essential for intuition about MHD equilibria, waves, and instabilities. That mechanical picture is the subject of the next chapter.

4
Magnetic Pressure and Tension

4.1 The Rubber Band and the Balloon

Put your hands on opposite sides of a balloon and squeeze. The air inside pushes back equally in all directions—that is pressure. Now take a rubber band and stretch it between your fingers. It pulls along its length, trying to contract, but it does not push sideways—that is tension.

Magnetic fields do both.

A magnetic field exerts a pressure $B^2/(2\mu_0)$ perpendicular to itself, pushing field lines apart. And it exerts a tension B^2/μ_0 along itself, trying to shorten field lines like stretched rubber bands. This dual character is not a metaphor or an approximation. It is an exact rewriting of the Lorentz force $\mathbf{J} \times \mathbf{B}$ in terms of the Maxwell stress tensor.

This mechanical picture transforms how we think about MHD. Want to confine a plasma? You need magnetic pressure to balance gas pressure. Want to understand why sunspot umbrae are dark? Magnetic pressure suppresses convection. Want to know how Alfvén waves propagate? Magnetic tension provides the restoring force.

The rubber band will become our workhorse analogy. We will use it to understand waves in Chapter 5, the kink instability in Chapter 8, and the magnetorotational instability in Chapter 10. Master it now, and the rest of MHD becomes far more intuitive.

4.2 Pressure Balance in a Solar Flux Tube

Let us see magnetic pressure in action with a concrete example: a vertical magnetic flux tube in the solar photosphere.

Inside the tube there is a strong magnetic field B and a gas pressure p_i. Outside there is no field (or a much weaker one) and a higher gas pressure p_e. At the boundary, total pressure must balance:

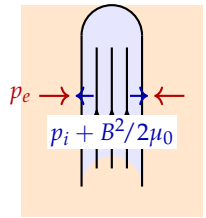

Figure 4.1: Pressure balance at a flux tube boundary: external gas pressure equals internal gas pressure plus magnetic pressure.

$$p_i + \frac{B^2}{2\mu_0} = p_e. \tag{4.1}$$

The magnetic pressure $B^2/(2\mu_0)$ supplements the internal gas pressure. This is why the gas pressure inside a flux tube is lower than outside—the magnetic field "makes up the difference."

Let us put in numbers for the solar photosphere. The external gas pressure is approximately $p_e \approx 1.2 \times 10^4$ Pa, about 0.12 atmospheres. A typical photospheric flux tube has a field strength $B \approx 0.15$ T (1500 gauss). The magnetic pressure is

$$\frac{B^2}{2\mu_0} = \frac{(0.15)^2}{2 \times 4\pi \times 10^{-7}} \approx 9000 \text{ Pa}.$$

From the pressure balance equation (4.1):

$$p_i \approx 12000 - 9000 = 3000 \text{ Pa}.$$

The internal gas pressure is only about 25% of external. Using the ideal gas law $p = \rho k_B T/m$ with roughly equal temperatures inside and outside, this means the internal density is also about 25% of external.

Lower density means lower opacity. We see deeper into the Sun inside the flux tube than outside. Since deeper means hotter, flux tubes appear bright—they are the "faculae" and "plage" that make the Sun slightly brighter during periods of high magnetic activity.

You might ask: if lower density makes flux tubes bright, why are sunspots dark? The answer is that sunspots have much stronger fields, $B \approx 0.2$–0.3 T, and the field is strong enough to suppress convection entirely. Without convective heat transport, the sunspot interior cools. The magnetic pressure still works the same way—it still reduces the internal gas pressure and density—but now the temperature is also lower, and lower temperature wins: sunspots are dark.

4.3 The Lorentz Force Decomposed

Now let us derive the pressure-tension picture rigorously. The magnetic force per unit volume on a current-carrying fluid is the Lorentz force:

$$\mathbf{f} = \mathbf{J} \times \mathbf{B}. \tag{4.2}$$

Using Ampère's law $\mathbf{J} = (1/\mu_0)\nabla \times \mathbf{B}$:

$$\mathbf{f} = \frac{1}{\mu_0}(\nabla \times \mathbf{B}) \times \mathbf{B}.$$

There is a standard vector identity:[1]

[1] This identity can be verified by writing out components, but it is worth memorizing: the cross product of a curl with itself gives a gradient minus a directional derivative.

$$(\nabla \times \mathbf{B}) \times \mathbf{B} = (\mathbf{B} \cdot \nabla)\mathbf{B} - \nabla\left(\frac{B^2}{2}\right).$$

Therefore:

$$\mathbf{f} = \frac{1}{\mu_0}(\mathbf{B} \cdot \nabla)\mathbf{B} - \nabla\left(\frac{B^2}{2\mu_0}\right). \tag{4.3}$$

The two terms have distinct physical meanings.

Magnetic Pressure

The second term, $-\nabla(B^2/2\mu_0)$, is the gradient of a scalar quantity. It acts exactly like a pressure gradient. The "magnetic pressure" is

$$p_B = \frac{B^2}{2\mu_0}. \tag{4.4}$$

This pressure pushes from regions of strong field to regions of weak field, perpendicular to the field lines. It is isotropic in the plane perpendicular to $\mathbf{B}$—it pushes equally in all directions within that plane.

For the solar photosphere example, with $B = 0.15$ T, we computed $p_B \approx 9000$ Pa. For comparison, atmospheric pressure at sea level is about 10^5 Pa, so the magnetic pressure in a sunspot is roughly 10% of atmospheric. Not huge, but comparable to the gas pressure in the solar photosphere.

Magnetic Tension

The first term, $(1/\mu_0)(\mathbf{B} \cdot \nabla)\mathbf{B}$, is more subtle. The operator $\mathbf{B} \cdot \nabla$ is a directional derivative along the field line. It measures how $\mathbf{B}$ changes as you move along the field.

Let us write $\mathbf{B} = B\hat{\mathbf{b}}$, where $B = |\mathbf{B}|$ is the magnitude and $\hat{\mathbf{b}}$ is the unit vector along the field. Then:

$$(\mathbf{B} \cdot \nabla)\mathbf{B} = B(\hat{\mathbf{b}} \cdot \nabla)(B\hat{\mathbf{b}}) = B\frac{\partial B}{\partial s}\hat{\mathbf{b}} + B^2(\hat{\mathbf{b}} \cdot \nabla)\hat{\mathbf{b}},$$

where $\partial/\partial s$ denotes the derivative along the field line.

The second part involves $(\hat{\mathbf{b}} \cdot \nabla)\hat{\mathbf{b}}$. For a unit vector, this is the curvature vector:

$$(\hat{\mathbf{b}} \cdot \nabla)\hat{\mathbf{b}} = \frac{\hat{\mathbf{n}}}{R},$$

where $\hat{\mathbf{n}}$ is the principal normal (pointing toward the center of curvature) and R is the radius of curvature.

Therefore the tension contribution to the force is:

$$\mathbf{f}_{\text{tension}} = \frac{B^2}{\mu_0 R}\hat{\mathbf{n}}. \tag{4.5}$$

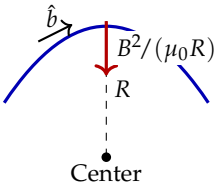

Figure 4.2: Magnetic tension: a curved field line exerts a force toward its center of curvature, with magnitude $B^2/(\mu_0 R)$.

This is exactly like the tension in a stretched string. A taut string under tension T, curved with radius R, exerts a restoring force per unit length T/R toward the center of curvature. For magnetic field lines, the "tension per unit area" is B^2/μ_0.

You might ask: why is the tension B^2/μ_0 but the pressure only $B^2/(2\mu_0)$? This asymmetry has a simple origin. Consider a field $\mathbf{B}$ pointing in the z-direction. The stress tensor (which we will meet shortly) has components $-B^2/(2\mu_0)$ in the x and y directions (pressure) but $+B^2/(2\mu_0)$ in the z direction. The tension force on a curved field line involves the change in this z-component as the direction changes, and the geometry gives an extra factor of 2.

4.4 *The Maxwell Stress Tensor*

The magnetic force can be written more elegantly as the divergence of a stress tensor. Define:[2]

$$T_{ij} = \frac{1}{\mu_0}\left(B_i B_j - \frac{B^2}{2}\delta_{ij}\right). \tag{4.6}$$

[2] The negative sign in front of the $B^2\delta_{ij}/2$ term is crucial. It ensures that the magnetic force is compressive (like pressure) in directions perpendicular to $\mathbf{B}$.

Then the force per unit volume is

$$f_i = \frac{\partial T_{ij}}{\partial x_j}.$$

To see what this tensor means, consider a field pointing in the z-direction: $\mathbf{B} = B\hat{\mathbf{z}}$. The stress tensor becomes

$$T = \frac{1}{\mu_0}\begin{pmatrix} -B^2/2 & 0 & 0 \\ 0 & -B^2/2 & 0 \\ 0 & 0 & +B^2/2 \end{pmatrix}.$$

The diagonal elements tell the story:

- $T_{xx} = T_{yy} = -B^2/(2\mu_0)$: negative stress (compression/pressure) perpendicular to $\mathbf{B}$
- $T_{zz} = +B^2/(2\mu_0)$: positive stress (tension) along $\mathbf{B}$

The magnetic field pushes outward perpendicular to itself and pulls inward along itself. This is precisely the balloon-and-rubber-band picture we started with.

You might ask: is this "real" stress, like the stress in a steel beam? Yes. You can integrate the Maxwell stress tensor over any closed surface to get the total electromagnetic force on the enclosed volume. If you build a box around a current-carrying wire in a magnetic field, the stress tensor correctly computes the force on the wire. The magnetic field transmits force through empty space via this stress.

4.5 The Plasma Beta

The ratio of gas pressure to magnetic pressure appears constantly in MHD. It has a name: the plasma beta.

$$\beta \equiv \frac{p}{B^2/(2\mu_0)} = \frac{2\mu_0 p}{B^2}. \tag{4.7}$$

This parameter tells you who is winning the tug-of-war between gas and field:

- $\beta \gg 1$: gas pressure dominates. The magnetic field is "weak"—it gets pushed around by the gas.
- $\beta \ll 1$: magnetic pressure dominates. The field is "strong"—the gas must conform to magnetic geometry.
- $\beta \sim 1$: equipartition. Neither dominates; they negotiate as equals.

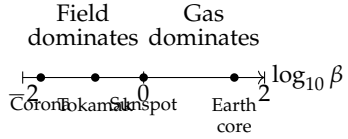

Figure 4.3: The plasma beta in various environments. The most interesting MHD physics often happens near $\beta \sim 1$.

Let us compute β for some astrophysical and laboratory plasmas.

Solar corona: $B \sim 0.01$ T, $n_e \sim 10^{15}$ m^{-3}, $T \sim 10^6$ K. Gas pressure $p = 2n_e k_B T \approx 0.03$ Pa. Magnetic pressure $B^2/(2\mu_0) \approx 40$ Pa. Therefore $\beta \approx 0.001$. The corona is magnetically dominated—plasma flows along field lines like cars on a highway, with no freedom to cross.

Tokamak: $B \sim 5$ T, $n_e \sim 10^{20}$ m^{-3}, $T \sim 10^8$ K (10 keV). Gas pressure $p \approx 3 \times 10^5$ Pa. Magnetic pressure $B^2/(2\mu_0) \approx 10^7$ Pa. Therefore $\beta \approx 0.03$. Achieving higher β is a major goal of fusion research—it means confining more plasma with the same magnet.

Earth's outer core: $B \sim 3 \times 10^{-4}$ T (at the core-mantle boundary), $\rho \sim 10^4$ kg/m^3, pressure $p \sim 10^{11}$ Pa. Magnetic pressure $B^2/(2\mu_0) \approx 0.04$ Pa. Therefore $\beta \sim 10^{12}$. The field is utterly negligible for the pressure balance—the core's structure is determined by gravity and rotation, not magnetism. Yet this tiny field is what gives Earth its magnetic field!

You might ask: if the core's field is so weak, how does it matter at all? The answer is that β measures pressure balance, not dynamical importance. Even a weak field can affect fluid motions through the Lorentz force, especially on large scales and long times. The geodynamo operates in the $\beta \gg 1$ regime, yet it works.

4.6 Force-Free Fields

There is a special class of magnetic configurations in which the Lorentz force vanishes entirely: $\mathbf{J} \times \mathbf{B} = 0$. These are called force-free fields.

For $\mathbf{J} \times \mathbf{B} = 0$, the current must be parallel to the field: $\mathbf{J} = \alpha \mathbf{B}$ for some scalar α. Using Ampère's law:

$$\nabla \times \mathbf{B} = \mu_0 \mathbf{J} = \mu_0 \alpha \mathbf{B}. \tag{4.8}$$

This is an eigenvalue equation for the curl operator.[3]

Three important cases:

1. $\alpha = 0$: current-free or "potential" field. Then $\nabla \times \mathbf{B} = 0$, so $\mathbf{B} = -\nabla \psi$ for some scalar potential, and $\nabla^2 \psi = 0$ (Laplace's equation).

2. $\alpha =$ constant: linear force-free field. The equation $\nabla \times \mathbf{B} = \alpha \mathbf{B}$ has analytical solutions.

3. $\alpha = \alpha(\mathbf{x})$: nonlinear force-free field. Much harder to solve; requires numerical methods.

[3] The solutions are called "Beltrami fields" in the mathematical literature. They have remarkable topological properties—the field lines can be knotted and linked in complex ways.

Force-free fields are excellent models for the solar corona, where $\beta \ll 1$. The gas pressure is negligible, so there is no pressure gradient to balance the Lorentz force. The only way the magnetic field can be in equilibrium is if the Lorentz force is zero.

A Worked Example: The Coronal Arcade

Consider a simple model of magnetic loops in the solar corona. The photospheric magnetic field varies sinusoidally: $B_z(x, z = 0) = B_0 \sin(kx)$, representing alternating magnetic polarities on the solar surface.

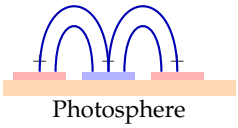

Figure 4.4: A potential-field arcade: field lines arch from positive (red) to negative (blue) polarity regions on the solar surface.

For a potential field ($\alpha = 0$), we solve $\nabla^2 \psi = 0$ with the boundary condition $\partial \psi / \partial z = -B_0 \sin(kx)$ at $z = 0$, and requiring the field to decay as $z \to \infty$. The solution is:

$$\psi = \frac{B_0}{k} \sin(kx) e^{-kz},$$

giving field components

$$B_x = -\frac{\partial \psi}{\partial x} = -B_0 \cos(kx) e^{-kz}, \quad B_z = -\frac{\partial \psi}{\partial z} = B_0 \sin(kx) e^{-kz}.$$

The field lines are the curves $\psi =$ constant, which form arched loops connecting regions of opposite polarity. The height of the arcade is set by the wavelength: loops with wavelength $\lambda = 2\pi/k$ rise to heights of order λ.

This is a current-free solution. Adding twist to the field lines—having $\alpha \neq 0$—changes the arcade shape. More twisted fields (larger $|\alpha|$) have lower-lying loops. This makes physical sense: the tension in twisted field lines pulls them down, while potential fields maximize their height.

4.7 Historical Note: Maxwell's Mechanical Universe

The Maxwell stress tensor carries his name because Maxwell himself introduced it in 1861. But for Maxwell, it was not merely a mathematical convenience. He believed it described real mechanical stresses in a physical medium—the luminiferous aether.

Maxwell imagined space filled with rotating molecular vortices, and the magnetic field as the rotation of these vortices. Neighboring vortices rotating in the same direction would push apart (like two meshing gears trying to turn the same way), creating magnetic pressure. The stress tensor emerged naturally from this mechanical picture.

We have long since abandoned the aether. There is no medium, no vortices, no gears. Yet the stress tensor survives intact. You can still use it to compute the force on any current-carrying conductor—the mathematics does not care whether the aether exists.

This is a common pattern in physics: a model may be wrong, but if it predicts correctly, the mathematical structures often survive. Maxwell's "wrong" model gave us the "right" stress tensor. One wonders how many of our current models will suffer the same fate—correct predictions emerging from incorrect ontology, with the mathematics outliving the physical picture that birthed it.

4.8 Why Sunspots Are Dark

Let us return to sunspots with our new tools. A sunspot is a region of intense magnetic field, $B \approx 0.2$–0.3 T, much stronger than the surrounding photosphere where $B \approx 0.01$ T or less.

The magnetic pressure in a sunspot is

$$p_B = \frac{B^2}{2\mu_0} \approx \frac{(0.25)^2}{2 \times 4\pi \times 10^{-7}} \approx 25000 \text{ Pa}.$$

This is larger than the external gas pressure (~ 12000 Pa), which seems paradoxical. How can the sunspot be in pressure balance?

The answer involves depth. The pressure balance condition $p_i + B^2/(2\mu_0) = p_e$ holds at each depth, but the external gas pressure increases rapidly with depth in the solar atmosphere. The sunspot field spreads out (becomes weaker and occupies more area) with depth, so the magnetic pressure decreases. At some depth, p_B and p_e become comparable, and below that depth, the flux tube maintains equilibrium.

At the visible surface, the sunspot interior has much lower gas pressure and density than the surroundings. But here is the crucial point: the sunspot is also cooler.

You might ask: why is it cooler? Because the magnetic field suppresses convection. Convection requires fluid elements to move across field lines, but with $\beta \ll 1$ in the sunspot interior, cross-field motion is strongly inhibited. Heat that would normally be carried upward by convection is blocked. The sunspot interior cools.

The effective temperature of a sunspot umbra is about 4000 K, compared to 5800 K in the surrounding photosphere. By the Stefan-Boltzmann law, the radiative flux goes as T^4, so the sunspot radiates

$$\frac{F_{\text{spot}}}{F_{\text{phot}}} = \left(\frac{4000}{5800}\right)^4 \approx 0.23.$$

The sunspot emits only about 23% as much light as its surroundings. It appears dark—not because it emits no light (a sunspot would outshine the full Moon if seen in isolation), but because the contrast with the surrounding photosphere is so stark.

This example shows how pressure and tension combine with the frozen-in constraint and energy transport to create observable phenomena. The magnetic field does not merely sit there; it actively shapes the thermal structure of the Sun.

4.9 Looking Ahead

We have established the mechanical picture of magnetic fields: pressure perpendicular to the field, tension along it. This picture becomes dynamical when we ask what happens when the field is perturbed.

Pluck a rubber band and it vibrates. The tension provides a restoring force; the mass provides inertia; together they produce oscillations. Magnetic field lines do the same thing. Perturb them, and they vibrate—these are Alfvén waves, carried by magnetic tension at the Alfvén speed $v_A = B/\sqrt{\mu_0 \rho}$.

But magnetic pressure can also propagate disturbances, combining with gas pressure to create magnetosonic waves. The full story of MHD waves—their speeds, polarizations, and physical character—is the subject of the next chapter.

5
Waves in a Magnetized Fluid

5.1 The Plucked String

Pluck a guitar string and it vibrates. The tension in the string provides the restoring force; the string's mass provides the inertia. Together, they set the oscillation frequency and the wave speed: $v = \sqrt{T/\mu}$, where T is the tension and μ is the mass per unit length.

Now imagine the string is made of plasma, and the tension comes from a magnetic field. We learned in the last chapter that magnetic field lines act like rubber bands under tension B^2/μ_0. If we "pluck" the field—displace a parcel of plasma perpendicular to the field direction—magnetic tension will try to restore it. But the plasma has inertia. The result is oscillation: the field line swings back and forth, and this disturbance propagates along the field.

This is an Alfvén wave, the signature oscillation of magnetohydrodynamics.

But that is not all. A magnetized plasma supports two additional wave modes: the fast and slow magnetosonic waves. These mix magnetic pressure with gas pressure, and their speeds depend on the angle of propagation relative to the field. Together, the three modes form a complete picture of how disturbances travel through a conducting fluid.

Understanding these waves is essential for everything from coronal heating to fusion plasma diagnostics to interstellar turbulence. And there is something remarkable about their discovery: Alfvén waves were predicted theoretically in 1942, in wartime Sweden, before anyone had seen them in a laboratory. Hannes Alfvén imagined them into existence by taking the frozen-in picture seriously.

5.2 The Alfvén Speed

Let us derive the wave speed by the simplest possible argument: dimensional analysis combined with physical intuition.

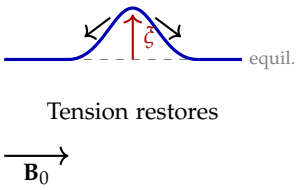

Figure 5.1: A kinked field line. Displacement ξ bends the line; magnetic tension pulls from both sides to straighten it.

Consider a uniform magnetic field $\mathbf{B}_0$ threading a conducting fluid of density ρ. Displace a fluid element perpendicular to the field. The field line bends, creating a kink. Magnetic tension—acting like the tension in a stretched string—tries to straighten the kink. But the fluid element has mass, so it overshoots. The result is oscillation.

For a string, the wave speed is $v = \sqrt{T/\mu}$, where T is tension (force) and μ is mass per unit length. For a magnetized plasma, the analogous quantities are:

- Tension per unit area: B_0^2/μ_0 (units: Pa = $\mathrm{N/m^2}$)
- Mass per unit volume: ρ (units: $\mathrm{kg/m^3}$)

The ratio has units of (velocity)^2:

$$\frac{B_0^2/\mu_0}{\rho} = \frac{B_0^2}{\mu_0 \rho} \quad [\mathrm{m^2/s^2}].$$

Taking the square root gives the Alfvén speed:

$$v_A = \frac{B_0}{\sqrt{\mu_0 \rho}}. \tag{5.1}$$

This is the characteristic velocity of MHD, as fundamental to magnetized plasmas as the speed of sound is to ordinary gases.

Numerical Examples

Let us compute v_A for some important environments.

Solar corona: $B \sim 10^{-3}$ T (10 gauss), $\rho \sim 10^{-12}$ $\mathrm{kg/m^3}$ (corresponding to $n_e \sim 10^{15}$ $\mathrm{m^{-3}}$). Then:

$$v_A = \frac{10^{-3}}{\sqrt{4\pi \times 10^{-7} \times 10^{-12}}} \approx \frac{10^{-3}}{1.1 \times 10^{-9}} \approx 900 \text{ km/s}.$$

Alfvén waves in the corona are fast—comparable to the solar wind speed. They can carry significant energy from the photosphere into the corona.

Tokamak fusion plasma: $B \sim 5$ T, deuterium density $n \sim 10^{20}$ $\mathrm{m^{-3}}$, giving $\rho \sim 3 \times 10^{-7}$ $\mathrm{kg/m^3}$. Then:

$$v_A = \frac{5}{\sqrt{4\pi \times 10^{-7} \times 3 \times 10^{-7}}} \approx 8 \times 10^6 \text{ m/s} \approx 3\%\, c.$$

The Alfvén speed in a tokamak is a significant fraction of the speed of light. This makes some relativistic corrections necessary for accurate wave physics.

Earth's outer core: $B \sim 3 \times 10^{-4}$ T, $\rho \sim 10^4$ $\mathrm{kg/m^3}$ (liquid iron). Then:

$$v_A = \frac{3 \times 10^{-4}}{\sqrt{4\pi \times 10^{-7} \times 10^4}} \approx \frac{3 \times 10^{-4}}{0.11} \approx 3 \text{ mm/s}.$$

Alfvén waves in Earth's core are glacially slow—comparable to the convective velocities that drive the geodynamo. This similarity of timescales is not a coincidence; it reflects the intimate coupling between flow and field in the dynamo process.

5.3 *Linearizing the MHD Equations*

Let us now derive the wave modes rigorously. We start with the ideal MHD equations:

$$\frac{\partial \rho}{\partial t} + \nabla \cdot (\rho \mathbf{v}) = 0, \tag{5.2}$$

$$\rho \frac{D\mathbf{v}}{Dt} = -\nabla p + \frac{1}{\mu_0}(\nabla \times \mathbf{B}) \times \mathbf{B}, \tag{5.3}$$

$$\frac{\partial \mathbf{B}}{\partial t} = \nabla \times (\mathbf{v} \times \mathbf{B}), \tag{5.4}$$

$$p = p(\rho), \quad c_s^2 = \frac{dp}{d\rho}, \tag{5.5}$$

where c_s is the sound speed, defined in Chapter 2.

Consider a uniform equilibrium: $\mathbf{B} = \mathbf{B}_0 = B_0\hat{\mathbf{z}}$, $\rho = \rho_0$, $p = p_0$, $\mathbf{v} = 0$. Now perturb this equilibrium:

$$\mathbf{B} = \mathbf{B}_0 + \mathbf{b}, \tag{5.6}$$

$$\rho = \rho_0 + \rho_1, \tag{5.7}$$

$$p = p_0 + p_1, \tag{5.8}$$

$$\mathbf{v} = \mathbf{v}_1, \tag{5.9}$$

where the perturbations are small: $|\mathbf{b}| \ll B_0$, etc.

Substituting into the MHD equations and keeping only first-order terms, we get the linearized equations:[1]

$$\frac{\partial \rho_1}{\partial t} + \rho_0 \nabla \cdot \mathbf{v}_1 = 0, \tag{5.10}$$

$$\rho_0 \frac{\partial \mathbf{v}_1}{\partial t} = -c_s^2 \nabla \rho_1 + \frac{1}{\mu_0}(\nabla \times \mathbf{b}) \times \mathbf{B}_0, \tag{5.11}$$

$$\frac{\partial \mathbf{b}}{\partial t} = \nabla \times (\mathbf{v}_1 \times \mathbf{B}_0). \tag{5.12}$$

[1] The linearization discards products of small quantities like $\mathbf{v}_1 \cdot \nabla \mathbf{v}_1$ or $\rho_1 \mathbf{v}_1$. This is valid when the perturbations are small compared to equilibrium values.

5.4 *Plane Wave Solutions*

Assume plane wave solutions where all perturbations vary as $\exp[i(\mathbf{k} \cdot \mathbf{r} - \omega t)]$. This replaces $\partial/\partial t \to -i\omega$ and $\nabla \to i\mathbf{k}$.

Let us choose coordinates so that $\mathbf{B}_0 = B_0\hat{\mathbf{z}}$ and $\mathbf{k}$ lies in the x-z plane at angle θ to $\mathbf{B}_0$:

$$\mathbf{k} = k(\sin\theta\,\hat{\mathbf{x}} + \cos\theta\,\hat{\mathbf{z}}).$$

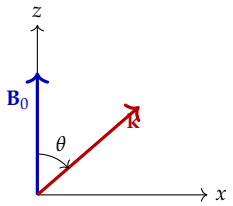

Figure 5.2: Geometry of wave propagation. The wavevector $\mathbf{k}$ makes angle θ with the background field $\mathbf{B}_0$.

The linearized equations become algebraic:

$$\omega \rho_1 = \rho_0 \mathbf{k} \cdot \mathbf{v}_1, \tag{5.13}$$

$$\omega \rho_0 \mathbf{v}_1 = c_s^2 \rho_1 \mathbf{k} - \frac{1}{\mu_0}(\mathbf{k} \times \mathbf{b}) \times \mathbf{B}_0, \tag{5.14}$$

$$\omega \mathbf{b} = -\mathbf{k} \times (\mathbf{v}_1 \times \mathbf{B}_0). \tag{5.15}$$

After substantial algebra—which we will not inflict upon you in full, though it is a worthwhile exercise—the dispersion relation emerges:[2]

$$\left(\omega^2 - k^2 v_A^2 \cos^2\theta\right)\left[\omega^4 - \omega^2 k^2 (v_A^2 + c_s^2) + k^4 v_A^2 c_s^2 \cos^2\theta\right] = 0. \tag{5.16}$$

This factors into three modes.

[2] The key steps involve eliminating ρ_1 and $\mathbf{b}$ in favor of $\mathbf{v}_1$, obtaining a matrix equation, and requiring the determinant to vanish for nontrivial solutions.

5.5 *The Three MHD Wave Modes*

The Alfvén Wave

The first factor in (5.16) gives:

$$\omega^2 = k^2 v_A^2 \cos^2\theta. \tag{5.17}$$

The phase velocity is:

$$v_{\text{ph}} = \frac{\omega}{k} = v_A |\cos\theta|.$$

This is the Alfvén wave. Its properties:

- The wave propagates fastest along the field ($\theta = 0$), with $v_{\text{ph}} = v_A$.
- At $\theta = 90$ (perpendicular to $\mathbf{B}_0$), the phase velocity is zero. Alfvén waves cannot propagate perpendicular to the field.
- The velocity perturbation $\mathbf{v}_1$ is perpendicular to both $\mathbf{k}$ and $\mathbf{B}_0$—it points in the y-direction in our coordinate system.
- The wave is transverse and incompressible: $\nabla \cdot \mathbf{v}_1 = 0$, so there is no density perturbation.

You might ask: if Alfvén waves don't compress the plasma, what do they do? They shake the field lines sideways. Imagine wiggling a garden hose—the hose itself moves, but the water inside doesn't compress. Similarly, Alfvén waves displace field lines without changing the magnetic field strength or the plasma density.

The group velocity of the Alfvén wave is particularly interesting. Since $\omega = k v_A \cos\theta$, we have:

$$\mathbf{v}_g = \nabla_{\mathbf{k}} \omega = v_A \hat{\mathbf{z}} = v_A \hat{\mathbf{b}}_0.$$

The group velocity points along the background field, regardless of the direction of $\mathbf{k}$. Energy in Alfvén waves travels strictly along field lines. This is the mathematical statement of the "plucked string" picture: disturbances propagate along the string, not perpendicular to it.

The Fast and Slow Magnetosonic Waves

The second factor in (5.16) gives a quadratic in ω^2:

$$\omega^4 - \omega^2 k^2 (v_A^2 + c_s^2) + k^4 v_A^2 c_s^2 \cos^2\theta = 0. \tag{5.18}$$

Solving for the phase velocity:

$$v_{\text{ph}}^2 = \frac{1}{2}\left[(v_A^2 + c_s^2) \pm \sqrt{(v_A^2 + c_s^2)^2 - 4 v_A^2 c_s^2 \cos^2\theta}\right]. \tag{5.19}$$

The $+$ sign gives the *fast magnetosonic wave*; the $-$ sign gives the *slow magnetosonic wave*. Unlike the Alfvén wave, these modes involve compression of both the plasma and the magnetic field.

Along the field ($\theta = 0$):

$$v_{\text{fast}} = \max(v_A, c_s), \quad v_{\text{slow}} = \min(v_A, c_s).$$

One mode propagates at the Alfvén speed, the other at the sound speed. Which is which depends on whether $v_A > c_s$ (low β) or $v_A < c_s$ (high β).

Perpendicular to the field ($\theta = 90$):

$$v_{\text{fast}} = \sqrt{v_A^2 + c_s^2}, \quad v_{\text{slow}} = 0.$$

The fast wave combines magnetic and gas pressure, propagating faster than either alone. The slow wave cannot propagate perpendicular to the field—like the Alfvén wave, it is "guided" by the field lines.

You might ask: what happens at intermediate angles? The waves interpolate smoothly between these limits. A useful mnemonic: at any angle, $v_{\text{slow}} \leq v_{\text{Alfvén}} \leq v_{\text{fast}}$. The three speeds are nested, with the Alfvén wave always between the magnetosonic pair.

5.6 The Friedrichs Diagram

The angular dependence of the wave speeds is best visualized with a *Friedrichs diagram*: a polar plot of phase velocity versus propagation angle.

In this diagram, the radial distance from the origin at angle θ represents the phase velocity for propagation at that angle to $\mathbf{B}_0$. For the typical case $v_A > c_s$ (low β plasma):

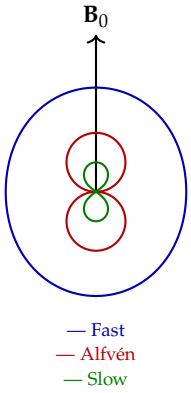

Figure 5.3: Friedrichs diagram for $v_A > c_s$. The radial distance from the origin is the phase velocity at that angle relative to $\mathbf{B}_0$.

- The **fast wave** forms the outermost curve, roughly elliptical.
- The **Alfvén wave** forms a figure-eight that touches the origin at $\theta = 90$.
- The **slow wave** forms the innermost curve, also touching the origin at $\theta = 90$.

When $v_A < c_s$ (high β), the diagram changes: the fast wave is more nearly circular, and the slow wave shrinks. In the special case $v_A = c_s$ ($\beta = 1$, equipartition), the Alfvén and slow waves become degenerate along the field direction.

This single diagram communicates what pages of equations cannot: the three-dimensional structure of wave propagation in MHD. Any disturbance can be decomposed into these three modes, each carrying energy at its own speed and direction.

5.7 *A Worked Example: Wave Damping in the Solar Wind*

Alfvén waves have been observed in the solar wind since the 1960s. Spacecraft measurements show correlated fluctuations in $\mathbf{v}$ and $\mathbf{B}$, with the characteristic phase relationship $\delta\mathbf{v} \propto \pm\delta\mathbf{B}/\sqrt{\mu_0\rho}$—the $+$ sign for outward-propagating waves, the $-$ sign for inward.

But here is a puzzle: if Alfvén waves propagate without compression, they should not dissipate in ideal MHD. Yet the fluctuation amplitude decreases with distance from the Sun. Why?

Several mechanisms contribute:

1. **Geometric expansion**: As the solar wind expands, the wave amplitude scales with the background field strength. $B \propto r^{-2}$ for a radial field, so δB decreases even without dissipation.
2. **Nonlinear steepening**: Large-amplitude Alfvén waves can steepen into shocks or generate compressional waves at higher harmonics. These compressional components can dissipate.
3. **Parametric decay**: An Alfvén wave can decay into a backward-propagating Alfvén wave plus a slow magnetosonic wave. This cascades energy to smaller scales.
4. **Turbulent cascade**: Counterpropagating Alfvén waves interact nonlinearly, transferring energy to smaller scales where it eventually dissipates.

Let us estimate the expansion effect. At 1 AU, $B \sim 5$ nT and $\rho \sim 5 \times 10^{-21}$ kg/m^3, giving $v_A \approx 60$ km/s. At 0.3 AU (near Parker Solar Probe's closest approach), $B \sim 50$ nT and $\rho \sim 5 \times 10^{-20}$ kg/m^3 (scaling roughly as r^{-2}), giving $v_A \approx 200$ km/s.

The ratio of Alfvén speeds is $200/60 \approx 3$. Meanwhile, B decreases by a factor of 10 from 0.3 AU to 1 AU. If wave amplitude δB scales with the background field, this geometric dilution alone accounts for much of the observed decrease—without any true dissipation. Disentangling geometric expansion from actual energy loss is an active area of research.

5.8 Historical Note: Alfvén's Prediction

In 1942, Hannes Alfvén published a remarkable paper in *Nature* titled "Existence of Electromagnetic-Hydrodynamical Waves." The paper is barely a page long. Alfvén simply writes down the wave equation, solves it, and states the result:

> "If a conducting liquid is placed in a constant magnetic field, every small transverse disturbance of the liquid will be propagated along the lines of force with the velocity $v = H/\sqrt{4\pi\rho}$."

(Here H is the magnetic field in Gaussian units.)

The prediction was not immediately accepted. Some physicists argued that resistivity would damp the waves before they could propagate. Others were skeptical of the idealized "infinite conductivity" assumption.

The first laboratory confirmation came in 1949, when Stig Lundquist in Sweden detected oscillations in liquid mercury at roughly the predicted frequency. The experiments were difficult—mercury is a poor conductor, so the waves were strongly damped—but the frequency dependence on field strength and density matched Alfvén's formula.

Definitive confirmation came from space. In the 1960s, the Mariner spacecraft detected clear Alfvén wave signatures in the solar wind: correlated oscillations of velocity and magnetic field, propagating outward from the Sun at the local Alfvén speed.

Alfvén received the Nobel Prize in Physics in 1970 for "fundamental work and discoveries in magnetohydrodynamics." The prize citation specifically mentioned the discovery of the waves that bear his name.

You might ask: how did Alfvén know to look for such waves in the first place? His insight came from taking the frozen-in picture seriously. If field lines are like strings attached to the fluid, and if strings can vibrate, then so can field lines. The mathematics followed from the physical intuition—not the other way around. This is a lesson worth remembering: the best predictions often come from taking your physical pictures more seriously than you think you should.

5.9 Waves in Inhomogeneous Media

So far we have assumed a uniform equilibrium. Real plasmas have gradients in density, temperature, and magnetic field strength. What happens to MHD waves in such environments?

The short answer: they reflect, refract, and convert between modes. A fast wave encountering a density gradient can partially convert into a slow wave or Alfvén wave. An Alfvén wave reaching a region where v_A changes will partially reflect.

Consider Alfvén waves in the solar atmosphere. Near the photosphere, $v_A \sim 10$ km/s. In the corona, $v_A \sim 1000$ km/s. This hundredfold increase in Alfvén speed means that waves propagating upward encounter a strong gradient.

The reflection coefficient for a wave at an interface where v_A changes from v_1 to v_2 is approximately:

$$R \approx \left(\frac{v_2 - v_1}{v_2 + v_1} \right)^2 .$$

For $v_2/v_1 = 100$, this gives $R \approx 0.96$. Almost all the wave energy reflects! Only about 4% is transmitted into the corona.

This presents a problem for coronal heating models that rely on Alfvén wave dissipation. How do the waves get into the corona if they mostly reflect at the transition region? Part of the answer is that the transition is not sharp—it has structure on scales comparable to the wavelength, reducing the reflection. Part is that higher-frequency waves have shorter wavelengths and can "tunnel" through the gradient. The full answer involves sophisticated wave physics that remains an active research area.

5.10 Philosophical Interlude: Why Three Modes?

You might wonder: why exactly three wave modes? Why not two, or four, or infinitely many?

The answer lies in the symmetries of the system. Ideal MHD has three fundamental degrees of freedom: the magnetic field (constrained by $\nabla \cdot \mathbf{B} = 0$, leaving two independent components), the velocity (three components), and the density (one component, with pressure determined by the equation of state). But these are coupled by the equations of motion. The number of independent wave modes equals the number of degrees of freedom, which for MHD is three.

In full plasma physics (without the MHD approximations), there are many more modes: Langmuir waves, ion acoustic waves, whistler waves, ion cyclotron waves, and so on. The MHD approximation filters these out by assuming quasineutrality and low frequency.

What remains are the three modes that survive on large scales and slow timescales.

This is a general principle: the number of wave modes tells you about the effective degrees of freedom in your system. One mode (like ordinary sound in a gas) means one restoring mechanism. Three modes in MHD means the interplay of gas pressure, magnetic pressure, and magnetic tension, each providing different restoring forces at different angles.

5.11 Looking Ahead

We have learned how disturbances propagate in a magnetized fluid: Alfvén waves along field lines, fast waves in all directions, slow waves guided by the field. But propagation is only half the story. What about equilibrium? Can a magnetic field confine a plasma—hold it in place against its thermal pressure? And if equilibrium is achieved, is it stable?

These questions lead us to MHD equilibria and the confinement problem. The tension and pressure we have studied create forces; when those forces balance, the plasma sits still. But balanced forces are not always stable forces. A ball at the top of a hill is in equilibrium, but a small push sends it rolling. Magnetic confinement faces similar challenges, and understanding them is essential for fusion energy. That is the subject of the next chapter.

Part II

Instabilities and Dynamics

6
Equilibria and the Confinement Problem

6.1 The Dream and Its Difficulty

Imagine building a cage out of nothing but magnetic fields—invisible walls that push without touching, that hold a hundred million degrees without melting. No material wall could survive such temperatures; tungsten melts at 3700 K, and we need 100 million K. But magnetic fields are immune to heat. Wrap the plasma in a sufficiently clever field configuration, and you might have a miniature star in a bottle.

The trouble is, the cage keeps trying to fall apart.

Magnetic confinement of hot plasma is one of the hardest engineering challenges ever attempted. The difficulty is not merely practical—better materials, stronger magnets, more power. The difficulty is mathematical. A fundamental theorem from MHD tells us that a plasma *cannot* confine itself. The field may push inward here, but it must push outward there. You cannot build a magnetic pressure cooker that is higher pressure inside than outside everywhere on the boundary.

This is why fusion reactors are so complicated. The magnetic cage cannot be built from the inside. It must be imposed from outside by massive superconducting magnets surrounding the machine. The plasma is caged, not self-confined. Understanding why the cage needs external support—and what we can do about it—is the subject of this chapter.

6.2 The Simplest Attempt: The Theta-Pinch

Let us try to confine a plasma with the simplest possible configuration: a straight cylinder with an axial magnetic field.

Imagine a cylinder of plasma with magnetic field $B_z(r)$ pointing along the axis. The field is stronger at the edge than in the middle. This creates a magnetic pressure gradient that pushes inward, confin-

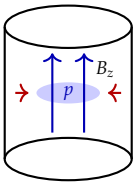

θ-pinch

Figure 6.1: The θ-pinch: an axial magnetic field compresses the plasma radially. But particles escape freely along the field lines.

ing the plasma radially.

The force balance in the radial direction is:

$$-\frac{dp}{dr} + J_\theta B_z = 0.$$

Using Ampère's law, $J_\theta = -(1/\mu_0)\partial B_z/\partial r$, we get:

$$\frac{dp}{dr} = -\frac{1}{\mu_0}\frac{\partial B_z}{\partial r}B_z = -\frac{1}{2\mu_0}\frac{\partial (B_z^2)}{\partial r}.$$

Integrating from the center (where $B_z = B_{\text{center}}$, $p = p_0$) to the edge (where $B_z = B_{\text{edge}}$, $p = 0$):

$$p_0 + \frac{B_{\text{center}}^2}{2\mu_0} = \frac{B_{\text{edge}}^2}{2\mu_0}. \tag{6.1}$$

This is pressure balance: the sum of gas pressure and magnetic pressure is constant across the plasma. The external field squeezes the plasma, and equilibrium is achieved.

So the θ-pinch works—radially. But what about the ends?

The field lines run straight through the cylinder and out both ends. Particles spiral along field lines freely. A thermal particle with speed $v_{\text{th}} \sim 10^6$ m/s (at 10 keV) crosses a 1-meter device in about 1 microsecond. The plasma leaks out the ends like water through a pipe.

For fusion, we need confinement times of order 1 second. The θ-pinch gives us 1 microsecond. We are off by a factor of a million.

You might ask: can we plug the ends? We could curve the field lines back on themselves, making a torus. Or we could add magnetic mirrors—regions of strong field that reflect particles. Both approaches have been tried. Both introduce new problems. The simple picture of straight field lines confining plasma radially captures the essence of the challenge: magnetic fields confine perpendicular to $\mathbf{B}$, not along $\mathbf{B}$.

6.3 *The Equilibrium Equation*

Let us now write down the general condition for MHD equilibrium. When the plasma is at rest ($\mathbf{v} = 0$), the momentum equation becomes:

$$\nabla p = \mathbf{J} \times \mathbf{B}. \tag{6.2}$$

The pressure gradient is balanced by the Lorentz force. Using Ampère's law $\mathbf{J} = (1/\mu_0)\nabla \times \mathbf{B}$ and the vector identity from Chapter 4:

$$\nabla p = \frac{1}{\mu_0}(\nabla \times \mathbf{B}) \times \mathbf{B} = \frac{1}{\mu_0}(\mathbf{B} \cdot \nabla)\mathbf{B} - \nabla\left(\frac{B^2}{2\mu_0}\right). \tag{6.3}$$

Rearranging:

$$\nabla\left(p + \frac{B^2}{2\mu_0}\right) = \frac{1}{\mu_0}(\mathbf{B}\cdot\nabla)\mathbf{B}. \tag{6.4}$$

The left side is the gradient of total pressure (gas plus magnetic). The right side is the magnetic tension force. In equilibrium, the total pressure gradient equals the tension.

Pressure Is Constant Along Field Lines

Taking the dot product of (6.2) with $\mathbf{B}$:

$$\mathbf{B}\cdot\nabla p = \mathbf{B}\cdot(\mathbf{J}\times\mathbf{B}) = 0,$$

since $\mathbf{B}$ is perpendicular to $\mathbf{J}\times\mathbf{B}$.

This means p is constant along each field line. In equilibrium, every field line is an isobar—a surface of constant pressure. The field lines and isobars coincide.

Similarly, taking the dot product with $\mathbf{J}$:

$$\mathbf{J}\cdot\nabla p = 0.$$

Current also flows along isobars. The current lines, field lines, and isobars all lie on the same surfaces.

These surfaces are called *flux surfaces*. In a well-confined plasma, flux surfaces are nested like the layers of an onion, with pressure decreasing from the hot core to the cool edge.

6.4 *The Virial Theorem: Why Self-Confinement Fails*

Now we come to the fundamental obstruction. Can a plasma confine itself—generate its own magnetic field and use it to hold itself together?

The virial theorem says no.

Physical Intuition

Think of a blob of plasma in empty space, carrying currents that generate a magnetic field. The gas pressure pushes outward everywhere. The magnetic pressure $B^2/(2\mu_0)$ is always positive, so it also pushes outward. Magnetic tension can pull inward where field lines are curved, but can the tension everywhere exceed the pressure?

Imagine integrating over the boundary of the plasma. The outward push of both gas and magnetic pressure must be balanced by the inward pull of tension. But tension only acts where field lines curve *into* the plasma. For a self-contained field—one that closes

on itself without external sources—the total magnetic force on any volume integrates to zero. The field can redistribute pressure, but it cannot provide net confinement.

The Mathematical Statement

Let us prove this rigorously. Consider a volume V bounded by a surface S that encloses the plasma. Take S to be a large sphere at radius R, far from the plasma, where both p and $\mathbf{B}$ fall to zero.

Start with the equilibrium equation (6.2) and take the dot product with the position vector $\mathbf{r}$:

$$\mathbf{r} \cdot \nabla p = \mathbf{r} \cdot (\mathbf{J} \times \mathbf{B}).$$

Integrate over the volume V:[1]

$$\int_V \mathbf{r} \cdot \nabla p \, dV = \int_S p \, \mathbf{r} \cdot d\mathbf{A} - 3 \int_V p \, dV.$$

[1] The identity $\nabla \cdot (p\mathbf{r}) = \mathbf{r} \cdot \nabla p + 3p$ helps convert the left side to a surface integral.

For large S where $p \to 0$, the surface integral vanishes, leaving $-3 \int_V p \, dV$.

For the right side, after some vector calculus:[2]

$$\int_V \mathbf{r} \cdot (\mathbf{J} \times \mathbf{B}) \, dV = -\int_V \frac{B^2}{2\mu_0} \, dV + \text{surface terms}.$$

[2] The manipulation involves the identity $\mathbf{r} \cdot (\mathbf{J} \times \mathbf{B}) = \mathbf{J} \cdot (\mathbf{B} \times \mathbf{r})$ and integration by parts. See Freidberg's *Ideal MHD* for details.

For a field that falls off at large distances (faster than $1/R$), the surface terms vanish. We are left with the **virial theorem**:

$$3 \int_V p \, dV + \int_V \frac{B^2}{2\mu_0} \, dV = 0. \tag{6.5}$$

But both integrals are positive! Gas pressure $p > 0$, and magnetic energy density $B^2/(2\mu_0) > 0$. The only way their sum can be zero is if both are zero—no plasma, no field.

Conclusion: A plasma cannot confine itself by its own magnetic field. External sources—currents in coils outside the plasma—are required.

This is not a technical limitation that better engineering might overcome. It is a mathematical impossibility, as certain as the impossibility of a perpetual motion machine. The virial theorem closes the door on self-confinement.

You might ask: surely with enough cleverness in the field geometry, one could evade this constraint? No. The virial theorem is not about local force balance—it is about global integrals. You can arrange for the field to push inward here and there, but the total inward push from a self-generated field must equal the total outward push. There is no topological trick, no clever configuration, that changes this arithmetic. The theorem is as fundamental as conservation of energy.

6.5 Confinement With External Coils

If self-confinement is impossible, we must use external coils. The virial theorem still applies, but now there is a surface contribution from the coil currents that can provide the missing inward force.

Consider a plasma surrounded by a perfectly conducting wall at the boundary S. The wall carries surface currents that support a jump in the tangential magnetic field. Inside the plasma, the equilibrium equation holds:

$$\nabla p = \mathbf{J} \times \mathbf{B}.$$

At the plasma-wall interface:

$$p + \frac{B^2}{2\mu_0} = \frac{B_{\text{wall}}^2}{2\mu_0}, \tag{6.6}$$

where B_{wall} is the field just inside the wall (supported by the wall currents).

The coils do not violate the virial theorem; they provide the external pressure that the theorem demands. The magnetic cage is held together by the scaffolding of the coils—remove the scaffolding, and the cage collapses. The plasma plus coils together satisfy force balance, but the plasma alone cannot.

Boundary Conditions

Real experiments have more complicated boundaries. Some important cases:

Perfectly conducting wall: The normal component of $\mathbf{B}$ must vanish at the wall: $\mathbf{B} \cdot \hat{\mathbf{n}} = 0$. Field lines are tangent to the wall. This is an idealization—real walls have finite resistivity—but it is often a good approximation on short timescales.

Vacuum region: Outside the plasma but inside the wall, there may be a vacuum region with no current. In this region, $\nabla \times \mathbf{B} = 0$, so $\mathbf{B} = -\nabla\chi$ for some scalar potential χ satisfying $\nabla^2\chi = 0$. The vacuum field connects the plasma to the coils.

Pressure discontinuity: If there is a sharp plasma edge with a current sheet, the tangential field jumps across the boundary: $[\![B_t]\!] = \mu_0 K$, where K is the surface current density.

6.6 A Worked Example: The Bennett Pinch

Let us work through a simple equilibrium analytically: the *Bennett pinch*, a cylindrical column of plasma carrying a uniform axial current.

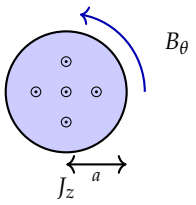

Figure 6.2: The Bennett pinch: axial current creates azimuthal field that pinches the plasma.

Consider a plasma cylinder of radius a carrying total current I. The current density is uniform: $J_z = I/(\pi a^2)$.

From Ampère's law, the azimuthal magnetic field is:

$$B_\theta(r) = \begin{cases} \dfrac{\mu_0 J_z r}{2} = \dfrac{\mu_0 I r}{2\pi a^2} & r < a \\ \dfrac{\mu_0 I}{2\pi r} & r > a \end{cases}$$

The radial force balance is:

$$\frac{dp}{dr} = -J_z B_\theta = -\frac{\mu_0 J_z^2 r}{2}.$$

Integrating from r to a (where $p = 0$ at the edge):

$$p(r) = \frac{\mu_0 J_z^2}{4}(a^2 - r^2) = \frac{\mu_0 I^2}{4\pi^2 a^4}(a^2 - r^2).$$

The central pressure is:

$$p_0 = p(0) = \frac{\mu_0 I^2}{4\pi^2 a^2}. \tag{6.7}$$

This is the **Bennett relation**: it tells us the current required to confine a given pressure in a cylinder of radius a.

Let us put in numbers. For $I = 1$ MA and $a = 1$ cm:

$$p_0 = \frac{4\pi \times 10^{-7} \times (10^6)^2}{4\pi^2 \times (10^{-2})^2} = \frac{10^5}{\pi \times 10^{-4}} \approx 3 \times 10^8 \text{ Pa} \approx 3000 \text{ atm}.$$

Enormous pressure! This is why early fusion researchers were excited by pinches—they seemed to offer high confinement with relatively modest currents.

The catch: the Bennett pinch is violently unstable. Perturbations grow exponentially, destroying the equilibrium in microseconds. We will study these instabilities—the kink and sausage modes—in Chapter 8. For now, the lesson is that equilibrium is necessary but not sufficient; stability is equally important.

You might ask: why bother with the Bennett pinch if it is unstable? Because it teaches us something important. The equilibrium exists—nature allows it mathematically. The problem is not force balance but fragility. The magnetic cage holds the plasma, but the slightest rattle breaks the bars. Understanding why requires understanding stability, which is the real frontier of MHD.

6.7 Historical Note: The Fusion Reckoning

In the 1950s, fusion seemed easy. Heat hydrogen hot enough and it will fuse—this was known from stellar physics. The first fusion

devices were built with optimism and secrecy. In the United States, Project Sherwood pursued pinches and mirrors. In Britain, the ZETA machine promised imminent success. In the Soviet Union, Andrei Sakharov and Igor Tamm developed the tokamak concept.

Edward Teller—"father of the hydrogen bomb"—predicted commercial fusion power within twenty years. He was not alone in his optimism.

Then reality intervened. Every confinement scheme was unstable. Plasmas kinked, sausaged, and squirmed out of their magnetic cages. The 1958 Geneva "Atoms for Peace" conference was a revelation: when the secret programs declassified their results, they all had the same problems. Nobody had fusion working.

The virial theorem was already known mathematically, but its implications for fusion were not fully appreciated. Researchers thought clever field configurations could evade it. They could not. The theorem is a thermodynamic statement about integrals; no local cleverness can circumvent a global constraint.

The path forward required external coils, sophisticated field geometries, and decades of work on stability. The "twenty years" became fifty, then seventy. As of this writing, ITER is under construction in France, aiming for net energy gain by the 2030s. The dream persists, but so does the difficulty.

You might ask: why is fusion so hard when the Sun does it effortlessly? The answer is gravity. The Sun is confined by its own weight—a force that scales as M^2/R^2 and is utterly dominant at stellar masses. Magnetic forces are a perturbation on the Sun, not the confinement mechanism. We cannot build a star on Earth; we must find another way.

6.8 The Beta Limit

Recall the plasma beta from Chapter 4:

$$\beta = \frac{p}{B^2/(2\mu_0)} = \frac{2\mu_0 p}{B^2}.$$

Higher β means more plasma pressure for a given field strength—more "bang for the buck" from your expensive magnets. But there is a limit.

Consider a tokamak with $B = 5$ T and central pressure $p_0 = 10^5$ Pa (about 1 atm). The beta is:

$$\beta = \frac{2 \times 4\pi \times 10^{-7} \times 10^5}{25} \approx 0.01 = 1\%.$$

Only 1% of the magnetic pressure is balancing the plasma! The field is vastly "overbuilt" relative to the plasma it confines.

Why so low? Because instabilities limit beta. Going above a few percent triggers modes that destroy confinement. This *beta limit* is one of the key constraints on fusion reactor design. A reactor with $\beta = 5\%$ is considered aggressive; $\beta = 10\%$ would be revolutionary.

You might ask: can we just use stronger magnets? To some extent, yes. Fusion power scales roughly as $\beta^2 B^4$, so doubling the field increases power 16-fold. But magnets are expensive, and there are engineering limits. The beta limit forces reactor designers into a delicate optimization.

6.9 Looking Ahead

We have established the fundamental constraint: magnetic confinement requires external coils. But what field geometry should we use?

The most successful approach is the tokamak: a torus with helical field lines that wind around both the long way (toroidal) and the short way (poloidal). This geometry has remarkable stability properties, which is why it has dominated fusion research for sixty years.

But the tokamak is not obvious. Why a torus? Why helical fields? What makes this configuration special? Understanding the tokamak requires understanding rotational transform, magnetic shear, and the delicate balance of forces in toroidal geometry. That is the subject of the next chapter.

7
The Tokamak: Fusion's Magnetic Cage

7.1 A Machine That Actually Works

In the late 1960s, Soviet physicists announced something remarkable: their "tokamak" device was confining plasma ten times better than anything else in the world. Western scientists were skeptical—Soviet plasma diagnostics had a mixed reputation, and extraordinary claims require extraordinary evidence.

In 1969, a British team flew to Moscow with their own Thomson scattering diagnostic, a laser-based technique for measuring electron temperature that the Soviets could not fake. They confirmed the results. The T-3 tokamak was achieving electron temperatures of 10 million kelvin with confinement times far exceeding previous devices.

Within five years, tokamaks were being built in every major fusion laboratory. The geometry was elegant: a doughnut-shaped chamber with magnetic field lines spiraling around the torus like stripes on a barber pole. The plasma current itself helped create the confining field. It seemed almost magical—a topology that actually worked.

Fifty years later, the tokamak remains the leading fusion concept. ITER, the experiment under construction in France at a cost exceeding $25 billion, is a tokamak. But understanding *why* tokamaks work—and the instabilities that limit them—took decades of effort. This chapter is about the geometry that makes confinement possible.

7.2 Why Straight Fields Fail in a Torus

We learned in the last chapter that a θ-pinch confines plasma radially but loses it out the ends. The obvious fix: bend the cylinder into a torus. Now the field lines close on themselves—no ends to leak through!

But this creates a new problem.

In a torus, the magnetic field varies with position. The field is

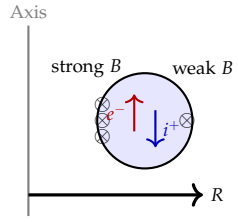

Figure 7.1: Cross-section: the toroidal field B_ϕ is stronger on the inboard side (closer to the central axis) and weaker on the outboard side. The gradient causes electrons and ions to drift in opposite vertical directions.

stronger on the inside (smaller major radius R) than on the outside:

$$B_\phi \propto \frac{1}{R}.$$

This gradient causes particles to drift. The drift velocity is:

$$\mathbf{v}_{\nabla B} = \frac{1}{q}\frac{\mathbf{B}\times\nabla B}{B^2}\frac{mv_\perp^2}{2B} \sim \frac{k_B T}{qBR}.$$

For a 10 keV plasma, $B = 5$ T, $R = 2$ m:

$$v_{\nabla B} \sim \frac{10^4 \times 1.6\times 10^{-19}}{1.6\times 10^{-19}\times 5\times 2} \approx 1000 \text{ m/s}.$$

Electrons and ions drift in opposite directions (they have opposite charge). This separates the charges, creating a vertical electric field $\mathbf{E}$. The electric field then drives an $\mathbf{E}\times\mathbf{B}$ drift that pushes the entire plasma outward, toward the outer wall.

The plasma slides off in milliseconds. Confinement fails.

You might ask: is there no way to cancel these drifts? There is—and it is the key insight behind the tokamak.

7.3 *Rotational Transform: The Saving Twist*

The solution is to twist the field lines.

If field lines do not just circle toroidally but also wind in the poloidal direction (around the cross-section of the torus), something remarkable happens. A particle drifting upward on the outside of the torus is carried by the twisted field line to the inside, where the gradient reverses and it drifts downward. Over a complete circuit, the drift averages to zero.

This twist is called *rotational transform*. In a tokamak, it is created by driving a toroidal current through the plasma. The current generates a poloidal magnetic field B_θ that adds to the toroidal field B_ϕ from the external coils. The result: helical field lines that spiral around the torus.

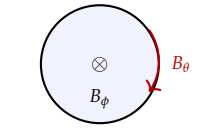

Figure 7.2: Field lines wind helically around the torus, combining toroidal (ϕ) and poloidal (θ) components.

Let us quantify the twist. Define the *safety factor* q:

$$q = \frac{\text{toroidal turns}}{\text{poloidal turns}} = \frac{rB_\phi}{RB_\theta}, \tag{7.1}$$

where r is the minor radius (distance from the plasma center) and R is the major radius.

The name "safety factor" reflects history: larger q means less twist, and less twist turns out to be safer against certain instabilities. A typical tokamak has $q \approx 1$ at the magnetic axis and $q \approx 3$–5 at the plasma edge.

What q Tells You

If $q = 2$, a field line makes two toroidal circuits for every poloidal circuit. After going around the torus twice, it returns to its starting point in the poloidal plane.

If q is irrational (say, $q = \sqrt{2}$), the field line never exactly closes. It densely covers a toroidal surface, called a *flux surface*, without ever repeating.

If $q = 1$, the field line closes after exactly one toroidal circuit. This turns out to be dangerous—perturbations with the same periodicity as the field line can resonate and grow. The $q = 1$ surface is where internal kink modes can develop.

You might ask: why not make q very large everywhere, to be maximally safe? Because large q means weak twist, weak poloidal field, and weak plasma current. The current provides both the twist and (via ohmic heating) some of the plasma heating. There is a tradeoff: too little twist loses the cancellation of drifts; too much twist risks current-driven instabilities.

7.4 The Grad-Shafranov Equation

Let us now make this picture mathematically precise. For a rigorous treatment of tokamak equilibrium, we need to solve the MHD force balance equation in toroidal geometry. The result is the *Grad-Shafranov equation*, named after Harold Grad and Vitaly Shafranov, who derived it independently in the late 1950s.

In axisymmetric equilibrium (no dependence on the toroidal angle ϕ), the magnetic field can be written as:

$$\mathbf{B} = \frac{1}{R}\nabla\psi \times \hat{\boldsymbol{\phi}} + \frac{F(\psi)}{R}\hat{\boldsymbol{\phi}}, \tag{7.2}$$

where ψ is the poloidal flux function (constant on flux surfaces), $F(\psi) = RB_\phi$, and $\hat{\boldsymbol{\phi}}$ is the toroidal unit vector.

The force balance equation $\nabla p = \mathbf{J} \times \mathbf{B}$ becomes, after considerable algebra:[1]

$$\Delta^* \psi = -\mu_0 R^2 \frac{dp}{d\psi} - F\frac{dF}{d\psi}, \tag{7.3}$$

where the *Grad-Shafranov operator* is:

$$\Delta^* = R^2 \nabla \cdot \left(\frac{\nabla}{R^2}\right) = R\frac{\partial}{\partial R}\left(\frac{1}{R}\frac{\partial}{\partial R}\right) + \frac{\partial^2}{\partial Z^2}.$$

This is an elliptic partial differential equation for $\psi(R, Z)$ given the profiles $p(\psi)$ and $F(\psi)$. Solving it, with appropriate boundary conditions from the coil geometry, gives the equilibrium flux surfaces.

[1] The derivation requires expressing $\mathbf{J}$ in terms of ψ and F, then projecting the force balance onto the poloidal plane. See Freidberg's *Ideal MHD* for the full calculation.

Physical Meaning

Each term in (7.3) has a physical interpretation:

Left side ($\Delta^* \psi$): Measures how the flux surfaces deviate from simple circular cross-sections. Non-zero $\Delta^* \psi$ means the surfaces are shaped—shifted, elongated, or triangular.

First term on right ($-\mu_0 R^2 \, dp/d\psi$): The pressure gradient. Higher central pressure pushes flux surfaces outward, creating the *Shafranov shift*: the magnetic axis is displaced outward from the geometric center.

Second term ($-F \, dF/d\psi$): The toroidal field gradient. If F varies with ψ (i.e., if B_ϕ changes across flux surfaces), this contributes to the equilibrium shape.

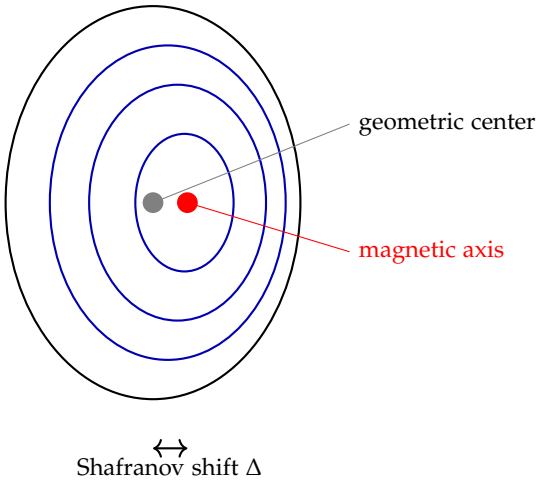

Figure 7.3: Shafranov shift: the magnetic axis is displaced outward from the geometric center due to pressure gradients. Flux surfaces nest around the shifted magnetic axis.

7.5 Flux Surfaces: The Onion-Skin Picture

Let us examine what the solutions to the Grad-Shafranov equation reveal. The plasma is organized into nested flux surfaces—toroidal shells, like the layers of an onion. This onion-skin structure is the foundation of tokamak confinement.

On each flux surface:

- Pressure is constant: $\mathbf{B} \cdot \nabla p = 0$ implies $p = p(\psi)$.
- Field lines lie entirely within the surface, winding helically without crossing to adjacent surfaces.
- The safety factor q is constant (for a given surface).

The magnetic axis—the innermost flux surface, which has degenerated to a curve—carries the highest pressure and hottest plasma.

Moving outward, pressure decreases, temperature drops, and the safety factor q increases.

This nested structure is the key to confinement. Plasma cannot easily cross flux surfaces because doing so requires crossing field lines, which is forbidden in ideal MHD. Transport across flux surfaces requires either collisions (classical transport), turbulent eddies (anomalous transport), or large-scale instabilities. The onion skin provides a thermal barrier: heat generated in the hot core must diffuse layer by layer to the cool edge.

You might ask: if flux surfaces are so confining, why is fusion hard? Because the nested structure is fragile. Instabilities can break flux surfaces, creating "magnetic islands" where field lines connect across what were previously isolated surfaces—like tunnels punched through the onion, letting heat escape directly. Even without instabilities, turbulence drives transport that exceeds classical predictions by factors of 10–100. The onion has leaky layers, and sometimes the layers tear.

7.6 A Worked Example: Computing q for a Tokamak

Let us compute the safety factor for a small tokamak with the following parameters:

- Major radius: $R_0 = 1.7$ m
- Minor radius: $a = 0.4$ m
- Toroidal field at the center: $B_{\phi 0} = 2.5$ T
- Plasma current: $I_p = 1$ MA

First, we estimate the poloidal field at the plasma edge. Treating the plasma current as a line current (a rough approximation):

$$B_\theta(a) \approx \frac{\mu_0 I_p}{2\pi a} = \frac{4\pi \times 10^{-7} \times 10^6}{2\pi \times 0.4} = 0.5 \text{ T}.$$

The safety factor at the edge, using (7.1):

$$q(a) = \frac{a B_\phi}{R_0 B_\theta} = \frac{0.4 \times 2.5}{1.7 \times 0.5} = \frac{1.0}{0.85} \approx 1.2.$$

This is too low! Tokamaks typically require $q_{\text{edge}} > 2$ to avoid certain instabilities (the external kink mode). With $q = 1.2$ at the edge, the plasma would be violently unstable.

To fix this, we could:

- Increase B_ϕ (requires larger, more expensive magnets)
- Decrease I_p (reduces heating and possibly confinement)

- Increase the aspect ratio R_0/a (larger machine)

Real tokamaks balance these tradeoffs carefully. ITER, for example, is designed with $R_0 = 6.2$ m, $a = 2.0$ m, $B_\phi = 5.3$ T, $I_p = 15$ MA, giving $q_{\text{edge}} \approx 3$.

7.7 Historical Note: From T-3 to ITER

The tokamak was invented by Igor Tamm and Andrei Sakharov at the Kurchatov Institute in Moscow in the early 1950s. The name is a Russian acronym: *toroidal'naya kamera s aksial'nym magnitnym polem*—toroidal chamber with axial magnetic field.[2]

[2] Some sources give a slightly different expansion, but all agree on the basic meaning.

The early tokamaks showed promise but nothing spectacular. Other configurations—stellarators, pinches, mirrors—were also being pursued. Then came T-3.

The T-3 tokamak achieved electron temperatures of 1 keV (about 10 million kelvin) with energy confinement times of tens of milliseconds—an order of magnitude better than any other device. The 1969 British verification mission settled the matter: tokamaks worked.

The subsequent history is a progression of ever-larger machines:

- **T-3** (1968): $T_e \sim 1$ keV, demonstrated the concept
- **PLT** (Princeton, 1978): First to reach $T_e \sim 5$ keV
- **TFTR** (Princeton, 1994): First D-T fusion reactions at significant power
- **JET** (Europe, 1997): Achieved $Q = 0.67$ (fusion power / input power)
- **ITER** (under construction): Target $Q = 10$

Each machine was larger, hotter, and better confined. But progress has been slower than the optimists hoped. The "engineering" problems—materials that can handle the heat, exhaust systems for the helium ash, avoiding disruptions that can damage the machine—have proven as difficult as the physics.

You might ask: why not just build a bigger machine now? Cost. JET cost about $1 billion in 1980s money. ITER will cost over $20 billion. A demonstration power plant would cost more still. Fusion is on a trajectory, but it is expensive, and the payoff is decades away.

7.8 The Stellarator Alternative

Let us consider the alternative. The tokamak is not the only path to fusion. A *stellarator* creates the rotational transform using external coils alone, without any plasma current.

The advantage: no current means no current-driven instabilities, and the device can operate in true steady state. The disadvantage: the coils must be spectacularly complex, twisted into three-dimensional shapes that are difficult to manufacture.

The Wendelstein 7-X stellarator in Germany, which began operations in 2015, has 70 superconducting coils, each a different shape, optimized by computer to create flux surfaces with good confinement properties. The engineering is a tour de force.

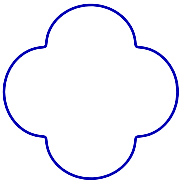

Figure 7.4: Stellarator coils must be non-planar and precisely shaped to create the required rotational transform.

Both concepts are actively pursued. ITER is a tokamak because tokamaks are better understood and have a longer track record. But stellarators may ultimately prove superior for a power plant, where steady-state operation is essential. The jury is still out.

7.9 Looking Ahead

We have established how tokamaks achieve equilibrium: nested flux surfaces created by a combination of toroidal and poloidal fields, with the twist (rotational transform) canceling particle drifts. The plasma is confined—but is it stable?

Equilibrium is necessary but not sufficient. A ball at the top of a hill is in equilibrium, but the slightest push sends it rolling down. The same is true for plasma: the equilibrium configuration may be unstable to small perturbations.

Current flowing through the plasma creates opportunities for instability. Pressure gradients push against the magnetic cage. Both can drive modes that destroy confinement. Understanding these instabilities—and how to avoid them—is the real frontier of fusion research. That is the subject of the next chapter.

8
Current-Driven Instabilities

8.1 When Current Becomes the Enemy

Run a current through a wire and nothing much happens—the wire stays straight. But run a current through a plasma, and all hell can break loose. The current creates a magnetic field, and that field can destabilize the very current that created it. The plasma writhes, kinks, and pinches.

These current-driven instabilities are among the most dangerous in fusion. A tokamak relies on a toroidal plasma current to create the confining poloidal field. But if that current is too strong, or too sharply peaked, the plasma becomes unstable. In the worst case, a "disruption" occurs: the plasma loses confinement in milliseconds, dumping hundreds of megajoules of energy onto the walls.

Think of the plasma as a coiled spring under tension. The current stores magnetic energy, and the plasma is always looking for ways to release it. The kink instability is the plasma's attempt to relax—to shorten its current path and reduce its magnetic stress. Understanding these instabilities took decades. The mathematics is subtle, but the physical pictures are intuitive. Let us build that intuition.

8.2 The Kink Instability: Current Shortening

Consider a straight column of current-carrying plasma—a Z-pinch. The axial current J_z creates an azimuthal magnetic field B_θ that wraps around the column. This field produces an inward $\mathbf{J} \times \mathbf{B}$ force that confines the plasma radially.

Now imagine the column develops a small helical kink—a sideways displacement that spirals around the axis. What happens?

The current path, which was straight, is now helical. But magnetic field lines—and the currents that create them—want to be as short as possible, because shorter paths mean less stored magnetic energy. If the kink can grow, the effective current path shortens, reducing the

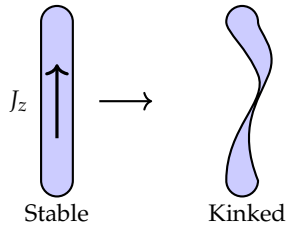

Figure 8.1: The kink instability: a helical displacement of the current column reduces the current path length and releases magnetic energy.

magnetic energy.

Let us see this energetically. The magnetic energy stored in the azimuthal field scales as:

$$W \sim \int \frac{B_\theta^2}{2\mu_0}\, dV \sim \frac{\mu_0 I^2}{4\pi} \times (\text{effective length}).$$

If the kink grows, the effective length of the current path decreases, W decreases, and energy is released. Released energy means instability—the perturbation grows.

This is the kink instability in its essence: the plasma trying to shorten its current path.

How Fast Does It Grow?

The growth rate of the kink is set by the Alfvén time—the time for magnetic signals to communicate across the plasma. For a cylinder of radius a:

$$\gamma \sim \frac{v_A}{a} \sim \frac{B_\theta}{\sqrt{\mu_0 \rho}\, a}.$$

Let us put in numbers for a fusion-relevant plasma: $n \sim 10^{20}$ m^{-3} (giving $\rho \sim 3 \times 10^{-7}$ kg/m^3 for deuterium), $B_\theta \sim 0.5$ T, $a \sim 0.3$ m. Then:

$$v_A = \frac{0.5}{\sqrt{4\pi \times 10^{-7} \times 3 \times 10^{-7}}} \approx 8 \times 10^5 \text{ m/s},$$

and

$$\gamma \sim \frac{8 \times 10^5}{0.3} \approx 3 \times 10^6 \text{ s}^{-1}.$$

The growth time is $\tau \sim 1/\gamma \sim 0.3\ \mu$s. This is *fast*—much faster than the energy confinement time of seconds. An unstable kink can destroy confinement in microseconds.

8.3 Stabilization by Axial Field

The kink can be stabilized by adding an axial magnetic field B_z—precisely what we have in a tokamak.

With both B_θ and B_z present, the field lines are helical. A kink perturbation would have to bend these helical field lines, which costs energy due to magnetic tension. If the axial field is strong enough, the tension cost exceeds the energy gain from current shortening, and the kink is stabilized.

The criterion for stability is the celebrated Kruskal-Shafranov condition:

$$q = \frac{aB_z}{RB_\theta} > 1. \tag{8.1}$$

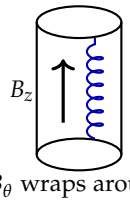

Figure 8.2: Adding an axial field B_z creates helical field lines. Bending them costs energy, stabilizing the kink.

Here q is the safety factor we met in Chapter 7. The condition says: if the field lines make more than one toroidal turn before completing a poloidal turn, the kink is stable.

You might ask: why exactly $q > 1$? The answer involves resonance. When $q = 1$, a field line closes on itself after exactly one toroidal circuit. A helical perturbation with the same periodicity can grow without "unwinding"—every point on the field line sees the same phase of the perturbation. For $q > 1$, the field line does not close after one turn, so perturbations average out.

8.4 The Internal Kink and Sawteeth

In a tokamak, the safety factor varies across the plasma: typically $q \approx 1$ near the magnetic axis and $q \approx 3$–5 at the edge. If $q < 1$ somewhere inside the plasma, an internal kink can develop.

The $m = 1$ internal kink is particularly dangerous. It represents a sideways displacement of the plasma core—the hot center sloshes to one side. At the $q = 1$ surface, field lines are resonant with this $m = 1$, $n = 1$ perturbation.

In many tokamaks, the internal kink manifests as the "sawtooth instability"—periodic crashes in which the hot core mixes with cooler surrounding plasma. The central temperature drops suddenly (the "crash"), then slowly rebuilds as heating continues, then crashes again. The cycle repeats with a period of tens to hundreds of milliseconds.

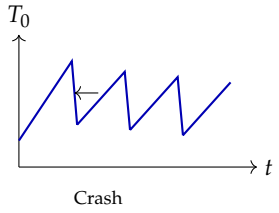

Figure 8.3: Sawtooth oscillations: the central temperature rises slowly, then crashes rapidly as the internal kink mixes hot and cold plasma.

Sawteeth are not catastrophic—the plasma survives them—but they limit performance by flattening the temperature profile and expelling energetic particles from the core. Controlling or avoiding sawteeth is an active area of research.

8.5 External Kinks and Disruptions

If the plasma boundary is free to move—if there is no nearby conducting wall—external kinks can develop. These are $m = 1$ modes that shift the entire plasma column sideways.

External kinks are unstable when $q_{\text{edge}} < 1$, which is why tokamaks are designed with $q_{\text{edge}} > 2$ or higher. But even with $q_{\text{edge}} > 1$, external kinks can be triggered by other events—a loss of plasma current control, a sudden cooling of the edge, an accumulation of impurities.

When an external kink grows without bound, the result is a *disruption*: complete loss of plasma confinement in milliseconds. The plasma thermal energy and magnetic energy are dumped onto the walls.

Let us estimate the energy involved for ITER:

- Plasma thermal energy: $W_{\text{th}} \approx 350$ MJ
- Magnetic energy in the poloidal field: $W_{\text{mag}} \approx 400$ MJ
- Total: ~ 750 MJ

During the thermal quench (the first phase of a disruption), this energy is released in about 10 ms:

$$P \sim \frac{W_{\text{th}}}{\tau} \sim \frac{350 \text{ MJ}}{0.01 \text{ s}} = 35 \text{ GW}.$$

Distributed over the wall area of ~ 700 m^2:

$$\text{Heat flux} \sim \frac{35 \text{ GW}}{700 \text{ m}^2} = 50 \text{ MW/m}^2.$$

This is roughly ten times the steady-state limit for tungsten. Without mitigation, the wall would melt.

You might ask: how do you mitigate a disruption? The strategy is to inject massive amounts of impurities—neon or argon gas—at the first sign of trouble. The impurities radiate the thermal energy isotropically as light, spreading it over the entire wall instead of dumping it locally. The target is to reduce peak heat flux below 10 MW/m^2.

Disruption mitigation is one of the critical engineering challenges for ITER. A single unmitigated disruption could end the machine's career.

8.6 *The Sausage Instability*

The kink is not the only current-driven instability. Consider again a Z-pinch, but now imagine a perturbation that pinches the column at regular intervals—a "sausage" or $m = 0$ mode.

Where the column narrows, the azimuthal field B_θ is stronger (same current, smaller circumference). Stronger B_θ means stronger inward pinch force. So the narrow regions get narrower, and the wide regions get wider. The instability feeds on itself.

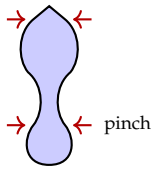

Sausage mode

Figure 8.4: The sausage instability: where the column is narrower, B_θ is stronger, and the inward pinch force is enhanced.

The sausage mode is stabilized by an axial field even more easily than the kink—any B_z provides a restoring force because the field lines must stretch as the column pinches. In tokamaks, the strong toroidal field completely suppresses sausage modes.

8.7 *Historical Note: The Perhapsatron and Early Pinches*

In the 1950s, pinch devices were the great hope of fusion research. Los Alamos built the "Perhapsatron"—so named because fusion was

"perhaps" possible. The machine was a toroidal Z-pinch: current flowed around the torus, creating a poloidal field that pinched the plasma inward.

Early results were tantalizing. Neutrons were detected—a sign of fusion reactions! But closer examination revealed that the neutrons came not from thermonuclear fusion but from instability-driven acceleration. The plasma was so violently unstable that ions were accelerated to MeV energies and produced neutrons through beam-target reactions, not thermal equilibrium.

The instabilities were dramatic. Films from the era show plasma columns writhing and kinking like untended fire hoses. Researchers called them "firehose modes"—the plasma whipped around, bounced off walls, and extinguished in milliseconds.

Understanding came from Martin Kruskal and Vitaly Shafranov, who independently derived the stability criterion in 1958. Their analysis explained why simple pinches failed: without a strong axial field, kinks are inevitable. The Kruskal-Shafranov limit ($q > 1$) pointed the way toward tokamaks—add enough axial field to stabilize the kink, and confinement becomes possible.

You might ask: if the physics was understood in 1958, why did fusion take so long? Because stability is necessary but not sufficient. Even with $q > 1$, tokamaks face other instabilities (pressure-driven modes, resistive modes, edge-localized modes) and anomalous transport that exceeds classical predictions by orders of magnitude. Each problem solved reveals the next.

8.8 Normal Mode Analysis: The Mathematical Framework

Let us now make the stability analysis precise. We linearize the ideal MHD equations about an equilibrium and look for exponentially growing solutions.

Write all quantities as equilibrium plus perturbation:

$$\mathbf{B} = \mathbf{B}_0 + \mathbf{B}_1, \quad \mathbf{v} = \mathbf{v}_1, \quad p = p_0 + p_1, \quad \rho = \rho_0.$$

The linearized ideal MHD equations are:

$$\frac{\partial \mathbf{B}_1}{\partial t} = \nabla \times (\mathbf{v}_1 \times \mathbf{B}_0), \tag{8.2}$$

$$\rho_0 \frac{\partial \mathbf{v}_1}{\partial t} = -\nabla p_1 + \frac{1}{\mu_0} \left[(\nabla \times \mathbf{B}_1) \times \mathbf{B}_0 + (\nabla \times \mathbf{B}_0) \times \mathbf{B}_1 \right]. \tag{8.3}$$

For a cylindrical equilibrium with $\mathbf{B}_0 = B_\theta(r)\hat{\boldsymbol{\theta}} + B_z(r)\hat{\mathbf{z}}$, we assume perturbations of the form:

$$\mathbf{v}_1 \propto e^{\gamma t + im\theta + ikz}.$$

This is *normal mode analysis*: we decompose arbitrary perturbations into Fourier modes characterized by growth rate γ and wavenumbers (m, k). If any mode has $\mathrm{Re}(\gamma) > 0$, the equilibrium is unstable.

Substituting into the linearized equations gives a system of coupled ODEs in the radial variable r. The boundary conditions are:

- Regularity at $r = 0$
- Matching to external vacuum field at $r = a$ (or to a conducting wall)

The eigenvalue problem determines which values of γ are allowed. For a uniform current channel carrying current I in an external axial field B_z, the stability boundary is precisely $q = 1$.

8.9 Looking Ahead

We have seen that current drives instabilities—the kink and its relatives. The plasma is a coiled spring, and too much current makes the spring snap.

But current is not the only driver of instability. Pressure gradients can also destabilize the plasma, even when the current is perfectly stable. When magnetic field lines curve, a pressure gradient can create an effective "gravity" that pushes plasma off the field lines. These pressure-driven instabilities—interchange modes, ballooning modes—set the famous "beta limit" on tokamak performance.

Understanding the interplay between current-driven and pressure-driven instabilities is essential for optimizing fusion devices. That is the subject of the next chapter.

9
Pressure-Driven Instabilities

9.1 The Heavy Fluid Above the Light

Hold a glass of water upside down. For a moment—perhaps a tenth of a second—nothing happens. Then the water falls.

This is the Rayleigh-Taylor instability. Heavy fluid above light fluid is unstable; the interface ripples, fingers of dense material penetrate the less dense, and gravity does its work. No amount of surface tension can prevent it. The only question is how fast.

Now imagine the same physics with magnetic field lines. The "heavy" fluid is hot, high-pressure plasma. The "light" fluid is vacuum—or more precisely, the low-pressure region supported by magnetic pressure. If the field curves the wrong way, with its center of curvature on the plasma side, the plasma can "fall" through the field just as water falls through air.

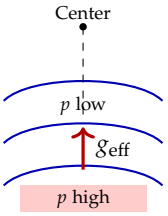

Figure 9.1: Bad curvature: the field curves away from the plasma, creating an effective gravity that can drive instability.

This is the *interchange instability*, and its more sophisticated cousin the *ballooning mode*. Unlike the current-driven instabilities of the last chapter, these modes do not require any plasma current. They are driven purely by pressure gradients interacting with curved magnetic fields.

These pressure-driven instabilities set the ultimate limit on how much pressure a tokamak can confine—the famous "beta limit." Understanding them is understanding why fusion cannot be made arbitrarily better simply by turning up the heating power.

9.2 Good Curvature and Bad Curvature

Let us build intuition for when pressure-driven instabilities occur.

Consider a plasma confined by curved magnetic field lines. The field is stronger on the concave side (closer to the center of curvature) and weaker on the convex side. This gradient creates an effective

gravity:

$$g_{\text{eff}} \sim \frac{v_{\text{th}}^2}{R_c} \sim \frac{k_B T}{m R_c}, \tag{9.1}$$

where R_c is the radius of curvature and v_{th} is the thermal velocity.

If the pressure gradient points in the same direction as this effective gravity—high-pressure plasma "above" low-pressure vacuum in the effective gravitational field—the system is unstable. The plasma wants to fall through the field.

This leads to the crucial distinction:

Bad curvature: The field curves away from the plasma. The center of curvature is on the plasma side. Pressure gradient and effective gravity are aligned. Unstable.

Good curvature: The field curves toward the plasma. The center of curvature is on the vacuum side. Pressure gradient and effective gravity oppose each other. Stable.

A tokamak has both. On the outboard side (low-field side), the toroidal field curves away from the plasma—bad curvature. On the inboard side (high-field side), the field curves toward the plasma—good curvature.

You might ask: if bad curvature exists in every tokamak, why doesn't everything go unstable immediately? The answer is magnetic shear.

9.3 *Stabilization by Magnetic Shear*

Magnetic shear—the variation of the field line pitch with radius—is the primary stabilizer of interchange modes.

In a tokamak, the safety factor q increases with radius: $q \approx 1$ at the center, $q \approx 3$–5 at the edge. This means the field line pitch changes as you move outward. A perturbation that is aligned with field lines at one radius is misaligned at neighboring radii.

This shear has two effects. First, it localizes the instability: a mode that tries to extend radially finds itself fighting against field lines that twist differently at each radius. Second, it provides a restoring force: displacing plasma across field lines stretches those lines, and magnetic tension resists the stretch.

The competition between destabilizing pressure gradient and stabilizing shear determines the stability boundary.

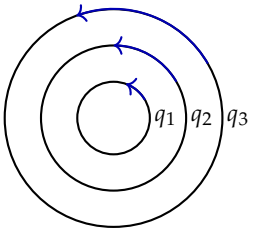

Figure 9.2: Magnetic shear: the field line pitch changes with radius (q increases outward), localizing perturbations.

9.4 *The Energy Principle*

Let us now make this quantitative. The most powerful tool for MHD stability analysis is the *energy principle*: if every possible perturbation increases the potential energy of the system, the equilibrium is stable.

Consider a small displacement $\boldsymbol{\xi}$ from equilibrium. The change in potential energy is:[1]

$$\delta W = \frac{1}{2}\int dV \left[\frac{|\mathbf{Q}_\perp|^2}{\mu_0} + \frac{B^2}{\mu_0}|\nabla \cdot \boldsymbol{\xi}_\perp + 2\boldsymbol{\xi}_\perp \cdot \boldsymbol{\kappa}|^2 + \gamma p |\nabla \cdot \boldsymbol{\xi}|^2 - 2(\boldsymbol{\xi}_\perp \cdot \nabla p)(\boldsymbol{\xi}_\perp \cdot \boldsymbol{\kappa}) \right], \tag{9.2}$$

where $\mathbf{Q} = \nabla \times (\boldsymbol{\xi} \times \mathbf{B})$ is the perturbed magnetic field, $\boldsymbol{\kappa} = (\hat{\mathbf{b}} \cdot \nabla)\hat{\mathbf{b}}$ is the field line curvature, and γ is the adiabatic index.

[1] The derivation involves considerable algebra, integrating by parts and using the equilibrium condition. See Freidberg's *Ideal MHD* for details.

The first three terms are always positive—they represent magnetic and compressional energy stored in the perturbation. The last term is the crucial one:

$$-2(\boldsymbol{\xi}_\perp \cdot \nabla p)(\boldsymbol{\xi}_\perp \cdot \boldsymbol{\kappa}). \tag{9.3}$$

This term can be negative when ∇p and $\boldsymbol{\kappa}$ point in the same direction—precisely the bad curvature situation. If this negative contribution outweighs the positive stabilizing terms, $\delta W < 0$ for some perturbation, and the system is unstable.

9.5 Interchange Modes

Let us consider the simplest pressure-driven instability: the *interchange mode*. Imagine two adjacent flux tubes of equal magnetic flux but different pressure. If we swap them—interchange their positions—what happens to the energy?

In a region of bad curvature, the tube originally at larger radius (lower field strength, larger volume) contains more plasma at higher pressure. When it moves inward (to smaller volume, higher field strength), it gets compressed. Meanwhile, the inner tube expands as it moves outward.

If the outer tube started with higher pressure, swapping releases energy: the plasma effectively "falls" in the effective gravity. This is the interchange instability.

The stability criterion involves a quantity called the Mercier criterion:

$$D_M > 0 \quad \text{for stability}, \tag{9.4}$$

where D_M includes contributions from the pressure gradient, field line curvature, and magnetic shear. In regions of bad curvature without shear, $D_M < 0$ and the plasma is interchange-unstable.

You might ask: what happens physically when the interchange mode develops? The flux tubes mix. Plasma from the high-pressure core penetrates into the low-pressure edge, and vice versa. The pressure profile flattens. In a tokamak, this enhanced transport degrades confinement.

9.6 *Ballooning Modes*

Let us now turn to a more sophisticated instability. Interchange modes are highly localized perpendicular to the field. Ballooning modes are more subtle: they localize *along* the field line in the bad curvature region.

Consider a flux surface in a tokamak. On the outboard side (bad curvature), pressure-driven perturbations want to grow. On the inboard side (good curvature), they are suppressed. A ballooning mode exploits this by "ballooning" out on the bad curvature side while remaining small on the good curvature side.

The mathematics involves solving an eigenvalue problem along the field line. The result: stability requires the pressure gradient to be below a critical value that depends on the local shear and curvature.

The ballooning stability limit, combined with the kink stability limit from Chapter 8, determines the maximum achievable beta in a tokamak.

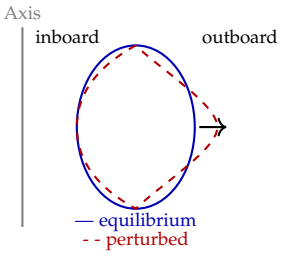

Figure 9.3: Ballooning mode: the perturbation (dashed) bulges outward only on the outboard (bad curvature) side, while the inboard side stays near equilibrium.

9.7 *The Beta Limit*

We have discussed beta—the ratio of plasma pressure to magnetic pressure—several times. Now we can understand what limits it.

The empirical *Troyon limit* summarizes decades of stability analysis:

$$\beta_{\max}(\%) = \beta_N \times \frac{I_p\ (\text{MA})}{a\ (\text{m}) \times B_T\ (\text{T})}, \tag{9.5}$$

where $\beta_N \approx 2.8$ for standard tokamak operation. This scaling emerges from stability codes that solve the energy principle for realistic tokamak equilibria.

Let us compute the beta limit for ITER: $I_p = 15$ MA, $a = 2.0$ m, $B_T = 5.3$ T.

$$\beta_{\max} = 2.8 \times \frac{15}{2.0 \times 5.3} \approx 2.8 \times 1.4 \approx 4\%.$$

At $\beta = 4\%$ and $B_T = 5.3$ T, the corresponding pressure is:

$$p = \beta \times \frac{B^2}{2\mu_0} = 0.04 \times \frac{(5.3)^2}{2 \times 4\pi \times 10^{-7}} \approx 4.5 \times 10^5 \text{ Pa} \approx 4.5 \text{ atm}.$$

Four and a half atmospheres. That is the maximum stable pressure in the core of ITER—roughly the pressure inside a bicycle tire. For all the sophistication of tokamak physics, the result is a plasma at modest pressure, held in place by an elaborate magnetic cage.

You might ask: can you beat the Troyon limit? Somewhat. "Advanced tokamak" scenarios with optimized current profiles can

achieve $\beta_N \approx 5$. Spherical tokamaks—devices with very low aspect ratio (fat tori)—exploit favorable geometry to reach $\beta \sim 40\%$ in some cases. But these are exceptions, not the rule. The beta limit remains a fundamental constraint.

9.8 Edge-Localized Modes: The Price of Confinement

In 1982, researchers at the ASDEX tokamak in Germany discovered *H-mode*—a high-confinement regime where a transport barrier forms at the plasma edge. Energy confinement nearly doubled. This was excellent news for fusion.

But H-mode came with a catch: edge-localized modes, or ELMs.

In H-mode, the steep edge pressure gradient approaches the local stability limit. Periodically, this gradient exceeds the threshold, triggering a ballooning-like instability. The instability saturates, expelling energy and particles from the edge. The gradient relaxes, stability is temporarily restored, the gradient rebuilds under heating, and the cycle repeats.

Each ELM deposits energy onto the divertor plates in a millisecond. For current tokamaks, this is manageable. For ITER, with its much larger stored energy, uncontrolled ELMs could deposit megajoules per square meter, destroying the divertor in months of operation.

You might ask: how do you control ELMs? Several strategies are under development:

- **Magnetic perturbations**: Small non-axisymmetric fields can destabilize tiny ELMs continuously, preventing the large periodic crashes.
- **Pellet pacing**: Injecting frozen fuel pellets triggers small ELMs at a controlled frequency.
- **Operating regimes**: Some regimes (like "QH-mode") achieve H-mode confinement without ELMs, though not yet reliably.

ELM control is one of the critical challenges for ITER. The physics is still being unraveled.

9.9 Historical Note: Discovering the Stability Landscape

The stability of magnetized plasmas was worked out piece by piece over decades.

The energy principle was formulated by Bernstein, Frieman, Kruskal, and Kulsrud in 1958—the same year as the Geneva confer-

ence that revealed the failures of early pinches. Their work provided the mathematical foundation for all subsequent stability analysis.

The Mercier criterion for interchange stability came from Claude Mercier in France in the 1960s. The ballooning mode analysis was developed by Connor, Hastie, and Taylor in the 1970s. The Troyon limit was established empirically by Francis Troyon in 1984, after analyzing stability boundaries across many tokamak scenarios.

Each contribution built on the last. The result is a detailed map of the stability landscape: which regions of parameter space are stable, which are unstable, and why. This map guides every aspect of tokamak design.

But the map is not complete. Edge physics, in particular, remains poorly understood. The transition from L-mode to H-mode, the dynamics of ELMs, the role of turbulence at the plasma edge—these are active research areas. The stability of burning plasmas, where alpha particles from fusion reactions contribute significant pressure, has never been tested experimentally. ITER will be the first machine to explore this regime.

9.10 Looking Ahead

We have now covered the two great classes of MHD instabilities: current-driven (Chapter 8) and pressure-driven (this chapter). Together, they constrain the operating space of tokamaks: the current must not exceed the Kruskal-Shafranov limit; the pressure must not exceed the beta limit.

But our focus has been entirely on fusion—the challenge of confining hot plasma for energy production. MHD has much wider applications. In the next chapter, we leave the laboratory and enter the cosmos.

The magnetorotational instability (MRI) is perhaps the most important instability in astrophysics. It operates wherever a conducting fluid rotates differentially in the presence of a magnetic field—which is to say, in almost every accretion disk around a black hole, neutron star, or young star. Understanding angular momentum transport in these disks requires understanding the MRI. That is where we turn next.

10
The Magnetorotational Instability

10.1 The Disk That Shouldn't Work

For decades, astrophysicists had an embarrassing problem: accretion disks shouldn't work.

Gas orbiting a black hole or young star has enormous angular momentum. To fall inward and feed the central object, the gas must somehow get rid of that angular momentum—transfer it elsewhere, radiate it away, something. But the molecular viscosity of astrophysical gas is pathetically small. A straightforward calculation shows that gas at 1 AU from the Sun, relying on molecular viscosity alone, would take longer than the age of the universe to spiral inward.

Yet disks accrete. We see it happening. Quasars blaze with the luminosity of a trillion suns, powered by gas falling onto supermassive black holes. Young stars double their mass by swallowing their birth disks. X-ray binaries flicker as gas streams onto neutron stars. Something transports angular momentum outward at a rate a billion times faster than molecular viscosity can explain.

For years, astrophysicists simply parameterized their ignorance. Shakura and Sunyaev's famous "α-prescription" posited a turbulent viscosity $\nu \sim \alpha c_s H$, where c_s is the sound speed, H is the disk thickness, and α is a dimensionless fudge factor between 0.01 and 0.1. The prescription was useful—it let people calculate disk structure—but it explained nothing. Where did the turbulence come from? What set α? Nobody knew.

Then in 1991, Steve Balbus and John Hawley found the answer. A weak magnetic field in a differentially rotating disk is violently unstable. The instability drives turbulence, and turbulent stress transports angular momentum. The "magnetorotational instability"—MRI for short—turns out to be the engine of accretion throughout the universe.

10.2 Springs in Orbit

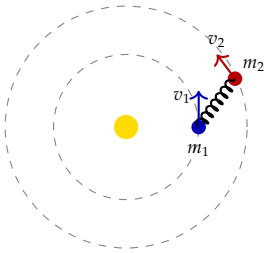

Figure 10.1: Two masses connected by a spring. The inner mass orbits faster, stretching the spring as it pulls ahead.

Let us build intuition with a mechanical analogy.

Consider two masses connected by a spring, both orbiting a central star. Place the inner mass at radius r_1 and the outer mass at radius $r_2 > r_1$. In a Keplerian orbit, angular velocity decreases with radius: $\Omega \propto r^{-3/2}$. The inner mass orbits faster than the outer mass.

What happens? Initially the spring is relaxed. But the inner mass pulls ahead while the outer mass falls behind. The spring stretches.

Now the spring exerts forces. It pulls backward on the inner mass, subtracting angular momentum. It pulls forward on the outer mass, adding angular momentum.

A mass that loses angular momentum spirals inward. A mass that gains angular momentum spirals outward. So the inner mass moves to a smaller radius, the outer mass to a larger radius. But this increases their separation further! The spring stretches more, the forces grow stronger, the separation increases faster.

This is a runaway: a feedback loop where any small displacement amplifies itself. The system is unstable.

You might ask: what if the spring is very stiff? Then small displacements produce large restoring forces before the masses have time to move radially. The spring oscillates but doesn't run away. Stability requires a stiff spring.

Here is the key insight: magnetic field lines behave like springs. Magnetic tension, as we developed in Chapter 4, acts to straighten bent field lines, just as a stretched spring pulls its endpoints together. If a field line threads through two fluid elements at different radii, differential rotation will stretch that field line, and magnetic tension will transfer angular momentum from the inner element to the outer.

If the field is weak—the magnetic "spring" is soft—the instability wins. If the field is strong—the spring is stiff—oscillations dominate and stability prevails. The MRI is the instability of weak magnetic fields in differential rotation.

10.3 The Instability Criterion

Let us now derive when the instability occurs.

Consider a disk of gas orbiting with angular velocity $\Omega(r)$ and threaded by a weak vertical magnetic field B_z. We'll analyze stability using a local approximation: zoom in on a small patch of the disk and treat it as a Cartesian box with the radial direction along x, the azimuthal direction along y, and the vertical direction along z.

In this local frame, the differential rotation appears as a shear flow: $v_y = -q\Omega x$, where $q = -d\ln\Omega/d\ln r$ is the shear parameter. For a

Keplerian disk, $\Omega \propto r^{-3/2}$, so $q = 3/2$.

The linearized MHD equations for perturbations proportional to $\exp(ik_z z - i\omega t)$ give a dispersion relation. After some algebra that I will spare you,[1] the result for axisymmetric perturbations ($k_r = k_\phi = 0$) is:

$$\omega^4 - \omega^2 \left[\kappa^2 + 2(k_z v_A)^2\right] + (k_z v_A)^2 \left[(k_z v_A)^2 + \kappa^2 - 4\Omega^2\right] = 0, \quad (10.1)$$

where $\kappa^2 = 2\Omega(2\Omega - r\, d\Omega/dr)$ is the square of the epicyclic frequency and $v_A = B_z/\sqrt{\mu_0 \rho}$ is the Alfvén speed.

[1] The full derivation involves linearizing the momentum equation, induction equation, and continuity equation, eliminating the density perturbation, and solving the resulting fourth-order polynomial. See Balbus & Hawley (1991) for details.

For a Keplerian disk, $\kappa^2 = \Omega^2$. The dispersion relation becomes:

$$\omega^4 - \omega^2 \left[\Omega^2 + 2(k_z v_A)^2\right] + (k_z v_A)^2 \left[(k_z v_A)^2 - 3\Omega^2\right] = 0.$$

Instability requires $\omega^2 < 0$ for some real k_z. Using the quadratic formula:

$$\omega^2 = \frac{1}{2}\left[\Omega^2 + 2(k_z v_A)^2 \pm \sqrt{(\Omega^2 + 2(k_z v_A)^2)^2 - 4(k_z v_A)^2\left((k_z v_A)^2 - 3\Omega^2\right)}\right].$$

The negative root can be negative (giving instability) when the last term inside the square root dominates. Working through the algebra, instability occurs when:

$$(k_z v_A)^2 < 3\Omega^2. \quad (10.2)$$

This is remarkable. The criterion says: if the field is weak enough that the Alfvén crossing time $(k_z v_A)^{-1}$ exceeds the rotation period Ω^{-1}, the system is unstable. There is no lower bound on the field strength—arbitrarily weak fields are unstable, just at long wavelengths.

10.4 Maximum Growth Rate

Let us find the fastest-growing mode.

Taking the derivative of ω^2 with respect to k_z and setting it to zero, the most unstable wavenumber is $k_z v_A = \sqrt{15/16}\,\Omega \approx 0.97\,\Omega$. Substituting back:

$$\gamma_{\max} = \frac{3}{4}\Omega. \quad (10.3)$$

The maximum growth rate is three-quarters of the orbital frequency! This is extraordinarily fast. An e-folding takes only $4/(3\Omega) \approx 1.3$ orbital periods. Within a few orbits, any weak magnetic field will be amplified enormously.

You might ask: doesn't this mean the MRI destroys itself? After all, as the field grows, eventually $(k_z v_A)^2 > 3\Omega^2$ and the instability shuts off.

Precisely so. The MRI amplifies the magnetic field until the field becomes strong enough to stabilize the flow. But then the field decays (through reconnection, which we'll discuss in the next chapter), the stability condition is violated again, and the MRI restarts. The saturated state is a dynamic balance: turbulence maintained by an instability that keeps shutting itself off and restarting.

Numerical simulations confirm this picture. The saturated MRI produces magnetic stresses with:

$$\frac{\langle B_r B_\phi \rangle}{\mu_0} \sim \alpha \, \rho c_s^2,$$

where $\alpha \sim 0.01$–0.1 matches the phenomenological values inferred from observations. The MRI naturally produces the right level of angular momentum transport.

10.5 Why Weak Fields Are Essential

You might ask: if strong magnetic fields are stabilizing, and weak fields are unstable, is there a minimum field strength for the MRI?

Yes, but it's a geometric constraint, not a stability threshold. The MRI requires the unstable wavelength to fit inside the disk. The most unstable wavelength is:

$$\lambda_{\rm MRI} = \frac{2\pi}{k_z} \sim \frac{2\pi v_A}{\Omega}.$$

For this to fit within the disk thickness H:

$$\frac{2\pi v_A}{\Omega} < H.$$

Since $H \sim c_s/\Omega$ for a thin disk, this requires $v_A < c_s/(2\pi)$, or in terms of plasma beta:

$$\beta = \frac{p_{\rm gas}}{p_{\rm mag}} = \frac{2c_s^2}{v_A^2} > 2(2\pi)^2 \approx 80.$$

The field must be weak—the magnetic pressure must be less than about one percent of the gas pressure. This is not a stringent requirement; most astrophysical disks have $\beta \sim 100$–10^4.

But the field cannot be zero. Without any magnetic field, there are no springs, no tension, and no instability. Purely hydrodynamic Keplerian disks are stable.[2]

This is why the MRI was such a revelation. It showed that weak magnetic fields don't just modify disk dynamics—they enable the entire accretion process.

[2] This is the Rayleigh criterion: a rotating flow is stable if angular momentum increases outward. Keplerian disks have $L = r^2\Omega \propto r^{1/2}$, which does increase outward. Without magnetic fields, Keplerian disks don't accrete.

10.6 A Protoplanetary Disk

Let us work through a concrete example: a protoplanetary disk around a young Sun-like star.

At a distance of 10 AU from a solar-mass star, the orbital parameters are:

$$\begin{aligned}\Omega &= \sqrt{\frac{GM_\odot}{r^3}} = \sqrt{\frac{6.67 \times 10^{-11} \times 2 \times 10^{30}}{(1.5 \times 10^{12})^3}} \\ &= \sqrt{\frac{1.33 \times 10^{20}}{3.4 \times 10^{36}}} = \sqrt{3.9 \times 10^{-17}} \\ &\approx 6.3 \times 10^{-9} \text{ rad/s}.\end{aligned}$$

The orbital period is $P = 2\pi/\Omega \approx 10^9$ s ≈ 32 years, consistent with what we expect at 10 AU.

For a typical protoplanetary disk at this radius:[3]

- Temperature $T \approx 50$ K
- Sound speed $c_s = \sqrt{k_B T/\mu m_p} \approx 500$ m/s (for molecular hydrogen)
- Disk thickness $H \sim c_s/\Omega \approx 8 \times 10^{10}$ m ≈ 0.5 AU
- Surface density $\Sigma \sim 10$ kg/m^2
- Midplane density $\rho \sim \Sigma/H \approx 10^{-10}$ kg/m^3

[3] These values come from the "minimum mass solar nebula" model and observations of T Tauri disk systems.

Now suppose the disk has a weak magnetic field with $\beta = 100$. The magnetic pressure is:

$$\frac{B^2}{2\mu_0} = \frac{p_{\text{gas}}}{\beta} = \frac{\rho c_s^2}{\beta} = \frac{10^{-10} \times (500)^2}{100} = 2.5 \times 10^{-7} \text{ Pa}.$$

Solving for the field strength:

$$B = \sqrt{2\mu_0 \times 2.5 \times 10^{-7}} = \sqrt{6.3 \times 10^{-13}} \approx 8 \times 10^{-7} \text{ T} = 8 \ \mu\text{G}.$$

This is a very weak field—about a hundred thousand times weaker than Earth's magnetic field. Yet it's enough to drive the MRI.

The Alfvén speed is:

$$v_A = \frac{B}{\sqrt{\mu_0 \rho}} = \frac{8 \times 10^{-7}}{\sqrt{4\pi \times 10^{-7} \times 10^{-10}}} = \frac{8 \times 10^{-7}}{\sqrt{1.3 \times 10^{-16}}} \approx 70 \text{ m/s}.$$

The most unstable wavelength is:

$$\lambda_{\text{MRI}} = \frac{2\pi v_A}{\Omega} = \frac{2\pi \times 70}{6.3 \times 10^{-9}} \approx 7 \times 10^{10} \text{ m} \approx 0.5 \text{ AU}.$$

This is comparable to the disk thickness—the MRI wavelength fits comfortably within the disk.

The growth time is:

$$\tau_{\rm MRI} = \frac{4}{3\Omega} = \frac{4}{3 \times 6.3 \times 10^{-9}} \approx 2 \times 10^8 \text{ s} \approx 6 \text{ years}.$$

Within about six years—a small fraction of the 32-year orbital period—any initial perturbation will have grown by a factor of e. After a few orbits, the disk is thoroughly turbulent.

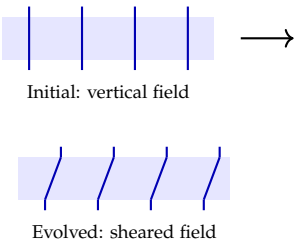

Figure 10.2: MRI evolution: initially vertical field lines are sheared by differential rotation, amplifying the field.

10.7 Forgotten and Rediscovered

The MRI has a peculiar history. It was discovered three times.

In 1959, Evgeny Velikhov at the Kurchatov Institute in Moscow was studying the stability of rotating conducting fluids—a question motivated by plasma confinement for fusion. He found that rotation stabilized some instabilities but created new ones when combined with magnetic fields. His analysis contained what we now call the MRI, but applied to cylindrical plasmas, not disks.

In 1961, Subrahmanyan Chandrasekhar at the University of Chicago published his monumental treatise *Hydrodynamic and Hydromagnetic Stability*. Chandrasekhar was cataloging every instability known to fluid mechanics, and he included the case of rotating magnetized fluids. His equations are equivalent to Velikhov's. But Chandrasekhar was interested in the mathematical structure of stability theory, not in astrophysical applications. The result sat in a book that everyone owned but few read carefully.

You might ask: how did such an important result stay hidden for thirty years?

The answer lies in the sociology of science. Velikhov was a plasma physicist thinking about fusion reactors. Chandrasekhar was a mathematical physicist building a taxonomy of instabilities. Neither was thinking about accretion disks. And the astrophysicists struggling with the angular momentum problem in disks weren't reading papers on magnetized Taylor-Couette flow.

Meanwhile, the accretion disk community invented elaborate workarounds. The α-prescription let people calculate disk structure without understanding the physics. Some proposed that disks were convective. Others invoked spiral waves. A few even suggested that disks didn't really accrete—that the gas fell in through some other mechanism entirely.

Then in 1991, Steve Balbus at the University of Virginia and John Hawley at the University of Virginia reexamined the problem. They knew about the old stability analyses. They also knew about accretion disks. They put two and two together.

Their paper "A Powerful Local Shear Instability in Weakly Magnetized Disks" showed that any disk with decreasing angular velocity and any magnetic field at all is unstable. The growth rate is fast—comparable to the orbital frequency. The instability naturally produces turbulent stresses of the right magnitude to explain observed accretion rates.

The paper was initially rejected. One referee complained that the result was "well known." In a sense it was—to anyone who had read Chandrasekhar carefully. But its implications for accretion had never been drawn.

After publication, the impact was immediate. Within a few years, numerical simulations confirmed the picture. By the end of the decade, the MRI was the standard model for angular momentum transport in accretion disks. Balbus and Hawley's paper now has over 4,000 citations.

The lesson is sobering. For thirty years, the solution to a major astrophysical problem sat in textbooks, waiting for someone to notice. Progress came not from new observations or more powerful computers, but from asking the right question.

10.8 Laboratory Verification

You might ask: can we see the MRI in the laboratory?

The challenge is formidable. The MRI requires a conducting fluid in differential rotation with a weak magnetic field. Most fluids aren't good conductors. Those that are—liquid metals like gallium or sodium—have high magnetic diffusivity, which damps the MRI before it can grow.

The magnetic Reynolds number $Rm = vL/\eta$, where η is the magnetic diffusivity, must exceed unity for the MRI to operate. For liquid gallium, $\eta \approx 0.2$ m^2/s. With $L \sim 0.1$ m and $v \sim 1$ m/s (typical for a laboratory experiment), $Rm \sim 0.5$—too small.

Nevertheless, experimenters persevered. The Princeton MRI Experiment uses liquid gallium in a Taylor-Couette apparatus: two concentric cylinders with the fluid in the gap between them. The inner cylinder rotates faster than the outer (mimicking Keplerian shear), and axial magnetic fields are applied.

In 2022, the Princeton group definitively detected the MRI in liquid metal, confirming the mechanism that had been theoretically understood for decades. Earlier experiments at Maryland and HZDR Dresden had shown suggestive results, but the Princeton detection was the first unambiguous laboratory confirmation.[4]

What we can say is that the basic physics is confirmed. Rotating conducting fluids with weak magnetic fields do show instabilities

[4] The difficulty is that laboratory experiments operate near marginal stability, where multiple instabilities compete. Clean detection of the MRI requires careful control of boundary conditions and magnetic field geometry.

consistent with the MRI mechanism. The spring analogy works.

10.9 Why Angular Velocity, Not Angular Momentum?

Let us return to a subtle point that deserves emphasis.

The classical Rayleigh criterion for rotating flows says: stability requires angular momentum $L = r^2\Omega$ to increase outward, $dL/dr > 0$. A Keplerian disk has $L \propto r^{1/2}$, which does increase outward. By Rayleigh's criterion, Keplerian disks are stable.

The MRI criterion says: instability occurs if angular velocity Ω decreases outward, $d\Omega/dr < 0$. A Keplerian disk has $\Omega \propto r^{-3/2}$, which does decrease outward. By the MRI criterion, Keplerian disks are unstable.

How can both be true? The answer is that they apply to different situations:

- **Rayleigh**: hydrodynamic (no magnetic field)
- **MRI**: magnetohydrodynamic (with magnetic field)

The magnetic field enables a new channel for instability. Without it, angular momentum exchange requires direct collisions between fluid elements—a process governed by angular momentum gradients. With it, magnetic tension can transfer angular momentum across finite distances—a process governed by the shear rate, which depends on angular velocity gradients.

The MRI destabilizes flows that hydrodynamics declares stable. This is why weak magnetic fields are so important in astrophysics: they change the fundamental stability properties of rotating systems.

10.10 The Saturated State

You might ask: if the MRI grows exponentially, why doesn't it amplify the magnetic field to arbitrarily large values?

The instability is self-limiting. As the field amplifies, eventually $(k_z v_A)^2 > 3\Omega^2$ and the instability shuts off. But then other processes take over.

The amplified field is tangled and turbulent. Magnetic reconnection (Chapter 11) dissipates some of the field energy as heat. Turbulent cascade transfers energy to small scales where it dissipates. The field strength decreases until the MRI criterion is satisfied again, and the instability restarts.

The saturated state is a balance: the MRI amplifies the field, dissipation reduces it, and the two processes reach a dynamic equilibrium. This equilibrium determines the level of turbulence and hence the effective viscosity of the disk.

Numerical simulations show that the saturated state depends on details: the strength and geometry of the net magnetic flux, the ionization fraction of the disk (which affects the coupling between gas and field), and even the numerical resolution of the simulation. The MRI is easy to understand in its linear phase but subtle in its nonlinear behavior.

What we can say with confidence: the MRI produces turbulent stresses that transport angular momentum outward at rates consistent with observed accretion. The basic mechanism works. The details are still being worked out.

10.11 Dead Zones and Layered Accretion

Not all disks are ideal conductors. In protoplanetary disks, the dense midplane can be so cold that there are few free electrons. Without charged particles, there's no coupling between gas and field, and the MRI cannot operate.

These "dead zones" create a layered structure. The surface layers of the disk, ionized by stellar X-rays and cosmic rays, are MRI-active and turbulent. The dense midplane is quiescent, protected from ionizing radiation by the gas above it.

Angular momentum transport in such a disk is complicated. The active surface layers can accrete while the dead zone sits passively. Material may accumulate at the boundaries between active and dead regions. Some models suggest that dead zones are where planetesimals form—the quiescent midplane allows dust to settle and clump without being disrupted by turbulence.

The geography of dead zones depends on temperature, density, ionization sources, and even the abundance of small dust grains (which soak up free electrons). It's a rich problem that connects disk physics to planet formation.

10.12 The Engine of Cosmic Accretion

Let us step back and appreciate what the MRI accomplishes.

A cosmic conspiracy seems to prevent accretion. Molecular viscosity is negligible. Hydrodynamics is stable. Angular momentum conservation appears to lock gas in eternal orbits.

But the universe found a loophole. The tiniest magnetic field—so weak it exerts negligible force directly—enables a powerful instability that drives turbulence and transports angular momentum. The weakness of the field is essential, not a limitation. A strong field would be stable.

The MRI powers quasars, the brightest objects in the universe. It

enables young stars to grow by consuming their birth material. It determines the structure of accretion disks around black holes in X-ray binaries. Everywhere that gas orbits a compact object and slowly spirals inward, the MRI is likely at work.

And the solution sat in textbooks for thirty years, waiting for someone to ask the right question. Physics is universal, but recognizing which physics applies where requires connecting communities and asking new questions about old results.

10.13 Looking Ahead

The MRI grows by stretching magnetic field lines, building up magnetic energy through the work done against magnetic tension. But this process cannot continue forever. Eventually the field becomes too contorted, too stressed. The frozen-in approximation breaks down. Field lines find shortcuts, rearranging their topology and releasing stored energy.

This is magnetic reconnection—the subject of our next chapter. Where the MRI is a story of gradual amplification, reconnection is a story of sudden release. Together, they form a cycle that regulates magnetic energy in plasmas throughout the universe.

11
Magnetic Reconnection

11.1 When Frozen-In Fails

On March 13, 1989, the entire province of Quebec went dark. Six million people lost power for nine hours. Transformers melted. The northern lights were visible as far south as Texas.

The cause was not equipment failure or human error. Two days earlier, a coronal mass ejection—a billion tons of magnetized plasma—had erupted from the Sun. When it slammed into Earth's magnetic field, something catastrophic happened at the boundary. Where the solar field pointed southward and Earth's field pointed northward, the opposing fields annihilated each other. Magnetic energy that had traveled ninety million miles from the Sun released in Earth's magnetosphere, driving currents through the ionosphere that induced voltages in power lines below.

This is magnetic reconnection: the process by which field lines break and rejoin, changing magnetic topology and releasing stored energy. It is the great exception to Alfvén's frozen-in theorem. Most of the time, in most of space, field lines are frozen into the plasma and cannot change their connections. But in thin current sheets where opposing fields meet, resistivity matters, topology changes, and energy is released.

Reconnection powers solar flares, accelerates the solar wind, triggers auroral substorms, and limits plasma confinement in fusion devices. It is the violent counterpoint to the frozen-in order that we have celebrated through nine chapters of this book. Understanding when and how the frozen-in constraint fails is essential to understanding how the magnetic universe actually works.

11.2 Opposing Fields in Contact

Let us begin with the simplest picture.

Imagine two regions of plasma, each carrying a magnetic field,

being pushed together by some external flow. On the left, the field points upward. On the right, it points downward. Where they meet, the field must reverse direction, passing through zero.

At the interface, $\nabla \times \mathbf{B} \neq 0$, which means (by Ampère's law) there must be a current. This current is concentrated in a thin layer—the current sheet. The thickness of the sheet is set by a competition: the external flow pushes the fields together, trying to make the sheet thinner; resistive diffusion spreads the current out, trying to make the sheet thicker. The equilibrium thickness depends on how fast the fields are being pushed together.

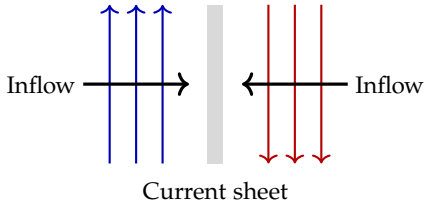

Figure 11.1: Opposing magnetic fields pushed together form a current sheet where the field reverses.

In this current sheet, something remarkable can happen. The frozen-in theorem requires infinite conductivity; real plasmas have finite resistivity. In most of space, this resistivity is negligible—the magnetic Reynolds number is enormous, and field lines are effectively frozen. But in the current sheet, where gradients are steep and the field passes through zero, resistivity matters.

Think of it this way: field lines are like threads sewn into a fabric. Normally the threads move with the fabric and cannot be cut. But at the current sheet, the fabric is thin and the scissors of resistivity can snip the threads. When threads from opposite sides are cut, they can be reconnected in new ways.

This is the essence of magnetic reconnection: field lines that were connected to plasma on the left become connected to plasma on the right, and vice versa. The topology of the magnetic field changes. Energy stored in the stressed field configuration is released.

11.3 *The Sweet-Parker Model*

Let us now make this quantitative.

In 1957, Eugene Parker at the University of Chicago and, independently, in 1958, Peter Sweet in England, worked out the simplest self-consistent model of steady reconnection. Their geometry is elegant: a long, thin current sheet of length L (the system size) and thickness $\delta \ll L$.

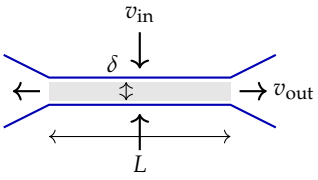

Figure 11.2: Sweet-Parker geometry: plasma flows in slowly (v_{in}), reconnects in the thin sheet (thickness δ, length L), and is expelled at $v_{\text{out}} \sim v_A$.

Plasma flows into the sheet from above and below at velocity v_{in}, carrying magnetic flux with it. Inside the sheet, the field reconnects, and plasma is expelled horizontally at velocity v_{out}.

Mass conservation relates the velocities:

$$v_{\text{in}} \cdot L = v_{\text{out}} \cdot \delta.$$

The mass flowing into the sheet from the sides must equal the mass flowing out the ends.

The outflow velocity is set by the magnetic tension of the newly reconnected field lines, which catapult the plasma out like a slingshot.

This gives $v_{\text{out}} \sim v_A$, the Alfvén speed.

For the inflow velocity, we balance Ohm's law. In the sheet, the convective electric field $v_{\text{in}} \times B$ must be balanced by resistive dissipation ηJ, where $J \sim B/(\mu_0 \delta)$ is the current density. This gives:

$$v_{\text{in}} B \sim \eta \frac{B}{\mu_0 \delta}, \quad \text{so} \quad v_{\text{in}} \sim \frac{\eta}{\mu_0 \delta}.$$

Combining with mass conservation:

$$\frac{v_{\text{in}}}{v_A} = \frac{\delta}{L}, \quad \text{and} \quad v_{\text{in}} \sim \frac{\eta}{\mu_0 \delta}.$$

Eliminating δ:

$$\frac{v_{\text{in}}}{v_A} = S^{-1/2}, \tag{11.1}$$

where $S = \mu_0 L v_A / \eta$ is the Lundquist number.[1]

The sheet thickness follows:

$$\frac{\delta}{L} = S^{-1/2}.$$

[1] The Lundquist number is essentially the magnetic Reynolds number $Rm = LV/\lambda$ using the Alfvén speed as the characteristic velocity: $S = Lv_A/\lambda$, where $\lambda = \eta/\mu_0$ is the magnetic diffusivity. In reconnection problems, v_A is the natural velocity scale because it determines the outflow speed.

11.4 The Problem: Too Slow

Let us apply Sweet-Parker to the solar corona.

A typical active region has:

- System size $L \sim 10^7$ m (about 10 Mm, or 10,000 km)
- Magnetic field $B \sim 0.01$ T (100 G)
- Density $n \sim 10^{15}$ m^{-3}
- Temperature $T \sim 10^6$ K

The Alfvén speed is:

$$v_A = \frac{B}{\sqrt{\mu_0 \rho}} = \frac{B}{\sqrt{\mu_0 n m_p}} = \frac{0.01}{\sqrt{4\pi \times 10^{-7} \times 10^{15} \times 1.7 \times 10^{-27}}} \approx 7 \times 10^6 \text{ m/s}.$$

The magnetic diffusivity in a fully ionized plasma is set by Coulomb collisions:[2]

$$\lambda = \frac{\eta}{\mu_0} \sim 1 \text{ m}^2/\text{s}.$$

[2] This is the Spitzer resistivity, which depends on temperature as $\eta \propto T^{-3/2}$. At coronal temperatures, resistivity is very low.

The Lundquist number is:

$$S = \frac{L v_A}{\lambda} = \frac{10^7 \times 7 \times 10^6}{1} = 7 \times 10^{13}.$$

The Sweet-Parker reconnection rate is:

$$\frac{v_{\text{in}}}{v_A} = S^{-1/2} = (7 \times 10^{13})^{-1/2} \approx 1.2 \times 10^{-7}.$$

The inflow velocity is $v_{\text{in}} \approx 1.2 \times 10^{-7} \times 7 \times 10^{6} \approx 0.8$ m/s—still just a walking pace.

The reconnection time is:

$$\tau_{\text{SP}} = \frac{L}{v_{\text{in}}} = \frac{10^7}{0.8} \approx 1.2 \times 10^7 \text{ s} \approx 5 \text{ months}.$$

But solar flares release their energy in minutes! The largest flares reach peak power in under ten minutes and decay over an hour. Sweet-Parker predicts reconnection times tens of thousands of times longer than observed.

You might ask: perhaps the reconnection region is much smaller than the active region? This helps somewhat—reducing L increases the rate. But even shrinking L by a factor of 1000 only speeds up reconnection by a factor of $\sqrt{1000} \approx 30$. The discrepancy is too large to fix by adjusting geometry.

Something fundamental is wrong with Sweet-Parker. Or rather, something fundamental is missing.

11.5 *Faster Reconnection*

The Sweet-Parker rate $v_{\text{in}}/v_A \sim S^{-1/2}$ is set by the aspect ratio of the current sheet: $\delta/L = S^{-1/2}$. A long, thin sheet processes magnetic flux slowly because the outflow bottleneck is narrow.

You might ask: can the sheet be shorter? Harry Petschek at the Avco-Everett Research Laboratory proposed in 1964 that it could. Instead of a single extended current sheet, Petschek imagined a compact diffusion region surrounded by standing slow-mode shocks.

In Petschek's model, the diffusion region where resistivity matters is tiny—of order δ^2 rather than $\delta \times L$. The shocks extending from this region do most of the work, converting magnetic energy to kinetic energy as plasma crosses them. The reconnection rate becomes:

$$\frac{v_{\text{in}}}{v_A} \sim \frac{\pi}{8 \ln S} \approx 0.01\text{–}0.1. \tag{11.2}$$

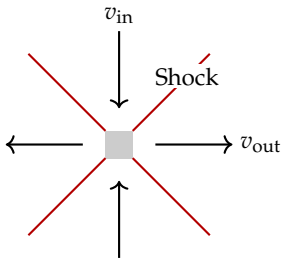

Figure 11.3: Petschek geometry: a small diffusion region (gray) with standing shock waves (red) that do most of the energy conversion.

This matches observations! Flares, substorms, and other reconnection events typically show rates of 0.01–0.1 times the Alfvén speed.

But there was a problem. When researchers ran computer simulations of resistive MHD, starting from smooth initial conditions, Petschek's geometry didn't emerge. The current sheet stubbornly evolved toward the Sweet-Parker configuration. You had to impose Petschek's geometry by hand; it wasn't self-consistent.

For thirty years, this was a puzzle. Why did nature achieve fast reconnection while simulations predicted slow reconnection?

11.6 Beyond Single-Fluid MHD

The resolution came from going beyond standard MHD.

Let us return to Ohm's law. The simplest form, $\mathbf{E} + \mathbf{v} \times \mathbf{B} = \eta \mathbf{J}$, treats the plasma as a single conducting fluid. But plasma consists of two species: ions and electrons. The full generalized Ohm's law includes additional terms:

$$\mathbf{E} + \mathbf{v} \times \mathbf{B} = \eta \mathbf{J} + \frac{1}{ne}(\mathbf{J} \times \mathbf{B} - \nabla p_e) + \frac{m_e}{ne^2}\frac{\partial \mathbf{J}}{\partial t}. \tag{11.3}$$

The term $\mathbf{J} \times \mathbf{B}/(ne)$ is the Hall term. It becomes important when the current sheet thickness δ approaches the ion skin depth:

$$d_i = \frac{c}{\omega_{pi}} = \sqrt{\frac{m_i}{\mu_0 n e^2}},$$

where $\omega_{pi} = \sqrt{ne^2/(\varepsilon_0 m_i)}$ is the ion plasma frequency.

For coronal parameters ($n \sim 10^{15}$ m^{-3}):

$$d_i = \sqrt{\frac{1.7 \times 10^{-27}}{4\pi \times 10^{-7} \times 10^{15} \times (1.6 \times 10^{-19})^2}} \approx 7 \text{ m}.$$

You might ask: how can physics at the 7-meter scale affect dynamics at the 10,000-km scale?

The answer lies in the reconnection geometry. As reconnection proceeds, the current sheet thins. In Sweet-Parker, $\delta = LS^{-1/2}$; for our coronal example, $\delta \approx 10^7 \times (7 \times 10^{13})^{-1/2} \approx 1$ m. The sheet naturally thins to the ion skin depth scale!

At this scale, ions and electrons no longer move together. Electrons, being much lighter, can flow through the diffusion region carrying the current. Ions, heavier and slower to respond, are left behind. The plasma becomes "two-fluid" rather than single-fluid MHD.

This decoupling changes everything. The effective outflow speed for electrons is much higher than for ions. The aspect ratio constraint that doomed Sweet-Parker is broken. The reconnection rate jumps to $\sim 0.1\, v_A$, matching observations.[3]

[3] Hall MHD and kinetic simulations consistently show reconnection rates of 0.1–0.2 v_A, nearly independent of the Lundquist number once S is large enough for the current sheet to thin to the ion scale.

11.7 The Plasmoid Instability

There is another route to fast reconnection that doesn't require leaving MHD entirely.

In 2007, Loureiro, Schekochihin, and Cowley showed that at very high Lundquist number, the Sweet-Parker current sheet becomes unstable. It tears into a chain of magnetic islands—plasmoids—separated by secondary current sheets.

The instability is a variant of the tearing mode we encountered in Chapter 8, but applied to a reconnecting current sheet rather than a static one. When $S > S_{\text{crit}} \approx 10^4$, the sheet fragments before it can reach the Sweet-Parker aspect ratio.

Plasmoid chain

Figure 11.4: At high Lundquist number, the current sheet fragments into a chain of plasmoids separated by X-points.

Each secondary current sheet can itself fragment, creating a hierarchy of scales. The net effect is to increase the effective reconnection rate: instead of one slow Sweet-Parker sheet, there are many smaller reconnection sites operating in parallel.

The plasmoid-mediated reconnection rate scales differently from Sweet-Parker:

$$\frac{v_{\text{in}}}{v_A} \sim S^{-\alpha}, \quad \text{with } \alpha \approx 0.3\text{–}0.4.$$

This is faster than Sweet-Parker ($\alpha = 0.5$) though still dependent on S. For very large S, the plasmoid instability may be the dominant mechanism enabling fast reconnection.

11.8 A Solar Flare

Let us now apply our understanding to a concrete event: a large solar flare.

Consider an active region with the following parameters:[4]

[4] These values are typical for X-class flares, the most powerful category in the standard classification.

- Linear size $L \sim 3 \times 10^7$ m (30 Mm)
- Magnetic field strength $B \sim 0.05$ T (500 G)
- Coronal density $n \sim 10^{16}$ m^{-3}

The magnetic energy stored in this region is:

$$E_{\text{mag}} = \frac{B^2}{2\mu_0} \times L^3 = \frac{(0.05)^2}{2 \times 4\pi \times 10^{-7}} \times (3 \times 10^7)^3.$$

Let us compute step by step:

$$\frac{B^2}{2\mu_0} = \frac{2.5 \times 10^{-3}}{8\pi \times 10^{-7}} = \frac{2.5 \times 10^{-3}}{2.5 \times 10^{-6}} = 1000 \text{ J/m}^3.$$

The volume is $L^3 = (3 \times 10^7)^3 = 2.7 \times 10^{22}$ m^3.

So:

$$E_{\text{mag}} = 1000 \times 2.7 \times 10^{22} = 2.7 \times 10^{25} \text{ J}.$$

For reference, this is about 6×10^9 megatons of TNT equivalent—six billion hydrogen bombs.

Not all this energy is released in a flare; typically 10–50% is converted. Taking 30%:

$$E_{\text{flare}} \approx 8 \times 10^{24} \text{ J}.$$

If the flare lasts $\tau \approx 1000$ s (about 15 minutes), the average power is:

$$P = \frac{E_{\text{flare}}}{\tau} = \frac{8 \times 10^{24}}{1000} = 8 \times 10^{21} \text{ W}.$$

The Sun's total luminosity is 4×10^{26} W, so this flare outputs about 2×10^{-5} of the Sun's power—but concentrated in a region that is only $\sim 10^{-6}$ of the solar surface. Locally, the power density exceeds the quiet Sun by a factor of 20.

You might ask: where does this energy go?

The answer: everywhere. Reconnection heats plasma to tens of millions of degrees, producing thermal X-rays. It accelerates electrons to relativistic speeds, producing hard X-rays and gamma rays when they slam into denser material. It drives mass motions (jets, eruptions) and launches shock waves into the heliosphere. The March 1989 storm was triggered by just such an eruption—a coronal mass ejection carrying 10^{12} kg of plasma at 1000 km/s.

11.9 Reconnection in the Laboratory

You might ask: can we study reconnection in the laboratory?

Indeed we can. The Magnetic Reconnection Experiment (MRX) at Princeton has been studying reconnection physics since 1995. The device creates opposing magnetic fields in a toroidal geometry and drives them together, forming a current sheet that reconnects.

MRX has confirmed many theoretical predictions: the formation of current sheets, the acceleration of plasma to Alfvén speeds, the role of Hall physics in speeding up reconnection. The measured reconnection rate of $\sim 0.1\, v_A$ matches both simulations and astrophysical observations.

More recently, NASA's Magnetospheric Multiscale (MMS) mission, launched in 2015, has directly observed reconnection in Earth's magnetosphere. The four MMS spacecraft fly in tight formation (sometimes separated by only 10 km), allowing them to resolve the electron diffusion region—the tiny central zone where electrons decouple from ions.

MMS observations have confirmed the Hall physics picture. They've seen the characteristic quadrupolar magnetic field pattern predicted by two-fluid theory. They've measured electron jets consistent with theory. The 50-year-old puzzle of fast reconnection is now largely solved, at least for the collisionless plasmas of near-Earth space.

11.10 When Does Reconnection Happen?

We have discussed how reconnection happens fast, but not what triggers it.

The fundamental requirement is a current sheet—a region where opposing magnetic fields meet. Such sheets form naturally when magnetized plasmas are pushed together by external flows, or when field lines are sheared and twisted.

But a current sheet can exist for a long time without reconnecting. The sheet must thin to the scale where fast reconnection is enabled (the ion skin depth for collisionless plasmas, or the scale where plasmoid instability sets in for resistive plasmas). This thinning is driven by the continued compression of the opposing fields.

Think of reconnection as a pressure relief valve. Magnetic stress builds up as fields are pushed together or twisted. The system resists, maintaining force balance through the current sheet. But the sheet keeps thinning, and eventually it reaches the critical scale. Then reconnection turns on suddenly, releasing the stored stress in a burst.

This is why reconnection events are often impulsive. The buildup is gradual—days for a solar active region, hours for a magnetospheric substorm. The release is rapid—minutes for a flare, seconds for a substorm onset. The metaphor of a loaded spring, held at bay until a trigger releases it, captures the physics.

11.11 The Broken Threads

Let us step back and appreciate what reconnection means for our understanding of magnetized plasmas.

Through most of this book, we have treated magnetic field lines as inviolable. They are frozen into the plasma, carried along by its motions, unable to break or change their connections. This frozen-in property gives magnetic fields their dynamical importance—they link distant regions, transmit forces, and constrain plasma motions.

Reconnection is where this picture fails. In thin current sheets, under the right conditions, the threads can be cut and resewn. Topology changes. Energy is released.

But reconnection does not invalidate the frozen-in picture; it completes it. The frozen-in approximation is accurate almost everywhere—in the vast volumes of space where current densities are low and resistivity is negligible. Reconnection happens only in special places: the thin sheets where opposing fields meet. These sites are rare but important, like the seams in a quilt. Most of the fabric is continuous; only at the seams can the pattern change.

The combination of frozen-in dynamics and localized reconnection

produces the behavior we observe: long periods of gradual evolution punctuated by sudden restructuring events. Magnetic flux accumulates, stresses build, and then a flare or substorm releases the tension. The cycle repeats.

This interplay—order and catastrophe, frozen and reconnecting—is how the magnetic universe actually operates.

11.12 *Looking Ahead*

We have now surveyed the major instabilities and dynamic processes of MHD: waves that carry information and energy, equilibria that balance forces, kinks and interchanges that disrupt those equilibria, the magnetorotational instability that drives accretion, and reconnection that releases magnetic energy.

But our treatment has been idealized. Real astrophysical systems are turbulent—filled with fluctuations on all scales, energy cascading from large to small, structures forming and dissolving in a chaotic dance. MHD turbulence is richer than its hydrodynamic cousin because of the magnetic field's anisotropy: fluctuations are different parallel and perpendicular to the field.

Understanding this turbulence—its statistics, its energy cascade, its role in transport and heating—is the subject of our next chapter.

Part III

Turbulence and Astrophysical Applications

12
MHD Turbulence

12.1 Cream in Coffee

Pour cream into coffee and watch it swirl. The patterns are beautiful—whorls and filaments, stretching and folding, chaos in a cup. Each pour is different. The details are unpredictable, yet something is universal: the cream always mixes, always creates the same kind of intricate structure, always reaches the same end state.

This is turbulence. It is the most common state of fluids in the universe, from the atmosphere we breathe to the gas between the stars. Understanding it requires giving up on predicting individual motions and instead describing statistics—how energy is distributed across scales, how fluctuations correlate in space and time, how the chaos organizes itself.

Now imagine the coffee is a plasma threaded by magnetic field lines. The cream doesn't just swirl—it swirls differently along the field than across it. Try to stir perpendicular to the field, and magnetic tension resists; stir along the field, and the fluid moves freely. The field imposes a direction, and the turbulence becomes anisotropic.

MHD turbulence is what happens when magnetic fields meet chaos. It governs the solar wind streaming past Earth, the interstellar medium filling the space between stars, the transport of angular momentum in accretion disks, and the confinement of plasma in fusion reactors. Understanding it requires extending Kolmogorov's classic picture of hydrodynamic turbulence to something richer and more structured.

12.2 Kolmogorov's Legacy

Let us begin with the foundation: Kolmogorov's 1941 theory of hydrodynamic turbulence.

The central insight is deceptively simple. Energy is injected into the fluid at large scales—by stirring the coffee, by convection in the

atmosphere, by jets in an accretion disk. This energy cannot stay at large scales; nonlinear interactions transfer it to smaller scales. An eddy of size L breaks into eddies of size $L/2$, which break into eddies of size $L/4$, and so on. The cascade continues until the eddies are so small that viscosity dissipates their energy as heat.

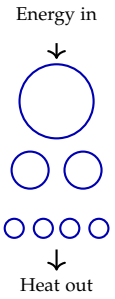

Figure 12.1: The turbulent cascade: energy flows from large eddies to small, where it dissipates as heat.

In the "inertial range"—the range of scales between injection and dissipation—the only relevant quantity is the energy cascade rate ε, measured in watts per kilogram. Dimensional analysis then determines everything.

An eddy of size ℓ has characteristic velocity v_ℓ. Its kinetic energy per mass is v_ℓ^2, and its turnover time is $\tau_\ell \sim \ell/v_\ell$. The rate at which energy cascades through this scale is:

$$\varepsilon \sim \frac{v_\ell^2}{\tau_\ell} \sim \frac{v_\ell^3}{\ell}.$$

Since ε is constant throughout the inertial range (what comes in must go out), we can solve for the velocity:

$$v_\ell \sim (\varepsilon \ell)^{1/3}. \tag{12.1}$$

Smaller eddies have smaller velocities. This is the Kolmogorov scaling.

The energy spectrum follows. The energy per unit wavenumber $E(k)$ represents how much kinetic energy resides in eddies of size $\ell \sim 1/k$. Since energy density scales as $v_\ell^2 \sim (\varepsilon\ell)^{2/3} \sim \varepsilon^{2/3}k^{-2/3}$, and $E(k)$ is energy per unit k, we need one more factor of k^{-1}:

$$E(k) \sim \varepsilon^{2/3} k^{-5/3}. \tag{12.2}$$

This $k^{-5/3}$ power law is one of the most robust results in physics. It has been verified in laboratory experiments, atmospheric measurements, and numerical simulations spanning decades of scale. The cream mixing into your coffee obeys it. So does the interstellar medium.

12.3 *Adding a Magnetic Field*

Let us now add a uniform magnetic field $\mathbf{B}_0$ and see what changes.

The field introduces a preferred direction. Perturbations can propagate along $\mathbf{B}_0$ as Alfvén waves, traveling at speed $v_A = B_0/\sqrt{\mu_0\rho}$. An eddy that tries to stretch field lines feels magnetic tension pulling back. The turbulence is no longer isotropic.

Consider a thought experiment. You're stirring the plasma perpendicular to the field. Magnetic tension resists, converting kinetic energy into magnetic perturbations. You're stirring parallel to the

field. Nothing special happens—the fluid moves freely, carrying the field lines along.

This asymmetry is the heart of MHD turbulence. Energy cascades differently in different directions.

You might ask: how do different scales communicate in MHD turbulence?

In hydrodynamic turbulence, eddies directly interact: a large eddy advects smaller eddies, shearing them and transferring energy. In MHD turbulence, there's an additional mechanism: Alfvén waves.

Imagine two Alfvén wave packets propagating in opposite directions along $\mathbf{B}_0$. When they collide, they interact nonlinearly, distorting each other and transferring energy to smaller scales. But the interaction only lasts for the collision time $\tau_A \sim \ell_\parallel / v_A$, where $\ell_\parallel$ is the scale of the wave packet along the field.

If the wave packets are narrow (small $\ell_\parallel$), they pass through each other quickly, barely interacting. If they are wide (large $\ell_\parallel$), they interact for a long time. The efficiency of energy transfer depends on this geometry.

12.4 *Critical Balance*

The key insight, due to Peter Goldreich and S. Sridhar in 1995, is what they called "critical balance."

The idea is simple: the turbulent cascade is most efficient when two timescales are equal.

One timescale is the eddy turnover time perpendicular to the field:

$$\tau_{\text{eddy}} \sim \frac{\ell_\perp}{v_\ell},$$

where $\ell_\perp$ is the eddy size perpendicular to $\mathbf{B}_0$ and v_ℓ is the turbulent velocity at that scale.

The other timescale is the Alfvén wave crossing time parallel to the field:

$$\tau_A \sim \frac{\ell_\parallel}{v_A},$$

where $\ell_\parallel$ is the eddy extent along $\mathbf{B}_0$.

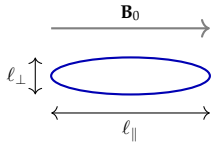

Figure 12.2: Critical balance: eddies are elongated along the magnetic field, with $\ell_\parallel \gg \ell_\perp$ at small scales.

Critical balance states that these timescales are comparable throughout the cascade:

$$\tau_{\text{eddy}} \sim \tau_A, \quad \text{i.e.,} \quad \frac{\ell_\perp}{v_\ell} \sim \frac{\ell_\parallel}{v_A}. \tag{12.3}$$

Why should this be true? If $\tau_{\text{eddy}} \ll \tau_A$, the eddy turns over before Alfvén waves can propagate across it. The interaction is essentially hydrodynamic, and the eddies quickly cascade to smaller scales. If $\tau_{\text{eddy}} \gg \tau_A$, Alfvén waves cross the eddy many times before it turns

over; the nonlinear interaction is weak, and the cascade is slow. The most efficient cascade occurs when the two timescales are comparable.

Let us work out the consequences.

From Kolmogorov scaling in the perpendicular direction, $v_\ell \sim (\varepsilon \ell_\perp)^{1/3}$. Substituting into critical balance:

$$\frac{\ell_\perp}{(\varepsilon \ell_\perp)^{1/3}} \sim \frac{\ell_\parallel}{v_A}.$$

Solving for $\ell_\parallel$:

$$\ell_\parallel \sim \frac{v_A}{\varepsilon^{1/3}} \ell_\perp^{2/3}. \tag{12.4}$$

The parallel scale grows more slowly than the perpendicular scale as we go to smaller eddies. Eddies become increasingly elongated along the field at small scales.

At the outer scale L, suppose $\ell_\parallel \sim \ell_\perp \sim L$ (the turbulence is injected isotropically). At smaller scales:

$$\frac{\ell_\parallel}{\ell_\perp} \sim \left(\frac{L}{\ell_\perp}\right)^{1/3}.$$

An eddy ten times smaller than the injection scale is elongated by a factor of $10^{1/3} \approx 2$. An eddy a thousand times smaller is elongated by a factor of 10. At small scales, the turbulence is essentially two-dimensional: structures vary rapidly perpendicular to the field but slowly parallel to it.

12.5 Energy Spectra

The energy spectra follow from critical balance.

In the perpendicular direction, the cascade proceeds essentially as in Kolmogorov turbulence:

$$E(k_\perp) \sim \varepsilon^{2/3} k_\perp^{-5/3}. \tag{12.5}$$

The familiar $-5/3$ slope persists.

In the parallel direction, the spectrum is steeper. Energy is transferred to smaller perpendicular scales more readily than to smaller parallel scales. The parallel spectrum is:

$$E(k_\parallel) \sim v_A \varepsilon^{1/2} k_\parallel^{-2}. \tag{12.6}$$

The $k_\parallel^{-2}$ slope means energy drops off more rapidly with decreasing parallel scale. Most of the fluctuation energy resides in structures that are elongated along the field.

You might ask: does this theory actually work?

The solar wind provides a natural laboratory. Spacecraft at 1 AU measure fluctuations in magnetic field and velocity over many decades of scale. The observations show:

- A $k^{-5/3}$ spectrum in the perpendicular direction, as predicted.
- Anisotropy consistent with critical balance: smaller structures are more elongated along the field.
- Fluctuations dominated by Alfvénic modes (velocity and magnetic field fluctuations correlated as expected for Alfvén waves).

The Goldreich-Sridhar theory, developed for an idealized case, captures the essential physics of turbulence in the solar wind.

12.6 The Historical Path

Let us pause to appreciate how this understanding emerged.

The first theories of MHD turbulence, by Philip Iroshnikov in 1964 and Robert Kraichnan in 1965, assumed isotropy. They reasoned that Alfvén waves propagating in opposite directions collide and interact, transferring energy to smaller scales. But each collision transfers only a small amount of energy—the waves partially pass through each other. The cascade is slower than in hydrodynamic turbulence, and the spectrum should be $E(k) \sim k^{-3/2}$, shallower than Kolmogorov's $-5/3$.

For thirty years, this was the standard picture. But observations stubbornly refused to cooperate. Solar wind measurements consistently showed $k^{-5/3}$ spectra, not $k^{-3/2}$. Something was wrong.

Goldreich and Sridhar's insight was that the isotropic assumption fails. When turbulence develops in a magnetized plasma, it naturally becomes anisotropic. Eddies elongate along the field. The cascade in the perpendicular direction is fast and Kolmogorov-like; the parallel direction is different.

You might ask: why didn't Iroshnikov and Kraichnan see this?

They were thinking about weak turbulence—the limit where Alfvén waves interact gently and perturbatively. In that regime, isotropy is a reasonable starting assumption. But in strong turbulence—the regime relevant to most astrophysical situations—the interactions are vigorous enough to enforce critical balance, and anisotropy develops spontaneously.

The debate between the Iroshnikov-Kraichnan picture and the Goldreich-Sridhar picture continued for years after 1995. Some theorists argued that anisotropy would be washed out by nonlinear mixing. High-resolution numerical simulations eventually settled

the matter: the Goldreich-Sridhar scaling holds, at least in the strong turbulence regime.

12.7 *Heating the Solar Corona*

Let us apply MHD turbulence to a long-standing puzzle: why is the solar corona so hot?

The Sun's visible surface, the photosphere, has a temperature of about 5800 K. Moving outward, the temperature drops through the chromosphere. Then something unexpected happens: the temperature rises sharply to over a million degrees in the corona. This violates our intuition that things should be cooler farther from a heat source.

The corona must be heated by some non-thermal mechanism. One leading candidate is Alfvénic turbulence.

Consider a coronal loop—an arc of magnetized plasma connecting two sunspots. Typical parameters are:

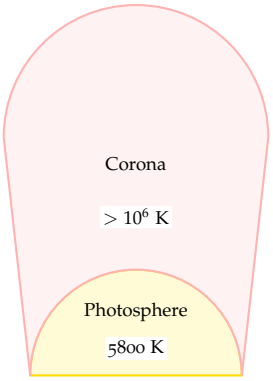

Figure 12.3: The coronal heating problem: temperature increases with height above the photosphere.

- Density: $n \sim 10^{14}$ m^{-3}
- Temperature: $T \sim 2 \times 10^6$ K
- Magnetic field: $B \sim 10^{-3}$ T (10 G)
- Loop length: $L \sim 10^8$ m (100 Mm)

The Alfvén speed is:

$$v_A = \frac{B}{\sqrt{\mu_0 n m_p}} = \frac{10^{-3}}{\sqrt{4\pi \times 10^{-7} \times 10^{14} \times 1.7 \times 10^{-27}}}.$$

Let me compute step by step:

$$\mu_0 n m_p = 4\pi \times 10^{-7} \times 10^{14} \times 1.7 \times 10^{-27} = 4\pi \times 1.7 \times 10^{-20} \approx 2.1 \times 10^{-19}.$$

$$\sqrt{\mu_0 n m_p} \approx 4.6 \times 10^{-10}, \quad v_A \approx \frac{10^{-3}}{4.6 \times 10^{-10}} \approx 2 \times 10^6 \text{ m/s} = 2000 \text{ km/s}.$$

Photospheric motions at the footpoints of the loop shake the magnetic field, launching Alfvén waves into the corona. The observed velocity fluctuations are about $\delta v \sim 30$ km/s at the driving scale.

The energy flux carried by Alfvén waves is the Poynting flux:[1]

$$F \sim \rho \, \delta v^2 \, v_A.$$

With $\rho = n m_p \approx 10^{14} \times 1.7 \times 10^{-27} \approx 1.7 \times 10^{-13}$ kg/m^3:

$$F \sim 1.7 \times 10^{-13} \times (3 \times 10^4)^2 \times 2 \times 10^6 = 1.7 \times 10^{-13} \times 9 \times 10^8 \times 2 \times 10^6 \approx 300 \text{ W/m}^2.$$

This matches the energy required to heat the quiet corona![2] The

[1] For Alfvén waves, the velocity perturbation δv and magnetic perturbation δB are related by $\delta v = \delta B / \sqrt{\mu_0 \rho}$. The Poynting flux $S = \delta \mathbf{E} \times \delta \mathbf{B} / \mu_0$ reduces to $\rho \, \delta v^2 \, v_A$.

[2] Active regions require up to 10^4 W/m^2, which can be supplied by larger wave amplitudes or additional heating mechanisms.

basic estimate works: Alfvén waves launched by photospheric motions carry enough energy to maintain the million-degree corona.

The point is that the basic physics works. Alfvénic turbulence, driven by photospheric motions and cascading to small scales where it dissipates, can heat the corona. The exact mechanism of dissipation at small scales remains debated—ion cyclotron damping, kinetic Alfvén waves, current sheet formation—but the energy is available.

12.8 Turbulence in the Interstellar Medium

You might ask: where else does MHD turbulence matter?

Everywhere. The interstellar medium—the gas and dust between the stars—is turbulent. Radio observations of pulsars reveal scintillation caused by density fluctuations in the intervening medium, and the statistics of this scintillation constrain the turbulent spectrum. The result: Kolmogorov-like, consistent with Goldreich-Sridhar.

Accretion disks are turbulent, driven by the MRI (Chapter 10). The MRI generates magnetic fluctuations that cascade to smaller scales, eventually dissipating and heating the disk.

Galaxy clusters contain hot, magnetized gas called the intracluster medium. This gas is stirred by mergers and by jets from central black holes, driving turbulence that mixes the gas and amplifies magnetic fields.

In each case, the basic framework—energy injection at large scales, cascade to small scales, dissipation at the viscous or resistive cutoff—applies. The details vary, but the physics is universal.

12.9 What We Don't Know

Let us be honest about limitations.

The Goldreich-Sridhar theory is for incompressible, Alfvénic turbulence with a strong mean magnetic field. Real astrophysical situations are messier:

- **Compressibility**: Fast and slow magnetosonic modes exist alongside Alfvén waves. How do they cascade? How do they couple?

- **Imbalance**: In the solar wind, Alfvén waves propagate predominantly outward from the Sun. This "imbalanced" turbulence may have different scaling.

- **Intermittency**: Energy is not distributed smoothly across scales but concentrated in coherent structures like current sheets. These structures can dominate the dissipation.

- **Kinetic effects**: At small scales, the MHD approximation breaks down. Ion and electron kinetics determine the dissipation mechanism.

You might ask: doesn't all this uncertainty undermine the theory?

Not entirely. The Goldreich-Sridhar scaling captures the dominant behavior in many situations. It's a skeleton on which more detailed models can be built. The $k^{-5/3}$ perpendicular spectrum is observed; the anisotropy is observed; critical balance is at least approximately satisfied. The theory works well enough to be useful.

But the details matter for specific applications. How much energy heats ions versus electrons? Where do cosmic rays scatter? What sets the efficiency of angular momentum transport in disks? These questions require going beyond the simplest theory, and the answers are still being worked out.

12.10 *The Shape of Chaos*

Let us close with a philosophical observation.

Turbulence is chaos, but it is organized chaos. The equations of motion are deterministic, yet the solutions are unpredictable in detail. We cannot say where each eddy will be, but we can say how the energy is distributed across scales. Order emerges from disorder.

The magnetic field adds another layer of organization. It imposes a direction, and the turbulence remembers this direction even at small scales. The cream in our magnetized coffee doesn't just mix randomly—it mixes preferentially perpendicular to the field. The chaos has a shape.

This interplay between chaos and order, between universal scaling and system-specific details, is what makes turbulence both fascinating and frustrating. It is the most common state of matter in the universe, governing phenomena from coffee cups to galaxy clusters, yet it remains one of the least understood areas of classical physics.

12.11 *Looking Ahead*

Turbulence cascades energy from large scales to small, where it dissipates. But turbulence can also do the reverse: amplify weak magnetic fields into strong ones. The dynamo mechanism uses turbulent motions, combined with rotation and helicity, to generate the large-scale magnetic fields we observe in planets, stars, and galaxies.

How does the Sun maintain its 11-year magnetic cycle? Why does Earth have a magnetic field at all? These questions require understanding how ordered fields emerge from chaotic flows. That is the

subject of our next chapter: dynamo theory.

13
Dynamo Theory

13.1 The Self-Made Field

Earth's magnetic field guides your compass, protects the atmosphere from the solar wind, and paints the aurora across polar skies. It has been here for at least 3.5 billion years—we know because ancient rocks preserve its signature in their magnetization. Without it, life on Earth might never have evolved; charged particles from the Sun would have stripped away the atmosphere long ago.

But magnetic fields don't last forever. Leave a magnetized piece of iron alone, and currents in it gradually die away through electrical resistance. The field decays. The same is true of Earth's field: without regeneration, ohmic dissipation would erase it in about 20,000 years.

Twenty thousand years is nothing on geological timescales. Yet the field persists for billions of years. Where does it come from?

The answer is wonderfully self-referential: the field makes itself. Deep in Earth's core, liquid iron churns in convective motions, rising and falling as heat escapes to the mantle above. This flowing conductor moves through the existing magnetic field, generating electrical currents by induction. The currents, in turn, create magnetic field. If the geometry is right, the regenerated field exceeds what was lost to dissipation. The field sustains itself, like a flame that burns its own fuel while creating more.

This is the dynamo mechanism. It operates in Earth's core, in the Sun's convection zone, in the liquid hydrogen of Jupiter, and probably in most stars and planets with substantial conducting fluid regions. Understanding how it works—and why it sometimes fails—is the subject of dynamo theory.

13.2 Why Simple Doesn't Work

Let us begin with a puzzle that stumped physicists for decades.

In 1919, Joseph Larmor asked whether the Sun's magnetic field

could be self-generated. He imagined a simple scenario: an axisymmetric flow in a rotating sphere, maintaining an axisymmetric field like a dipole. It seemed natural. The Sun is roughly axisymmetric. Its field is roughly dipolar. Why not?

In 1934, Thomas Cowling proved that this picture is impossible.

Cowling's theorem states: *No axisymmetric magnetic field can be maintained by axisymmetric fluid motions.*

The proof exploits a geometric fact. An axisymmetric field has points where the field strength vanishes—typically at the equator for a dipole. At these null points, the field lines close, and there's no way for axisymmetric motions to regenerate what diffusion destroys. The induction term $\nabla \times (\mathbf{v} \times \mathbf{B})$ cannot create field from nothing at a point where $\mathbf{B} = 0$.

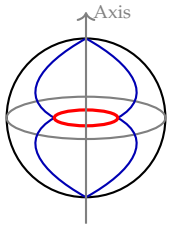

Figure 13.1: Cowling's theorem: the null points form a ring around the equator (shown as red ellipse). Axisymmetric flows cannot regenerate field where $B = 0$.

Think of it this way. The induction equation stretches and transports existing field. It can amplify what's there, move it around, twist it into new shapes. But at a true null point, there's nothing to stretch or transport. Diffusion steadily erases the field near the null, and induction cannot replenish it.

You might ask: if axisymmetric dynamos are impossible, how do the Sun and Earth have magnetic fields?

The answer is that real flows are not axisymmetric. Convection cells, rising plumes, and turbulent eddies have three-dimensional structure. When combined with rotation—which imposes a preferred handedness through the Coriolis force—these flows can evade Cowling's theorem and sustain a large-scale magnetic field.

The devil, as always, is in the details.

13.3 *The Kinematic Dynamo*

Let us approach the problem systematically.

We start by asking a simpler question: given a prescribed velocity field $\mathbf{v}(\mathbf{x}, t)$, will the magnetic field grow or decay? This is the kinematic dynamo problem. We ignore the back-reaction of the field on the flow (which would require solving the full momentum equation) and focus purely on the induction equation:

$$\frac{\partial \mathbf{B}}{\partial t} = \nabla \times (\mathbf{v} \times \mathbf{B}) + \lambda \nabla^2 \mathbf{B}, \tag{13.1}$$

where $\lambda = \eta/\mu_0$ is the magnetic diffusivity.

This is a linear equation in $\mathbf{B}$. Solutions are superpositions of modes that grow or decay exponentially: $\mathbf{B} \propto e^{\gamma t}$. If any mode has $\gamma > 0$, the flow is a kinematic dynamo—it amplifies magnetic field.

The competition is between induction (the first term) and diffusion (the second term). Dimensional analysis gives the magnetic Reynolds

number:

$$Rm = \frac{vL}{\lambda},$$

where v is a characteristic velocity and L is a characteristic length scale. If $Rm \ll 1$, diffusion wins and the field decays. If $Rm \gg 1$, induction dominates and dynamo action is possible.

The critical magnetic Reynolds number Rm_{crit} depends on the flow geometry. For most flows, $Rm_{\text{crit}} \sim 10$–100. Below this threshold, no dynamo occurs regardless of the flow pattern. Above it, the right kind of flow will amplify the field.

13.4 Mean-Field Electrodynamics

Real astrophysical flows are turbulent. Tracking every eddy is impossible. We need a statistical approach.

Let us decompose the magnetic field and velocity into mean and fluctuating parts:

$$\mathbf{B} = \langle \mathbf{B} \rangle + \mathbf{b},$$
$$\mathbf{v} = \langle \mathbf{v} \rangle + \mathbf{u},$$

where angle brackets denote an average (over time, space, or an ensemble of realizations).

Substituting into the induction equation and averaging, we get:

$$\frac{\partial \langle \mathbf{B} \rangle}{\partial t} = \nabla \times (\langle \mathbf{v} \rangle \times \langle \mathbf{B} \rangle + \boldsymbol{\mathcal{E}}) + \lambda \nabla^2 \langle \mathbf{B} \rangle, \tag{13.2}$$

where $\boldsymbol{\mathcal{E}} = \langle \mathbf{u} \times \mathbf{b} \rangle$ is the mean electromotive force (EMF) from the fluctuating fields.

This term $\boldsymbol{\mathcal{E}}$ is the heart of mean-field dynamo theory. The fluctuating velocity and fluctuating field, though individually chaotic, combine to produce a systematic mean EMF.

How do we evaluate $\boldsymbol{\mathcal{E}}$? In the simplest approximation, we expand in terms of the mean field and its derivatives:

$$\mathcal{E}_i = \alpha_{ij} \langle B \rangle_j + \beta_{ijk} \frac{\partial \langle B \rangle_j}{\partial x_k} + \cdots \tag{13.3}$$

For isotropic turbulence (no preferred direction), symmetry constrains the coefficients. The leading terms are:

$$\boldsymbol{\mathcal{E}} = \alpha \langle \mathbf{B} \rangle - \beta \nabla \times \langle \mathbf{B} \rangle, \tag{13.4}$$

where α and β are scalar coefficients.

The β term represents turbulent diffusion: random motions enhance the spreading of magnetic field, just as they enhance the mixing of cream in coffee. The effective diffusivity becomes $\lambda + \beta$, typically much larger than the molecular value λ.

The α term is more remarkable. It represents an EMF *parallel* to the mean field—something that doesn't happen in laminar flows. This is the famous "alpha effect."

13.5 The Alpha Effect

You might ask: how can turbulence generate an EMF parallel to the magnetic field?

The key is helicity. Helicity measures the "handedness" of a flow—the correlation between velocity and vorticity:

$$H = \langle \mathbf{u} \cdot (\nabla \times \mathbf{u}) \rangle = \langle \mathbf{u} \cdot \boldsymbol{\omega} \rangle.$$

A flow has positive helicity if it tends to twist like a right-handed corkscrew (velocity and vorticity aligned); negative helicity if it twists like a left-handed corkscrew (velocity and vorticity anti-aligned).

In a rotating system, helicity arises naturally. Consider a rising thermal plume in a convecting layer. As it rises, the Coriolis force deflects its motion, twisting it into a helical shape. In the Northern Hemisphere (where rotation is counterclockwise viewed from above), rising fluid twists counterclockwise—positive helicity. In the Southern Hemisphere, the twist is opposite.

Now consider what happens when this helical flow interacts with a horizontal magnetic field. The rising, twisting motion stretches and wraps the field lines. A horizontal field line gets lifted and twisted, generating a vertical component. Averaged over many such events, the turbulence produces a mean EMF that has a component parallel to the original mean field.

The quantitative result, derived by Steenbeck, Krause, and Rädler in the 1960s, is:

$$\alpha \approx -\frac{\tau}{3} \langle \mathbf{u} \cdot \boldsymbol{\omega} \rangle, \tag{13.5}$$

where τ is the correlation time of the turbulence. The negative sign reflects how the twist converts one component of field into another.

The alpha effect is the engine of large-scale dynamos. It converts toroidal field (wrapped around the rotation axis) into poloidal field (threading through the poles), and vice versa. This mutual conversion allows the field to sustain itself against diffusion.

13.6 The Solar Dynamo

Let us apply these ideas to the best-observed example: the Sun.

The Sun's magnetic field varies on an approximately 11-year cycle. Sunspots appear, grow numerous, then fade. The latitude where spots appear migrates from mid-latitudes toward the equator over

the cycle. And crucially, the field's polarity reverses every 11 years: north becomes south, south becomes north. The full magnetic cycle is thus 22 years.

The standard model is the $\alpha\omega$ dynamo:

The ω effect: The Sun rotates differentially—the equator rotates faster than the poles. This differential rotation stretches any poloidal field into toroidal field, winding it around the rotation axis like thread on a spool.

The α effect: Convective turbulence in the solar interior is helical due to the Coriolis force. This helicity converts toroidal field back into poloidal field.

The cycle operates as follows:

1. Start with a poloidal field (say, pointing out of the Northern Hemisphere).
2. Differential rotation stretches it into toroidal field.
3. The α effect converts the toroidal field into new poloidal field—but with opposite polarity!
4. Differential rotation stretches this new poloidal field into toroidal field of opposite sign.
5. The α effect again reverses the polarity.
6. After two half-cycles (22 years), the field returns to its original configuration.

You might ask: where exactly does this happen in the Sun?

The location is still debated, but the leading candidate is the tachocline—a thin shear layer at the base of the convection zone, about 200,000 km below the visible surface. Here, the differentially rotating convection zone meets the rigidly rotating radiative interior. The shear is strong, the ω effect is efficient, and magnetic flux can be stored without being immediately disrupted by convection.

The details remain contentious. How exactly flux rises from the tachocline to the surface, why the cycle is 11 years rather than some other period, and what causes occasional "grand minima" (like the Maunder Minimum of 1645–1715, when sunspots nearly vanished) are active research questions.

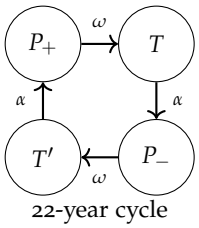

Figure 13.2: The $\alpha\omega$ dynamo cycle: differential rotation (ω) converts poloidal to toroidal field; the alpha effect (α) converts toroidal back to poloidal with reversed polarity.

13.7 *Earth's Dynamo*

Let us now turn to our own planet.

Earth's magnetic field is generated in the outer core—a shell of liquid iron about 2,200 km thick, lying between the solid inner core and

the rocky mantle. The liquid iron is an excellent electrical conductor, and it convects vigorously, driven by the heat escaping from the inner core and the latent heat released as the inner core slowly solidifies.

We can estimate whether conditions favor a dynamo.

The outer core has:

- Radius $R \approx 3.5 \times 10^6$ m
- Typical convective velocity $v \approx 5 \times 10^{-4}$ m/s (inferred from changes in the field over decades—the "secular variation")
- Magnetic diffusivity $\lambda \approx 1$ m^2/s (for liquid iron)

The magnetic Reynolds number is:

$$Rm = \frac{vR}{\lambda} = \frac{5 \times 10^{-4} \times 3.5 \times 10^6}{1} = 1750.$$

This is well above the critical value of $Rm_{\text{crit}} \sim 10$–50 required for dynamo action. Earth's core easily exceeds the threshold.

The energy required to maintain the dynamo comes from convection. Ohmic dissipation—the heating from electrical resistance—must be balanced by the power supplied by fluid motions. Estimates suggest the geodynamo requires about 10^{11}–10^{12} W (100 GW to 1 TW). This is a small fraction of Earth's total heat loss ($\sim 4 \times 10^{13}$ W), so there's plenty of power available.

You might ask: why doesn't Mars have a magnetic field?

Mars once had a dynamo. The oldest Martian crust, in the southern highlands, is strongly magnetized. But the dynamo shut off about 4 billion years ago. The likely reason: Mars is smaller than Earth, so its core cooled more quickly. Once the core cooled below the threshold for vigorous convection, the dynamo died.

Venus presents a different puzzle. It's nearly Earth's size, yet has no detected magnetic field. Perhaps Venus lacks a solid inner core (which in Earth releases latent heat that drives convection). Perhaps its mantle convects sluggishly, failing to extract enough heat from the core. The absence of a Venusian dynamo remains poorly understood.

13.8 Laboratory Dynamos

You might ask: can we create a dynamo in the laboratory?

The challenge is formidable. Laboratory flows have Rm of order unity or less—far below the threshold for dynamo action. To exceed $Rm_{\text{crit}} \sim 10$–50, you need either very large scales, very fast flows, or very low magnetic diffusivity.

In 1999, experimenters in Riga, Latvia, succeeded. They pumped liquid sodium through a helical pipe system at high velocity, creating

a flow with the right geometry to sustain a magnetic field. When the flow exceeded a critical speed, the field spontaneously grew from ambient noise and saturated at a finite amplitude. The dynamo worked.

The Karlsruhe experiment in Germany achieved similar success with a different geometry in 2000. More recent experiments in Cadarache, France (the VKS experiment) have demonstrated turbulent dynamos with polarity reversals reminiscent of Earth's.

These experiments are tours de force of engineering—liquid sodium is reactive, hot, and dangerous; the flows must be sustained for long periods; the diagnostics must measure fields inside opaque liquid metal. But they confirm that the physics of dynamos, worked out theoretically over decades, actually operates in nature.

13.9 Saturation and Back-Reaction

We have discussed kinematic dynamos, where the velocity field is prescribed. But real dynamos must eventually saturate: the field cannot grow forever.

Saturation occurs when the growing magnetic field back-reacts on the flow that generates it. As the field strengthens, the Lorentz force $\mathbf{J} \times \mathbf{B}$ opposes the motions that twist and stretch the field lines. Eventually, generation and dissipation balance.

Several mechanisms contribute to saturation:

- **Alpha quenching**: Strong magnetic fields suppress the helical turbulence that creates the alpha effect. The effective α decreases as B increases.
- **Direct suppression**: The Lorentz force directly opposes the shearing motions (the ω effect) that stretch field lines.
- **Flux loss**: In stars, buoyant magnetic flux rises through the convection zone and escapes at the surface, removing magnetic energy from the system.

The saturated field strength is determined by equipartition: roughly, the magnetic energy density $B^2/(2\mu_0)$ becomes comparable to the kinetic energy density $\rho v^2/2$ of the driving flow.

For the Sun, this gives:

$$B_{\rm sat} \sim \sqrt{\mu_0 \rho v^2}.$$

With convective velocities $v \sim 30$ m/s and density $\rho \sim 200$ kg/m^3 (deep in the convection zone):

$$B_{\rm sat} \sim \sqrt{4\pi \times 10^{-7} \times 200 \times 900} = \sqrt{2.3 \times 10^{-1}} \approx 0.5 \text{ T} = 5000 \text{ G}.$$

This is consistent with inferred field strengths in the solar interior.[1] The dynamo saturates at the level where magnetic and kinetic energies are comparable.

[1] Surface sunspot fields are typically 1000–3000 G, but the interior toroidal field at the base of the convection zone may be much stronger—perhaps 10^4–10^5 G.

13.10 The Seed Field

You might ask: where does the first magnetic field come from?

A dynamo amplifies existing field. It cannot create field from nothing. Some initial seed is required.

The answer comes from a mechanism called the Biermann battery. In a plasma where temperature and density gradients are not parallel, a current arises spontaneously. The electron pressure force $-\nabla p_e/n_e$ has a curl if ∇T_e and ∇n_e point in different directions:

$$\frac{\partial \mathbf{B}}{\partial t} \propto \nabla T_e \times \nabla n_e.$$

This is not a dynamo—it's a one-time injection of field from thermodynamic gradients. But it provides the seed. In a forming star, the collapse is never perfectly spherical; temperature and density gradients have different orientations. A weak field appears spontaneously, perhaps 10^{-20} T or less.

Then the dynamo takes over. Even starting from infinitesimal amplitude, exponential growth eventually produces the fields we observe. The origin of the seed doesn't matter much; the dynamo does the heavy lifting.

13.11 Order from Chaos

Let us close with a reflection on what dynamo theory tells us about the universe.

Turbulent convection seems chaotic—plumes rise and fall unpredictably, vortices form and dissolve, flows reverse without warning. Yet from this chaos, ordered magnetic fields emerge. The Sun's 22-year cycle, Earth's steady dipole (punctuated by reversals), the spiral magnetic patterns in galaxies—all arise from turbulent conducting fluids.

The key is not that turbulence creates order directly, but that it has the right statistical properties. On average, convection in a rotating system is helical. On average, the helicity converts one component of field into another. The chaos is essential—it provides the complexity needed to evade Cowling's theorem—but it operates through averages, not individual events.

This is a recurring theme in physics. Thermodynamics emerges from the chaos of molecular collisions. Fluid dynamics emerges from

the chaos of particle motions. And now we see that cosmic magnetism emerges from the chaos of turbulent flow. The universe builds order from disorder, structure from randomness, by the patient accumulation of statistical bias.

13.12 Looking Ahead

We have seen how magnetic fields are generated in convecting planets and stars. The same physics governs the interiors of all magnetized bodies, from brown dwarfs to white dwarfs to neutron stars.

In our final chapter, we turn to magnetic fields in the most extreme environments: accretion disks around black holes, the jets that blast out from active galactic nuclei, and the cosmic engines that power the most luminous objects in the universe. These systems operate at the frontier of MHD, where relativistic effects, radiation pressure, and extreme gravitational fields all come into play. Yet the basic principles—frozen-in flux, magnetic tension, pressure balance, dynamo action—remain our guides.

14
MHD in Stellar Interiors

14.1 The Rhythm of the Sun

Every eleven years, the Sun goes mad.

Sunspots multiply, spreading like dark bruises across the solar face. Flares erupt, releasing in minutes the energy that the Sun normally radiates in hours. Coronal mass ejections blast billion-ton clouds of magnetized plasma into space, sometimes aimed directly at Earth.

Then the frenzy subsides. Spots become rare, flares infrequent. The Sun enters a quiet phase, its surface almost unblemished. And after a few years of calm, the cycle begins again.

This rhythm has repeated for as long as we've watched—certainly since Galileo first turned his telescope sunward in 1610, and presumably for billions of years before. What drives it?

The answer lies deep inside the Sun, in regions we cannot directly observe. Convection churns the outer third of the star, carrying heat from the nuclear furnace below. Rotation winds these turbulent motions into systematic patterns. And from this choreography of flow and spin, magnetic fields are born.

Think of the Sun's magnetic field as a rope. Differential rotation—the equator spinning faster than the poles—winds the rope around the Sun, stretching and strengthening it. Turbulent convection twists the rope, knotting it into complex configurations. Eventually the tension becomes too great: the rope breaks through the surface as sunspots, releasing its stored energy as flares. Then the winding begins again.

We have met the dynamo mechanism in Chapter 13. Now we apply it to its best-observed example: the Sun. The solar dynamo is a testing ground for dynamo theory—a place where we can compare predictions against detailed observations spanning centuries. Yet despite this wealth of data, the solar dynamo remains incompletely understood. We know the pieces; assembling them into a complete

picture has proven frustratingly difficult.

14.2 *The Butterfly and the Cycle*

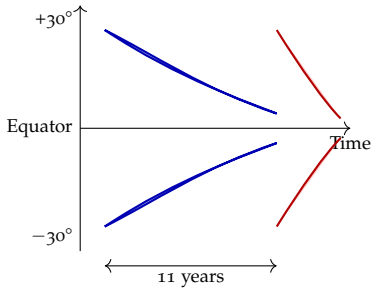

Figure 14.1: The butterfly diagram: sunspot latitude versus time. Spots appear at mid-latitudes and migrate toward the equator over each 11-year cycle.

Let us begin with what we observe.

The sunspot cycle was discovered by Heinrich Schwabe, a German pharmacist and amateur astronomer, who noticed the pattern in 1843 after seventeen years of daily observations. Modern data have refined his discovery:

The period averages about eleven years, though individual cycles range from nine to fourteen years. At cycle minimum, the Sun is nearly spotless; at maximum, hundreds of spots may dot its surface.

The latitude of spot emergence follows a striking pattern. At the start of a cycle, spots appear around $\pm 30°$ latitude. As the cycle progresses, new spots emerge closer and closer to the equator, reaching $\pm 5°$ at cycle's end. When plotted as latitude versus time, the pattern resembles butterfly wings—hence the "butterfly diagram."

The magnetic field adds another layer of regularity. In each hemisphere, the leading spot of a sunspot pair (leading in the direction of rotation) has consistent polarity throughout the cycle. But this polarity reverses from one cycle to the next: if northern-hemisphere leading spots are positive in one cycle, they're negative in the next.

This is Hale's polarity law, and it reveals something profound: the eleven-year sunspot cycle is really half of a twenty-two-year magnetic cycle. The Sun's large-scale field completely reverses polarity every eleven years, returning to its original state after twenty-two.

You might ask: what physical mechanism could produce such ordered behavior from the turbulent chaos of solar convection?

The answer is the $\alpha\omega$ dynamo, operating in the transition layer between the convection zone and the radiative interior.

14.3 *The Tachocline*

Let us descend into the Sun.

The outer thirty percent of the Sun, by radius, is the convection zone. Here, energy is transported by rising hot gas and sinking cool gas—the same process that bubbles soup in a pot. The convection zone rotates differentially: the equator completes a rotation in about 25 days, while the poles take about 35 days.

Below the convection zone lies the radiative interior. Here, energy is transported by photons diffusing through the dense plasma. And crucially, the radiative interior rotates nearly uniformly, like a solid body.

Between these two regions lies the tachocline—a thin layer, per-

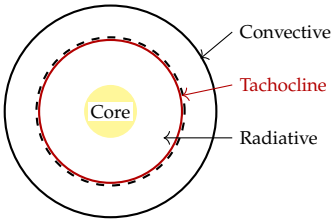

Figure 14.2: Solar structure: the tachocline is a thin shear layer between the differentially rotating convection zone and the uniformly rotating radiative interior.

haps 20,000 km thick (only 3% of the solar radius), where the rotation rate changes abruptly. This is where helioseismology, the study of solar oscillations, has revealed the Sun's internal structure with remarkable precision.

The tachocline is thought to be the seat of the solar dynamo. Here, the differential rotation is strongest—the ω effect that stretches poloidal field into toroidal field operates at maximum efficiency. And here, magnetic flux can be stored without being immediately disrupted by convective motions.

The dynamo cycle works as follows. Differential rotation in the tachocline stretches any poloidal (north-south) magnetic field into toroidal (east-west) field—winding the magnetic rope around the Sun like thread on a spool. The toroidal field is amplified until it becomes buoyantly unstable—the magnetic pressure makes it lighter than its surroundings. Flux tubes rise through the convection zone and emerge at the surface as sunspot pairs.

Meanwhile, the α effect—helical turbulence driven by the Coriolis force—converts some of the toroidal field back into poloidal field, but with reversed polarity. The cycle repeats, with the field oscillating between one polarity state and its opposite.

14.4 Rising Flux

Let us follow a magnetic flux tube as it rises from the tachocline to the surface.

At the base of the convection zone, the toroidal field may reach strengths of 10^4–10^5 G (1–10 T). Such fields are buoyant: magnetic pressure $B^2/(2\mu_0)$ partially replaces gas pressure p, reducing the density required for pressure balance. The tube is lighter than its surroundings by:

$$\frac{\Delta\rho}{\rho} \sim \frac{B^2}{2\mu_0 p}.$$

For $B = 10$ T and $p \sim 10^{13}$ Pa (typical tachocline pressure):

$$\frac{\Delta\rho}{\rho} \sim \frac{(10)^2}{2 \times 4\pi \times 10^{-7} \times 10^{13}} = \frac{100}{8\pi \times 10^6} \approx 4 \times 10^{-6}.$$

This tiny density deficit is enough. In the solar gravitational field ($g \approx 270$ m/s^2), the buoyancy acceleration is:

$$a = g\frac{\Delta\rho}{\rho} \approx 270 \times 4 \times 10^{-6} \approx 10^{-3} \text{ m/s}^2.$$

The rise velocity, balancing buoyancy against aerodynamic drag, is roughly:

$$v_{\text{rise}} \sim v_A \left(\frac{r_{\text{tube}}}{H_p}\right)^{1/2},$$

where v_A is the Alfvén speed inside the tube, r_{tube} is the tube radius, and H_p is the pressure scale height.[1] For realistic parameters, $v_{\text{rise}} \sim$ 100–1000 m/s.

[1] The pressure scale height $H_p = p/(\rho g) \approx 5 \times 10^7$ m in the lower convection zone.

The convection zone is about 2×10^8 m deep. At 100 m/s, the rise time is:

$$t_{\text{rise}} \sim \frac{2 \times 10^8}{100} = 2 \times 10^6 \text{ s} \approx 23 \text{ days}.$$

This matches observations: active regions emerge over timescales of weeks, consistent with flux tubes rising from the tachocline.

You might ask: why don't rising flux tubes get torn apart by convection?

The key is twist. A flux tube with purely toroidal field (field running along the tube's length) is vulnerable: convective eddies can kink and fragment it. But if the tube carries a component of field along its axis—if it's twisted like a rope—magnetic tension holds it together.

The twist comes from the Coriolis force. As the tube rises through the rotating Sun, it develops helical motions that generate axial field. This twist is essential for survival; simulations show that untwisted tubes disperse before reaching the surface.

14.5 The Period Problem

You might ask: why eleven years?

This is perhaps the most embarrassing question in solar physics. We can build models that produce eleven-year cycles, but we can't predict the period from first principles.

Dimensional analysis offers a start. The dynamo involves turbulent diffusion across the convection zone. A diffusion time is:

$$\tau_{\text{diff}} \sim \frac{L^2}{\eta_{\text{turb}}},$$

where $L \sim 2 \times 10^8$ m is the depth of the convection zone and $\eta_{\text{turb}} \sim 10^8$–$10^9$ m^2/s is the turbulent magnetic diffusivity.

This gives:

$$\tau_{\text{diff}} \sim \frac{(2 \times 10^8)^2}{10^{8.5}} = \frac{4 \times 10^{16}}{3 \times 10^8} \approx 10^8 \text{ s} \approx 3 \text{ years}.$$

This is the right order of magnitude, but the details—the factor of three or four needed to reach eleven years—depend sensitively on parameters we don't know well: the strength and spatial distribution of α, the precise rotation profile, the role of meridional circulation.

Moreover, the period varies from cycle to cycle. Cycle 23 lasted 12.6 years; cycle 24 lasted 11.0 years. Something modulates the dynamo on timescales we don't understand.

14.6 Grand Minima

The Sun doesn't always cycle smoothly. From about 1645 to 1715, sunspots nearly vanished. This "Maunder Minimum" coincided with the coldest part of the Little Ice Age in Europe—though whether the connection is causal remains debated.

Longer records, reconstructed from tree rings and ice cores, reveal other grand minima scattered through the past ten thousand years. The Sun apparently switches between states: sometimes cycling vigorously, sometimes barely cycling at all.

You might ask: what causes grand minima?

We don't know. Possibilities include:

- **Chaotic dynamics**: The nonlinear dynamo equations may have multiple attractors. The Sun might wander between them unpredictably.
- **Meridional circulation changes**: The slow poleward flow at the surface, and its return flow at depth, affects the dynamo period. Variations in this circulation could push the dynamo into quiescence.
- **External forcing**: Though unlikely, gravitational perturbations from planets have been suggested.

Whatever the cause, grand minima remind us that the Sun's apparent regularity is not guaranteed. The Maunder Minimum could happen again—and we would have little warning.

14.7 Angular Momentum Transport

Let us turn to a different problem: how does the Sun's interior rotate as it does?

The radiative interior rotates nearly uniformly, like a solid body. The convection zone rotates differentially. These rotation profiles are stable over solar evolution timescales. Something must enforce them.

The puzzle is sharpest at the tachocline. Angular momentum wants to flow from the fast-rotating equator to the slow-rotating poles, and from the differential convection zone into the uniform interior. Why doesn't it?

The answer returns us to our magnetic rope. Even a weak field threading the tachocline acts like a tether between the convection zone and the radiative interior. If one region tries to spin faster, it twists the magnetic tether, and the resulting tension pulls back.

The answer is magnetic fields. Even a weak poloidal field threading the tachocline couples the two regions. If the convection zone

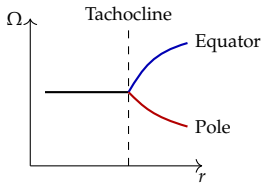

Figure 14.3: Solar rotation profile: uniform in the radiative interior, differential in the convection zone, with a rapid transition at the tachocline.

tries to spin up, it twists the field lines, generating toroidal field. This toroidal field exerts a Maxwell stress on the radiative interior, transferring angular momentum and resisting the spin-up.

Let us estimate the required field strength. The angular velocity contrast across the tachocline is $\Delta\Omega \sim 10^{-6}$ rad/s. The shear timescale is the time for differential rotation to wind up the field significantly:

$$\tau_{\text{shear}} \sim \frac{1}{\Delta\Omega} \approx 10^6 \text{ s} \approx 12 \text{ days}.$$

For magnetic coupling to be effective, the Alfvén crossing time across the tachocline must be comparable:

$$\tau_A = \frac{\delta}{v_A} \sim \tau_{\text{shear}},$$

where $\delta \sim 2 \times 10^7$ m is the tachocline thickness. This gives:

$$v_A \sim \frac{2 \times 10^7}{10^6} = 20 \text{ m/s}.$$

With density $\rho \sim 200$ kg/m^3 at the tachocline:

$$B = v_A \sqrt{\mu_0 \rho} = 20 \times \sqrt{4\pi \times 10^{-7} \times 200} \approx 20 \times 1.6 \times 10^{-2} \approx 0.3 \text{ T} = 3000 \text{ G}.$$

A field of a few thousand gauss threading the tachocline could enforce the observed rotation profile. This is weaker than the toroidal field in active regions (which may reach 10^5 G at the tachocline), but it's a significant structural element of the solar interior.

14.8 Beyond the Sun

You might ask: what about other stars?

Stars span an enormous range of magnetic properties. Solar-type stars show activity cycles similar to the Sun's, with periods ranging from about 7 to 25 years. More rapidly rotating stars tend to be more magnetically active, with stronger fields and shorter cycles.

Fully convective stars—those with masses below about 0.35 solar masses—lack the tachocline entirely. Yet many show strong magnetic fields and vigorous activity. Their dynamos must operate differently, perhaps through small-scale turbulent processes throughout the convective volume rather than the organized $\alpha\omega$ mechanism.

At the other extreme, a few percent of hot A and B stars have surface fields of thousands of gauss—far stronger than the Sun's. These are the Ap and Bp stars ("p" for peculiar). Their fields are probably not dynamo-generated but fossil remnants from star formation, frozen into the radiative envelope where no convection disrupts them.

Asteroseismology—the study of stellar oscillations—has opened a new window on internal rotation. In subgiant and red giant stars, the core rotates only about ten times faster than the envelope. This is far slower than expected from simple angular momentum conservation; as the core contracts, it should spin up dramatically. Magnetic torques are the leading explanation: fields threading between core and envelope transfer angular momentum, keeping the core from spinning too fast.

14.9 The Limits of Understanding

Let us be honest about what we don't know.

We cannot predict the amplitude or timing of solar cycles. Forecasts for cycle 24 predicted it would be strong; it was the weakest in a century. Forecasts for cycle 25 predicted weakness; it turned out stronger than expected. The Sun continues to surprise us.

We don't know where in the Sun the α effect operates. Is it distributed through the convection zone? Concentrated near the surface? Both? Different models give different answers, and observations cannot yet distinguish them.

We don't understand grand minima. We don't know why the Maunder Minimum happened, whether it will happen again, or what the consequences might be.

This is humbling. The Sun is our nearest star, observed in exquisite detail for centuries. Yet its internal dynamics remain partly mysterious. The dynamo equations are well-established; the difficulty is in the parameters and boundary conditions, in the complexity of three-dimensional turbulent convection coupled to magnetic fields and rotation.

14.10 Listening to Stars

Let us close with a reflection on method.

We cannot send probes into the solar interior. We cannot drill cores from distant stars. Everything we know about stellar magnetism comes from indirect inference: from the surface manifestations of deep processes, from the oscillations that probe internal structure, from the rotation and activity that reveal underlying dynamics.

This is indirect science at its best. Helioseismology revealed the tachocline—a structure nobody had predicted, essential for understanding the dynamo. Asteroseismology is revealing internal rotation rates that challenge our models of angular momentum transport. Each new observational technique opens new windows.

The Sun is a laboratory, but one we observe from afar. We form hypotheses, make predictions, and test them against the data. Sometimes we're right; often we're wrong. The cycle continues—in the Sun and in our understanding of it.

14.11 Looking Ahead

Stars generate magnetic fields in their interiors, and those fields emerge to dominate their surfaces, winds, and environments. But the most spectacular MHD phenomena occur around compact objects: neutron stars and black holes.

In our final chapter, we turn to accretion disks, relativistic jets, and the cosmic engines that power active galactic nuclei. These systems push MHD to its limits, where extreme gravity, relativistic flows, and enormous energies create phenomena unlike anything in quieter corners of the universe.

15
Accretion Disks, Jets, and Cosmic Engines

Look at a photograph of M87, the giant elliptical galaxy at the heart of the Virgo cluster, and you will see something extraordinary: a brilliant jet of plasma shooting 5000 light-years outward. This luminous beam is propelled by a black hole six billion times the mass of the Sun, fed by a disk of gas spiraling inexorably inward. Here is MHD at its most extreme. The gas swirls at speeds approaching that of light, heated to millions of degrees, threaded by magnetic fields strong enough to shape the flow of matter on scales larger than solar systems. The jet itself is launched from near the event horizon—the point of no return—accelerated by magnetic forces, squeezed by magnetic pressure, and somehow maintained as a coherent beam across distances that dwarf entire galaxies.

We have built up the MHD toolkit through these lectures: frozen-in flux, magnetic pressure and tension, waves, instabilities, turbulence, dynamos. Now we bring everything together to understand the most powerful engines in the universe. Accretion onto compact objects converts gravitational potential energy into radiation with efficiencies approaching 40%—far exceeding nuclear fusion's meager 0.7%. Jets channel a significant fraction of that power into narrow beams that reshape their cosmic environments, inflating bubbles in galaxy clusters, triggering or suppressing star formation, and announcing their presence across billions of light-years.

Think of these systems as cosmic water wheels—but instead of water falling onto paddles, it is magnetized plasma spiraling down a gravitational drain. The drain funnels energy; the magnetic field extracts it; the jet is the power output. This is the capstone of MHD: physics at its most energetic and most beautiful.

15.1 The Angular Momentum Problem

Let us begin with a puzzle that confronts any gas trying to fall onto a compact object. Gas carries angular momentum. If that angular mo-

mentum is conserved during infall, the gas cannot simply plummet to the center. Instead, it spirals in only until centrifugal force balances gravity, then orbits forever.

Consider gas at distance r from a central mass M, moving with orbital velocity v. Its specific angular momentum is

$$\ell = r \times v.$$

Conservation of angular momentum means the gas can fall no closer than the circularization radius, where centrifugal acceleration balances gravitational pull:

$$r_{\rm circ} = \frac{\ell^2}{GM}.$$

Let us put in numbers. Suppose gas at 100 AU from a solar-mass star orbits at approximately 3 km/s. The specific angular momentum is

$$\ell = r \times v \approx 100 \times 1.5 \times 10^{11}\ \text{m} \times 3000\ \text{m/s} = 4.5 \times 10^{16}\ \text{m}^2/\text{s}.$$

The circularization radius becomes

$$r_{\rm circ} = \frac{(4.5 \times 10^{16})^2}{6.67 \times 10^{-11} \times 2 \times 10^{30}} \approx \frac{2 \times 10^{33}}{1.3 \times 10^{20}} \approx 1.5 \times 10^{13}\ \text{m} \approx 100\ \text{AU}.$$

Wait—the gas cannot fall inward at all! It already sits at its circularization radius. If we started the gas at larger distance with the same specific angular momentum, it would spiral in and park at 100 AU, forming a disk. To actually accrete onto the central object, something must transport angular momentum outward, allowing the inner gas to spiral further in while the outer gas spirals out.

You might ask: could ordinary molecular viscosity do the job? After all, viscosity transports momentum in fluids. The viscous timescale for a disk of size r and kinematic viscosity ν is

$$\tau_{\rm visc} \sim \frac{r^2}{\nu}.$$

For ionized hydrogen at 10^4 K, kinematic viscosity is approximately $\nu \sim 10^{-4}\ \text{m}^2/\text{s}$. For our 100 AU disk:

$$\tau_{\rm visc} \sim \frac{(1.5 \times 10^{13})^2}{10^{-4}} \approx 2 \times 10^{30}\ \text{s} \approx 10^{23}\ \text{years}.$$

This is vastly longer than the age of the universe. Molecular viscosity cannot possibly explain observed accretion rates. Protoplanetary disks evolve on million-year timescales, not 10^{23}-year timescales. Something else must be happening.

The answer, as you might suspect, is magnetic. The magnetorotational instability we studied in Chapter 10 generates turbulence in

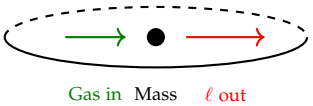

Figure 15.1: Angular momentum must flow outward for gas to accrete inward. The disk acts as a conveyor belt.

any differentially rotating disk threaded by a weak magnetic field. This turbulence acts like an effective viscosity, transporting angular momentum outward on dynamical timescales. Additionally, magnetic fields anchored in the disk can launch winds that carry angular momentum away entirely. Both mechanisms are fundamentally MHD phenomena. The angular momentum problem is really a magnetic problem.

15.2 *The Alpha-Disk Model*

In 1973, Nikolai Shakura and Rashid Sunyaev faced a dilemma. They wanted to model accretion disks, but they did not know the precise mechanism transporting angular momentum. Their solution was elegant: parameterize the ignorance. They assumed that turbulent stresses in the disk could be written as

$$T_{r\phi} = \alpha P,$$

where P is the total pressure (gas plus radiation) and α is a dimensionless parameter somewhere between 0.01 and 0.1. The symbol α has become so ubiquitous that these are universally called "alpha-disks."

You might ask: isn't this just sweeping the physics under the rug? In a sense, yes. Shakura and Sunyaev freely admitted they did not know what caused the turbulence. But the parameterization allowed them to build a complete model of disk structure that could be compared with observations. The bet was that whatever mechanism operated, it would produce stresses proportional to pressure. This turns out to be roughly correct for MRI-driven turbulence, vindicating their intuition decades before the MRI was understood.

The alpha prescription leads to a complete disk model. Let us sketch the structure. In steady state, mass flows inward at rate $\dot{M}$, and angular momentum flows outward. The viscous stress extracts angular momentum from inner annuli and deposits it in outer ones. Energy dissipated by this process heats the disk, which radiates from its surfaces.

The key relations for a geometrically thin, optically thick disk (one where the disk thickness H is much smaller than the radius r, and photons are trapped) are:

$$\dot{M} = 3\pi\nu\Sigma, \tag{15.1}$$

$$\nu = \alpha c_s H, \tag{15.2}$$

$$\sigma T_{\rm eff}^4 = \frac{3GM\dot{M}}{8\pi r^3}, \tag{15.3}$$

where Σ is the surface density, c_s is the sound speed, H is the disk scale height, $T_{\rm eff}$ is the effective temperature, and σ is the Stefan-Boltzmann constant. The last equation states that the local dissipation rate (proportional to $GM\dot{M}/r^3$) is radiated from the disk surface.

Let us estimate the temperature in an accretion disk around a stellar-mass black hole. Taking $M = 10\ M_\odot$ and $\dot{M} = 10^{-8}\ M_\odot/\text{yr} \approx 6 \times 10^{14}$ kg/s, at radius $r = 100$ km $= 10^5$ m:

$$T_{\rm eff}^4 = \frac{3 \times 6.67 \times 10^{-11} \times 2 \times 10^{31} \times 6 \times 10^{14}}{8\pi \times 10^{15} \times 5.67 \times 10^{-8}}.$$

The numerator is approximately 2.4×10^{36}, the denominator about 1.4×10^9, giving $T_{\rm eff}^4 \approx 1.7 \times 10^{27}$ and thus $T_{\rm eff} \approx 6 \times 10^6$ K. This is an X-ray temperature! And indeed, accreting stellar-mass black holes are among the brightest X-ray sources in the sky.

The alpha-disk model, despite its phenomenological foundation, has proven remarkably successful. When Balbus and Hawley identified the MRI in 1991, simulations confirmed that MRI-driven turbulence produces effective α values in the range 0.01 to 0.1, exactly what Shakura and Sunyaev had assumed. The cosmic water wheel works because magnetic turbulence churns the flow, carrying angular momentum outward like a system of interlocking gears.

15.3 When Magnetic Flux Accumulates

Something interesting happens when magnetic flux builds up near the central object. In a standard alpha-disk, the magnetic field is dynamically weak—it drives turbulence but does not significantly affect the overall flow pattern. But suppose more and more magnetic flux is advected inward, accumulating near the black hole. Eventually, the magnetic pressure becomes comparable to the ram pressure of the infalling gas:

$$\frac{B^2}{2\mu_0} \sim \rho v^2 \sim \rho \frac{GM}{r}.$$

In this "magnetically arrested disk" state, the field is strong enough to halt accretion temporarily. Gas piles up outside the magnetosphere until the pressure is sufficient to push through, leading to episodic accretion. The disk "breathes," with periods of quiescence punctuated by bursts of infall.

You might ask: why would flux accumulate in the first place? The answer involves the interplay between advection and diffusion. In a highly conducting disk, magnetic flux is frozen into the flow and advected inward with the accreting gas. If the inward advection exceeds outward diffusion (which can happen when $\dot{M}$ is high), flux

piles up at the center. Simulations show this naturally occurs in many circumstances.

Magnetically arrested disks have dramatic consequences for jet power. The strong magnetic field threading the black hole provides a direct conduit for extracting rotational energy. The jets from magnetically arrested disks are among the most powerful observed—precisely what we see in objects like M87. The cosmic water wheel, when the magnetic field grows strong enough, develops a powerful exhaust.

15.4 *Powering Jets: The Blandford-Znajek Mechanism*

How does a spinning black hole power a jet? The mechanism, proposed by Roger Blandford and Roman Znajek in 1977, remains one of the most remarkable applications of MHD—remarkable because it operates in a regime where spacetime itself is curved and rotating.

The basic idea is this: imagine magnetic field lines threading the event horizon of a spinning black hole. The black hole's rotation drags spacetime around with it—a phenomenon called frame dragging—which in turn drags the field lines. This rotation twists the field, generating a toroidal component. The twisted field carries angular momentum outward along the rotation axis, extracting energy from the black hole's spin.

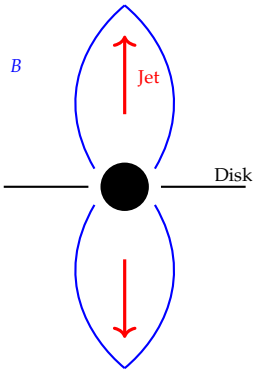

Figure 15.2: The Blandford-Znajek mechanism: field lines threading a spinning black hole extract rotational energy, powering jets along the poles.

Let us estimate the power. The gravitational radius of a black hole is $r_g = GM/c^2$. For a black hole of mass M threaded by magnetic field B and spinning with dimensionless parameter a/M (where $a/M = 1$ is maximal spin), the Blandford-Znajek power scales as

$$P_{\rm BZ} \sim \frac{B^2 r_g^2 c}{\mu_0} \left(\frac{a}{M}\right)^2.$$

For M87's black hole, $M \approx 6 \times 10^9\ M_\odot$, so

$$r_g = \frac{6.67 \times 10^{-11} \times 6 \times 10^9 \times 2 \times 10^{30}}{(3 \times 10^8)^2} \approx \frac{8 \times 10^{29}}{9 \times 10^{16}} \approx 9 \times 10^{12}\ \text{m}.$$

This is about 60 AU—the black hole's gravitational radius exceeds the size of our solar system out to Neptune's orbit.

Taking $B \sim 100\ \text{G} = 10^{-2}\ \text{T}$ (estimated from emission models and Event Horizon Telescope observations) and $a/M \sim 0.9$:

$$P_{\rm BZ} \sim \frac{(10^{-2})^2 \times (9 \times 10^{12})^2 \times 3 \times 10^8}{4\pi \times 10^{-7}} \times 0.81.$$

Working through:

$$P_{\rm BZ} \sim \frac{10^{-4} \times 8 \times 10^{25} \times 3 \times 10^8 \times 0.81}{1.3 \times 10^{-6}} \approx \frac{2 \times 10^{30}}{1.3 \times 10^{-6}} \approx 1.5 \times 10^{36}\ \text{W}.$$

Let us compare this to the Milky Way's total luminosity of about 3×10^{36} W. M87's jet carries power comparable to an entire galaxy! And this comes purely from extracting the rotational energy of the black hole via magnetic fields. The cosmic water wheel's exhaust is a galactic-scale searchlight.

You might ask: won't the black hole spin down eventually? Yes—but the timescale is long. A maximally spinning black hole of mass M contains rotational energy $E_{\rm rot} \sim 0.29Mc^2$. For M87's $6 \times 10^9 M_\odot$ black hole, this is about 3×10^{56} J. At $P_{\rm BZ} \sim 10^{36}$ W, the spin-down time is $\tau \sim 3 \times 10^{20}$ s $\sim 10^{13}$ years—a thousand times the age of the universe. M87 can afford to run its jet indefinitely.

15.5 Jet Collimation

Jets emerge from near the black hole, but they must travel enormous distances while remaining tightly collimated. M87's jet maintains an opening angle of only a few degrees over 5000 light-years. What keeps it so narrow?

The answer lies in magnetic hoop stress—the tension in toroidal magnetic field lines that we encountered back in Chapter 4. As the jet expands, any toroidal field component wrapping around it provides an inward-directed tension:

$$\text{Hoop stress} = \frac{B_\phi^2}{\mu_0 r}.$$

This stress acts like the tension in a wrapped rubber band, squeezing the jet toward the axis. If the jet tries to expand, it stretches the toroidal field, increasing the tension and pushing back.

The collimation is not perfect, of course. Close to the black hole, the jet is launched with some opening angle determined by the magnetic field geometry. As it propagates outward, the hoop stress pinches it progressively tighter. Eventually, at large distances, external pressure from the surrounding medium may take over the confinement role. The intergalactic medium, hot and diffuse though it is, provides a pressure floor that helps keep the jet narrow.

There is something almost paradoxical here. The jet is powered by energy extracted from near the event horizon, a region of extreme gravity. Yet the physics that keeps it collimated—magnetic tension—is the same phenomenon that confines plasma in a tokamak, operates in solar coronal loops, and shapes the Earth's magnetosphere. MHD is scale-invariant, or nearly so. The same equations that describe a laboratory plasma describe a galactic jet.

You might ask: what happens when the jet finally decollimizes? Eventually, at scales of hundreds of thousands of light-years, many

jets do lose their collimation. They form giant lobes—enormous bubbles of radio-emitting plasma inflated by the jet's kinetic energy. These lobes can span millions of light-years, dwarfing their host galaxies. They represent the ultimate dissipation of the jet's power, the final stage of the cosmic water wheel's output.

15.6 A Tale of Two Black Holes

Let us examine two very different accreting black holes to see how the same MHD physics produces vastly different observational signatures.

M87: The Roaring Giant

M87's black hole, at $6 \times 10^9\ M_\odot$, sits at the center of a giant elliptical galaxy. It is surrounded by hot gas from the intracluster medium—the Virgo cluster provides ample fuel. The accretion rate is relatively high, the magnetic flux has accumulated to the magnetically arrested state, and the result is a powerful jet that we see in radio, optical, and X-ray light.

The Event Horizon Telescope image of M87, released in 2019, showed a bright ring surrounding a dark shadow—the first direct image of a black hole's immediate environment. The ring is not the event horizon itself but the photon ring, where light orbits the black hole before escaping toward us. The asymmetry in the ring (brighter on one side) reveals the black hole's spin and the Doppler beaming of the approaching jet material.

The Event Horizon Telescope achieved angular resolution of about 20 microarcseconds—roughly the angular size of a donut on the Moon, as seen from Earth. This remarkable feat of very-long-baseline interferometry allowed astronomers to probe scales of just a few gravitational radii, where MHD reigns supreme.

Sagittarius A: The Quiet Neighbor*

Our own Milky Way harbors a supermassive black hole too: Sagittarius A*, lurking at the Galactic Center just 26,000 light-years away. With a mass of $4 \times 10^6\ M_\odot$—a thousand times smaller than M87's behemoth—it is in many ways a more modest object.

Yet Sgr A* presents a puzzle. Its luminosity is only about 10^{29} W, roughly 300 times the Sun's output. For a four-million-solar-mass black hole, this is pathetically dim. Let us calculate what we might expect.

The Eddington luminosity—the maximum luminosity for spherical accretion before radiation pressure blows away the infalling mate-

rial—scales as

$$L_{\rm Edd} = \frac{4\pi G M m_p c}{\sigma_T} \approx 1.3 \times 10^{31}\ {\rm W} \times \frac{M}{M_\odot}.$$

For Sgr A*:

$$L_{\rm Edd} \approx 1.3 \times 10^{31} \times 4 \times 10^6 \approx 5 \times 10^{37}\ {\rm W}.$$

The observed luminosity is $L \approx 10^{29}$ W, giving $L/L_{\rm Edd} \sim 2 \times 10^{-9}$. Sgr A* is a billion times fainter than it could be!

You might ask: is it simply starved for fuel? Partly. The Galactic Center does not provide the copious gas supply that M87 enjoys. But there is more to the story. At such low accretion rates, the disk becomes "radiatively inefficient." The gas is optically thin—photons escape before they can share energy efficiently between electrons and ions. The ions, which carry most of the gravitational energy, remain hot but do not radiate. Most of the energy is advected across the event horizon rather than radiated away.

This is the regime of radiatively inefficient accretion flows (RIAFs), sometimes called advection-dominated accretion flows (ADAFs). The disk is geometrically thick (puffed up by ion pressure), optically thin (transparent to its own radiation), and thermally inefficient. MHD still operates—the MRI still drives turbulence, magnetic fields still thread the flow—but the observational signature is very different from a thin, bright disk.

Sgr A* does show flares: sudden brightenings by factors of 10–100 that last minutes to hours. These may arise from magnetic reconnection events near the black hole, transient overdensities in the flow, or jets briefly pointing toward us. The flares provide valuable diagnostic information about the MHD processes occurring at the event horizon scale.

The Event Horizon Telescope also imaged Sgr A* in 2022, revealing a similar ring-and-shadow structure to M87 but with more variability—the smaller black hole evolves on shorter timescales (minutes rather than days), making the image harder to construct. Both images stand as triumphs of observational astronomy and confirmations of our theoretical models.

15.7 Disk Winds and Mass Loss

Not all the gas that approaches a black hole actually falls in. Magnetic fields anchored in the disk can launch powerful winds that carry mass, angular momentum, and energy away from the system.

The basic mechanism is centrifugal acceleration along inclined field lines. Imagine a field line emerging from the disk at an angle to

the vertical. Gas tied to this field line rotates with the disk at the footpoint but finds itself at a different radius along the field line—where the centrifugal force, if the field is inclined outward, exceeds gravity. The gas is flung outward along the field line like a bead on a rotating wire.

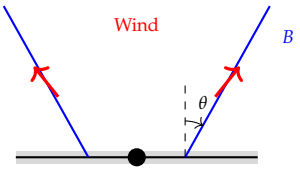

Figure 15.3: Disk winds are launched along inclined field lines. Gas is centrifugally accelerated away from the disk.

For the wind to be launched, the field line must be inclined at more than 30° from the vertical—the critical angle where centrifugal force along the field equals the gravitational component along the field. This is the Blandford-Payne mechanism, proposed in 1982, and it provides an alternative (or complement) to the Blandford-Znajek mechanism for powering outflows.

You might ask: which mechanism dominates, Blandford-Znajek or Blandford-Payne? It depends on the system. Blandford-Znajek requires a spinning black hole and strong magnetic flux threading the horizon—it extracts energy from the hole itself. Blandford-Payne can operate from any rotating disk with inclined magnetic fields—it extracts energy from the disk's rotation. In many systems, both likely contribute.

Disk winds have profound implications for the evolution of accreting systems. They can carry away a significant fraction of the inflowing mass, reducing the actual accretion rate onto the central object. They can remove angular momentum, potentially supplementing or even replacing the MRI as the agent of angular momentum transport in some regions. And they can inject energy and momentum into the surrounding environment, influencing star formation and galaxy evolution.

15.8 Jets Reshaping Galaxies

The jets we have discussed do not simply vanish into the void. They interact with their environment, and those interactions can reshape entire galaxies.

Consider a jet propagating through the hot gas that fills a galaxy cluster. The jet inflates a bubble—a cavity of relativistic plasma that displaces the thermal gas. These bubbles are visible in X-ray images as dark regions where the hot intracluster medium has been pushed aside. The Perseus cluster, one of the nearest and best-studied, shows multiple generations of bubbles, testimony to repeated outbursts from the central black hole over hundreds of millions of years.

The energy in these bubbles is enormous. A single bubble might contain 10^{52} J—comparable to a supernova. But unlike supernovae, which explode once, jet activity can repeat, injecting energy quasi-continuously. This "radio-mode feedback" is thought to solve a long-standing puzzle: why don't the centers of galaxy clusters cool down?

Hot gas radiates X-rays. In the dense centers of clusters, the cooling time can be as short as a hundred million years. Without heating, the gas should cool, sink toward the center, and form stars at prodigious rates. Yet we see relatively little star formation in cluster cores. The jet-inflated bubbles provide the missing heating, their energy gradually dissipating into the surrounding gas through sound waves, turbulence, and mixing. The black hole, through its jets, acts as a cosmic thermostat.

This feedback loop operates across an astonishing range of scales. The black hole itself is contained within its gravitational radius—perhaps 10^{13} m for a massive cluster central black hole. The jets extend to megaparsec scales—10^{22} m. That is nine orders of magnitude, from the event horizon to the cluster outskirts. MHD processes at the smallest scales determine the thermodynamic fate of gas at the largest.

15.9 Historical Interlude: From Quasars to Event Horizons

The story of our understanding of cosmic engines spans six decades of discovery.

In 1963, Maarten Schmidt measured the spectrum of a peculiar radio source called 3C 273. The emission lines were wildly redshifted—the object was receding at 16% of the speed of light, implying a distance of 2 billion light-years. Yet it appeared almost star-like, hence the name "quasi-stellar object" or quasar. At that distance, its apparent brightness implied a luminosity of 10^{40} W—a hundred times the entire Milky Way, from a region smaller than the solar system. What could possibly produce such power?

Donald Lynden-Bell, in 1969, proposed the answer: accretion onto supermassive black holes. The gravitational potential energy released as matter spirals toward a black hole exceeds even nuclear fusion in efficiency. A black hole accreting at its Eddington limit converts roughly 10% of the infalling mass to radiation—fifteen times more efficient than hydrogen fusion. This "gravitational engine" could explain quasar luminosities.

But how did the gas shed its angular momentum and actually fall in? Shakura and Sunyaev's 1973 alpha-disk model provided a framework, parameterizing the unknown turbulent viscosity. The model worked—it matched observations—but what generated the turbulence?

The answer came in 1991, when Steven Balbus and John Hawley resurrected a forgotten instability first noted by Velikhov in 1959 and Chandrasekhar in 1960. The magnetorotational instability, as we explored in Chapter 10, drives turbulence in any weakly magnetized,

differentially rotating disk. The angular momentum problem was solved—not by molecular physics, but by MHD.

Meanwhile, the jet story developed in parallel. Blandford and Znajek (1977) showed how spinning black holes could electromagnetically power jets. Blandford and Payne (1982) demonstrated how disk winds could be centrifugally launched. Numerical simulations in the 2000s—particularly by Jonathan McKinney, Alexander Tchekhovskoy, and collaborators—mapped out when each mechanism dominates and how magnetically arrested disks produce the most powerful jets.

The Event Horizon Telescope collaboration, culminating in the 2019 M87 image and 2022 Sgr A* image, brought these theoretical ideas face to face with observation. The images are consistent with our MHD models of accretion and jet launching. We can finally see the cosmic water wheel operating.

15.10 The Limits of MHD

Throughout these lectures, we have treated MHD as an excellent approximation. And it is—but every approximation has limits.

Near black hole event horizons, the gravitational field is strong enough that general relativity becomes essential. Standard MHD assumes flat spacetime; near a black hole, spacetime curves dramatically. The Blandford-Znajek mechanism itself emerges from the interplay of electromagnetism and general relativity in ways that classical MHD cannot fully capture. Modern simulations of black hole accretion use general relativistic MHD (GRMHD), extending the MHD equations to curved spacetime.

You might ask: does the plasma approximation even hold near a black hole? In many cases, yes. The plasma near Sgr A* or M87 is hot and dense enough that collective behavior dominates, and MHD (or its relativistic generalization) remains valid. But in some extreme environments—the pulsar magnetosphere, for instance—the plasma is so dilute that MHD breaks down and particle-by-particle "kinetic" descriptions become necessary.

At very small scales, MHD always breaks down eventually. The MRI generates structure down to the dissipation scale, where magnetic diffusivity and viscosity take over. In reconnection regions, electron and ion physics determine the actual reconnection rate. In shock fronts, particle acceleration requires kinetic treatment. MHD sets the large-scale stage, but microphysics determines the small-scale details.

These limitations remind us that MHD is a tool, not a truth. It describes conducting fluids magnificently over an enormous range of scales—from laboratory plasmas to galaxy clusters. But the universe

is not obligated to remain within MHD's domain of validity. As we push to ever more extreme environments, we must be prepared to go beyond.

15.11 What Remains Unknown

After fourteen chapters of MHD, you might think we have the universe figured out. We do not. Let me mention a few open questions that keep researchers busy.

Jet composition: What are jets actually made of? We know they contain magnetic fields and relativistic particles, but the mix of electrons, positrons, and protons remains uncertain. The answer matters because it determines how jets interact with their environment and how efficiently they radiate.

Magnetic flux origin: Where does the magnetic flux in accretion disks come from? Is it advected inward from large scales, generated by a disk dynamo, or some combination? The magnetic flux budget determines whether a disk reaches the magnetically arrested state and how powerful its jets can be.

Variability: Why do accreting black holes flicker? The variability timescales range from milliseconds to years, spanning many orders of magnitude. MHD turbulence, reconnection events, and disk instabilities all likely contribute, but connecting specific variability signatures to specific physical mechanisms remains challenging.

Jet feedback in detail: We know jets heat galaxy clusters, but exactly how? Sound waves? Mixing? Cosmic ray acceleration? Different heating mechanisms deposit energy at different locations and affect the gas differently. Getting the details right matters for understanding galaxy evolution.

The MAD threshold: What determines whether a disk reaches the magnetically arrested state? Can we predict from first principles which systems will have powerful jets and which will not?

These questions are not idle curiosities. They connect black hole physics to galaxy formation, cosmic ray acceleration, and the large-scale structure of the universe. The cosmic water wheel does not operate in isolation—it is coupled to its environment across all scales.

15.12 The Long View

We have traveled far in these lectures. We began with the simple observation that magnetic fields and conducting fluids interact—that currents create fields, fields push currents, and the two become locked together in the frozen-in-flux embrace. From this foundation we built: waves that carry magnetic energy, equilibria that con-

fine plasma, instabilities that rearrange it, turbulence that cascades it, dynamos that generate it, and now jets that focus it into cosmic searchlights.

MHD is an approximation, but it is a magnificent one. The same equations that describe a tokamak describe a stellar interior describe a black hole accretion disk. The magnetic Reynolds number might vary by factors of 10^{20} between these systems, yet the frozen-in-flux picture holds throughout. Alfvén waves propagate; magnetic pressure and tension act; the MRI operates; reconnection occurs. Scale-invariance, or something close to it, makes MHD remarkably portable.

And yet MHD is also specific. It is not the physics of all fluids but of conducting fluids. It is not the physics of all fields but of electromagnetic fields mediating collective plasma behavior. Its domain of validity is carved out by conditions: sufficient collisionality, sufficient magnetization, sufficiently slow phenomena compared to light and plasma oscillations. Within that domain, MHD is tremendously powerful. Outside it, other physics awaits.

The universe is full of magnetic plasma doing interesting things. Stars generate their own magnetic fields, then drive winds and explosions shaped by those fields. Accretion disks spin, heat, radiate, and power jets that reshape galaxies. The interstellar medium is stirred by supernovae, structured by magnetic pressure, and threaded by cosmic rays. Galaxy clusters harbor hot, magnetized gas whose cooling is regulated by black hole feedback.

What we have covered is a foundation. The real frontier involves numerical simulations that push the limits of computation, observations from radio to X-ray that probe MHD on scales from planets to clusters, and analytical theory that extracts insight from the mathematical structure. The field is very much alive.

In 1942, Hannes Alfvén proposed that conducting fluids support a new kind of wave—a slow, transverse oscillation mediated by magnetic tension. The community was skeptical; Fermi reportedly said the idea was "impossible." Eight decades later, Alfvén waves have been observed in the solar wind, the Earth's magnetosphere, and (indirectly) in accretion disk turbulence. Alfvén won the Nobel Prize. The universe, it turns out, pays attention to the physics even when physicists do not.

There is more to discover. There always is. But you now have the tools to understand it.

Bibliography

[1] Peter A. Davidson. *An Introduction to Magnetohydrodynamics*. Cambridge University Press, 2001.

[2] Eric Priest. *Magnetohydrodynamics of the Sun*. Cambridge University Press, 2014.

[3] Steven A. Balbus and John F. Hawley. A powerful local shear instability in weakly magnetized disks. *The Astrophysical Journal*, 376:214–222, 1991.

[4] Peter Goldreich and S. Sridhar. Toward a theory of interstellar turbulence. ii. strong alfvénic turbulence. *The Astrophysical Journal*, 438:763–775, 1995.